AN INVESTIGATION OF LIQUID VELOCITY MEASUREMENT USING PZT CYLINDERS

YAO-TING CHANG

An Investigation of Liquid Velocity Measurement Using PZT Cylinders

by

Yao-Ting Chang

Thesis Presented for the Degree of

Magister Technologiae

in the Department of Electrical Engineering

Cape Peninsula University of Technology

December 2006

Declaration

This thesis is submitted for the degree of Magister Technologiae in the Department of Electrical Engineering at the Cape Peninsula University of Technology. It has not been submitted before for any degree or examination at this or any other university. The author confirms it is his own, original work.

.....

Y.T Chang

30 November 2006

Acknowledgments

I would like to thank the following for their contribution towards this project:

- My supervisor, Associate Professor J Davies for his invaluable advice and guidance throughout this research work;
- B Prenzlow (University of Cape Town), for his discussion and insight into the adaptive mutation breeder algorithm;
- all the CIR members M Parker, S Kaplan, T Smith and others for their assistance;
- my gratitude goes to my family and close friends for their constant encouragement throughout these two years of study and,
- finally, financial support from the National Research Foundation (NRF).

An Investigation of Liquid Velocity Measurement Using PZT Cylinders

by

Yao-Ting Chang

Submitted to the department of Electrical Engineering
on March 31, 2007, in partial fulfillment of the
requirements for the degree of
Magister Technologiae

Synopsis

A novel ultrasonic velocimeter was developed in this study using a single element PZT cylinder encapsulated within an isothermal cavity. The rig was designed to hold a small sample volume of test liquid (typically less than 0.2ml), as a prerequisite for biological application. An admittance spectrum for the liquid filled cavity displayed sharp piezoelectric modes indicating strong coupling between the cylinder and liquid. This coupling was further improved by using liquid soap as a coupling agent. The phase velocity was measured, using the change in frequency associated with change in acoustic mode number. Early results indicated a change in frequency, with mode number decrease over the superimposed piezoelectric resonance providing a skewed value for phase velocity. This problem is evidenced in the literature precluding continuous wave interferometry as a realisable means of measuring phase velocity. This study examines the common problem of frequency pulling and resonant interaction between acoustic and piezoelectric modes. For the first time an alternative is shown to traditional "electro-acoustic" models, utilising an extension of Mason's transmission line model with the addition of a "mechanical-acoustic" transformer to represent energy coupling between the piezoelectric and surrounding liquid. It was found the transformer coupling coefficient could be described as the inner surface area of the cylinder. In an attempt to quantify the behaviour of this model it has been simplified into an "electro-acoustic" equivalent lumped circuit elements. Each liquid mode is represented as a series tuned LCR circuit. The solution to the frequency pulling was unravelled by implementing a stochastic optimiser (adaptive mutation breeder algorithm) to predict the coupling coefficient between mechanical and acoustic modes. It also predicts acoustic equivalent circuit parameters and further utilise it to extract the velocity of sound from the test liquid. Three test liquids were evaluated including water, FC43 and FC75 at a constant temperature of 30 °C±0.01 °C. Initial results indicate a strong correlation between the model and experiment with accumulative admittance errors falling below 5%. Subsequently it was possible to achieve phase velocity measurements with a "worst case" standard deviation of less than 3.74. It has been the hypothesis of this study to show, in concept, that inline tube velocimeter is plausible using continuous wave cylindrical interferometry.

Contents

List of Figures

Abbreviations and Symbols

Anglicised spelling has been used throughout this dissertation.

Abbreviations

AMBA	adaptive mutation breeder algorithm
PZT	lead zirconate titanate
KLM	Krimholtz, Leedom and Matthae

Symbols

A	Surface area of the transducer
a	Acceleration
B	Susceptance
C	Capacitance
C_o	Electrical capacitance of piezoelectric transducer
D	Electric displacement
d	Piezoelectric constant
$\mathbf{d}$	Distance between Tx and Rx
E	Voltage
F	Force
f_s	Series resonance frequency
f_p	Parallel resonance frequency
f_m	Maximum frequency
f_n	Minimum frequency
G	Conductance

h	Piezoelectric constant
I	Current
k	Wave number
L	Inductance
m	Mass
M_a	Mutual mechanical-acoustic coupling coefficient
N	Turn ratio of transformer
Q_m	Quality factor
R	Resistance
S	Strain
T	Stress
t	Thickness of the piezoelectric transducer
υ	Velocity
X	Reactance
x	Acoustic path length
Y	Admittance
$\mathbf{Y}$	Young's modulus
Z	Impedance
Z_o	Characteristic acoustic impedance
λ	Wavelength
k_{eff}	Electromechanical coupling factor
ξ	Displacement
ω	Angular frequency
ϵ^s	Clamped permittivity
s^ε	Electric compliance
ε^T	Dielectric constant
ρ	Density

Chapter 1

Introduction

1.1 Background

The use of piezoceramic transducers to produce ultrasound for research and industry has increased rapidly in recent years. Many new applications are continually developed and much of this is demonstrated in the literature[2][29]. As a result, a theoretical analysis of the fundamental operation for such devices is not only desirable, but vital.

In 1947, the first piezoelectric ceramic barium titanate ($BaTiO_3$) was a revolutionary discovery, and a decade later the discovery of lead zirconate titanate (PZT) shown by B Jaff[48] constituted a turning point in the field of piezoelectric ceramics. These polycrystalline materials could be rendered permanently piezoelectric by sintering and polling to provide a piezoelectric effect[2]. Ceramic materials possess several advantages over natural crystals (such as quartz and rochelle salt), including higher piezoelectric sensitivity (up to several hundred times) and ease of fabrication into a variety of shapes and sizes[48]. This is why PZT and $BaTiO_3$ remain the most popular and commonly used piezoelectric ceramics. Piezoelectric transducers are now used in a broad range of applications; few examples are as follows:

- Medical: HIFU (high intensity focused ultrasound)[15], IVUS (intravascular ultrasound)[4] and ultrasound imaging[1];

- industrial sensors: level detection, flow sensing, sonochemical devices and velocimeter[35];
- underwater signaling: echosounders, fish finders and sonar systems;
- automotive systems: movement detection, accelerometers;
- hydrophones: biological, military underwater communications;
- actuators: transformer, ultrasonic motors, Surface Acoustic Wave (SAW) devices[46] and,
- high power ultrasonics: ultrasonic drills, cleaning, welding[14].

It is the goal of this study to investigate the application of PZT ceramics as used in the field of liquid velocity measurement. Several techniques exist for determining the velocity of sound in liquids. The most popular approach is utilising the concept of "Time of Flight" and a continuous wave technique[16]. These methods require a complex design and accurate electronic instrumentation to measure the velocity of sound in the liquid.

This study attempts to develop a velocimeter using a single piezoelectric cylinder. Such a sensor is useful to connect and made for in-line pipe sensor and has no impact on the flow of the liquid inside the pipe. When a liquid is placed into a cylindrical piezoelectric transducer, the movement of the transducer is coupled to the liquid. An approximation of the behaviour of sound waves travelling in the liquid within the cylinder can be understood by modelling the inner electrode of the cylinder as a transmitter/receiver and the centre of the cylinder as a reflector. When a voltage is applied to the transducer, the transmitter vibrates and produces sound waves which travel through the liquid towards the reflector and then returns back towards the transmitter. While the wave is propagating at a designated frequency, the reflected signal is "added" to the next wave (superimposed), creating a standing wave. The significance of standing waves is that they provide for an accurate measurement of sound speed in the medium under isentropic conditions[16][38]. The physical performance of a single piezoelectric transducer can be adequately obtained by an equivalent circuit, representing the electrical and mechanical properties of the transducer. Although the theoretical analysis of

equivalent circuits for elementary piezoelectric transducers have been published at length in acoustic literature[19][30][31][39], the theory of an acoustic port coupling with liquid was not evident. Analysing the existing equivalent circuits, allowed for the design of an adequate electronic circuit to represent the liquid filled transducer.

1.2 Objectives

It is the purpose of this study to investigate:

- The resonant behaviour of an empty and liquid filled PZT cylinder;
- the acoustic series of loosely coupled modes generated within a PZT cylinder;
- a means of exciting liquid resonances by using a PZT cylinder held within an isothermal rig;
- a new electro-acoustic equivalent circuit model which represents a liquid filled PZT cylinder;
- an adaptive mutating breeder algorithm (AMBA)[23], which is incorporated in this study, for modelling the equivalent circuit mode and determining circuit parameters and,
- the velocity of sound of various test liquids e.g. distilled water, fluorocarbon FC43 and FC75 using the designed velocimeter.

1.3 Procedure

The resonance behaviours of empty and liquid filled PZT ceramic cylinders of varying sizes and diameters were studied for the purpose of measuring the velocity of liquids. Additionally, the optimum size and diameter of the ceramic cylinder required to yield the best results in the experiment was investigated. A test rig was designed to hold a PZT cylinder which was immersed in a water bath for it to achieve an isothermal

condition. The absolute admittance spectra with different test liquids was measured using an impedance analyser. The result indicated the frequency pulling existed between the piezoelectric and liquid resonance mode and such a pulling effect needed to be adequately removed. This study attempts to show an "electro-acoustic" model able to provide an intuitive understanding of the fundamental behaviour of a liquid filled PZT cylinder. Finally, the "electro-acoustic" circuit parameters were calculated by utilising AMBA and the velocity of sound is determined.

1.4 Scope and Limitations

This study focuses on experimental and mathematical modelling of acoustic resonance behaviour of PZT ceramic cylinders of varying sizes and diameters. Further geometries will not be included in this study. The test liquids used in this study were distilled water, FC75 and FC43. The study's significance is to provide results on the resonant behaviour of a PZT cylinder and to detail the behaviour of unique radial acoustic modes within a PZT cylinder. It is a desire to provide a new equivalent transmission line model that describes the behaviour of a PZT cylinder when coupling with liquid. Use of stochastic optimisers (constrained to the adaptive mutation breeder algorithm) as a means of determining equivalent circuit parameters and prediction liquid characteristics such as sound velocity from lumped transmission line parameters are also sought.

1.5 Development Plan

Chapter 2 reviews the background of current methods used for a velocimeter. Chapter 3 discusses the resonant behaviour of a PZT cylinder and investigates PZT cylinders with different materials and sizes. Transducers are explored to determine which will yield the best results. Chapter 4 reviews existing equivalent circuits in the literature including Mason[30], Redwood[41] and KLM[45] models. These models are excessively difficult to understand or to implement. These approximations are adequate for a single piezoelectric element resonating at its fundamental mode, but do not account for harmonics and

mechanical loading. A new "electro-acoustic" model is described at the end of this chapter which was used to represent the liquid filled PZT cylinder. Chapter 5 details the concept of AMBA and how it was implemented as a stochastic optimiser for predicting equivalent circuit parameters and extracting liquid properties such as the velocity of sound. Chapter 6 discusses the design criteria of a liquid velocimeter rig. The instrument set up and data acquisition are also discussed in this chapter. Chapter 7 summarises the findings and conclusions are drawn. Finally, Chapter 8 recommends future work.

Chapter 2

Velocity of Sound Measurement

Many methods have been developed over time to measure the properties of ultrasound as it propagates through liquid. There are several methods to obtain accurate measurement of phase velocity in a sample liquid. Many of these differ from one another, however, most may be regarded as a modification of a few fundamental measuring principles. Traditional and most used techniques include "time of flight" and the continuous wave technique. Each is briefly described in the following sections.

2.1 'Time of Flight' Method

This method is mostly used for the measurement of distance and speed of sound. A typical implementation of such a system involves one or two piezoelectric discs coupled to an acoustic cell[37]. A transmitter (Tx) and receiver (Rx) are placed at a defined distance. The sample liquid is placed in a cavity cell between transmitter and receiver. A sinusoidal pulse is emitted from a transmitter and the time measured for the signal to traverse the liquid and arrive at the receiver (see Fig.2-1). The disadvantage of this method is although the distance between the transmitter and receiver can be determined exactly, the time measurement is difficult to obtain. The signal that travels through the liquid medium is badly distorted (the signal is absorbed and dispersed by the medium, as the liquid acts as an acoustic filter[31]), thus an error is introduced into the measurement system. The debate of this method and several solutions are reviewed in the following

sections.

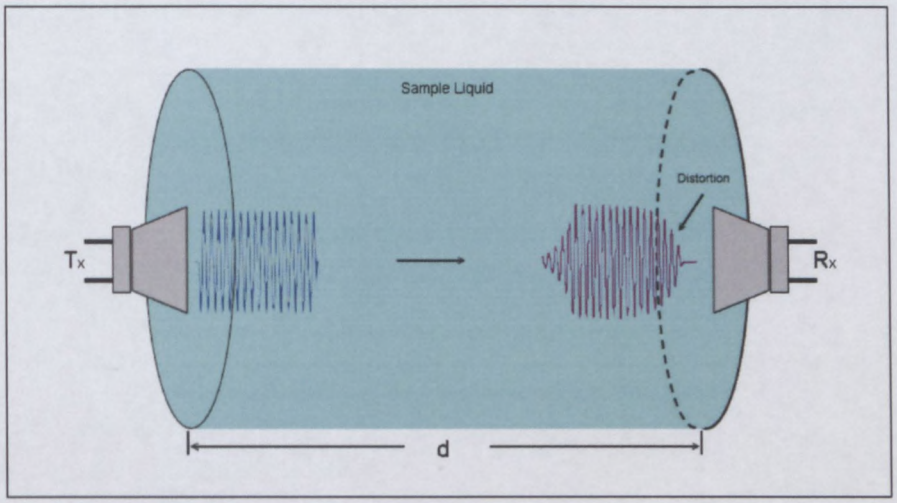

Figure 2-1: Illustration of "Time of Flight" method. The transmitted pulse travels in the liquid through the pre-defined distance '**d**'. The time taken between the pulse to travel from Tx to Rx allows the speed of sound to be determined. Note the distortion of the received pulse

2.1.1 Phase Echo Superposition (PES)

Phase of echoes are superposed in the medium, and round-trip time determined by maximising the amplitude of superposed echoes. The repetition frequency (rf) of the transmitter is adjusted so the time between pulses is equal to a multiple of the round-trip transit time[16]. This method has the advantage of easy operation and a possible extension of automatic measurement. Accurate measurement of the absolute value of sound velocity is a complex process; typically accuracy of 0.006% is required[33].

2.1.2 Pulse Echo Overlap (PEO)

The echo overlap uses similar analogy as PES method, the phase of echoes are overlapped with each other. However, only a single pulse is present in the sample medium at all time and no superposition of the waveforms occurs within the sample vessel[16]. This method enables an accurate determination of absolute value, but quick measurement is difficult

and an extension to an automatic measurement is not possible[36].

2.1.3 Sing-Around Method

A pulse generator sends a pulse of rf carrier which is fed to the transducer. After traversing the medium, the acoustic pulse is reconverted to the electronic pulse by the receiver and used to retrigger the transmitter. This method combines the accuracy and the advantages of automatic, instantaneous operation and recording. The problem of a self-oscillator type method is time delay caused by the acoustic delay due to the medium and the electronic component. Operation range is relatively small using the sing-around method and calibration is required for a particular class of liquids; it has a typical accuracy of 0.01%[12].

2.2 Continuous Wave and Phase Locking Technique

The continuous wave technique is an alternative method to the "time of flight" method and was originally proposed by Sehgal et al.[44]. Phase locking is implemented in continuous wave systems to eliminate threshold uncertainties[17]. The circuit required to perform phase locking has been widely used in telecommunication and is well understood. The output frequency tracks the input frequency by means of phase feedback mechanism using phase difference between the input and output signals[49]. This technique improves the sensitivity and real-time velocity measurement can be achieved. The theory behind the continuous wave locking technique is to place a transmitter a set distance from a receiver and generate a standing wave in the sample medium as shown in Fig.2-2. The transducer drives frequency or phase delay is a quadrature between the received signal[52]. The phase detector is used to determine the phase difference between the driving and receiving transducers. The output of the phase detector is used as feedback to drive the input of a voltage controlled oscillator[16].

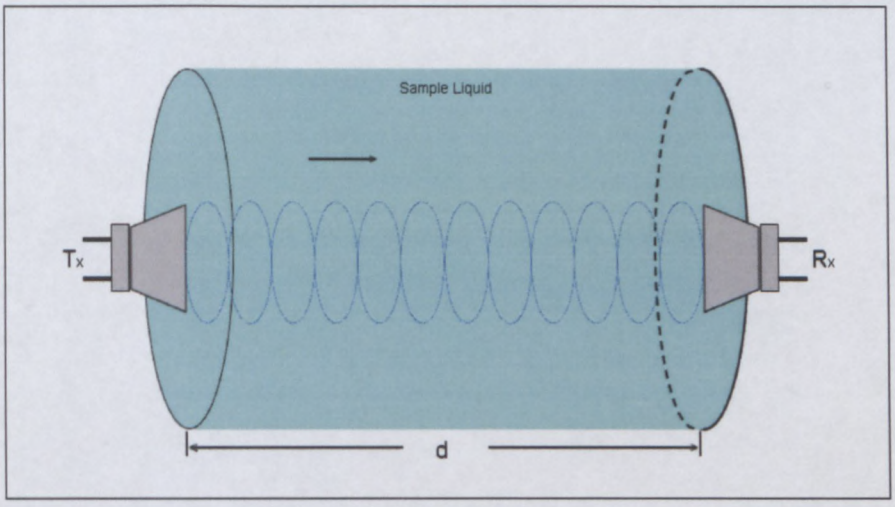

Figure 2-2: Illustration of a continuous wave system. The standing waves have been set up inside the liquid and the frequency of the standing wave depends on the speed of sound in the liquid

The frequency of the controlled wave is proportional to the speed of sound in the liquid. The velocity of sound (ν) in the liquid is defined by:

$$\nu = \frac{f \times d}{n} \tag{2.1}$$

where

f =frequency of the controlled wave;

d =distance between transmitter and receiver; and

n =number of waveform.

The velocity of the sound can be accurately determined, since the frequency and the distance between transducer is constant. The fractional change in the speed of sound is equal to the fractional change in the frequency.

$$\frac{\Delta f}{f_o} = \frac{\Delta \nu}{\nu_o} \tag{2.2}$$

where

f_o and ν_o are the initial frequency and speed of sound.

The continuous wave technique is proven to be more accurate than the "time of flight" method. However, there is ambiguity in this technique as the number of waves within the medium are unknown. The nonlinearities caused by the frequency pulling[16] has the difficulty in obtaining accurate results using this technique.

The study of the velocity of sound in liquid employed technique using a transmitting and a receiving transducer may cause problems such as transducer misalignment, diffraction effects, and mechanical and electrical coupling[28]. It is the study of this thesis to implement an alternative method for velocity of sound measurement. A single piezoelectric cylinder was used, acting as both transmitter and receiver. When such a transducer is submerged in a liquid, a standing wave was set up inside the piezoelectric cylinder. The liquid interacts with the dynamics of the PZT cylinder and changes its resonant behaviour. By measuring these changes, the liquid parameters such as velocity of sound, density and viscosity can be determined.[38]. The discussion of such a method will be the subject for the remainder of this study.

Chapter 3

Piezoelectric Cylinder Characteristics

Piezoelectric ceramics such as barium titanate ($BaTiO_3$) and lead zirconate titanate (PZT) have for many years been used as transducers and are used typically for the emission and detection of acoustic signals[48]. Piezoelectric ceramics are commonly used elements in underwater acoustics, ultrasonic instruments and transducer design. They may be sintered into many shapes including bars, plates, discs, rings, hemispheres and cylinders[2].

Each geometry of a PZT ceramic has unique vibrational modes determined by the material properties and poling direction, just as every mechanical geometry has a unique set of eigen modes and values. A hollow PZT cylinder is shown in Fig.3-1, poled in wall thickness, illustrating the direction of sound radiation, which is indicated by the dotted lines. The three main fundamental resonance modes of the cylinder are:

-radial;

-length and,

-thickness mode.

The resonance frequencies of the three fundamental modes are generally derived from the geometry of the cylinder and may be calculated using the following formulae:

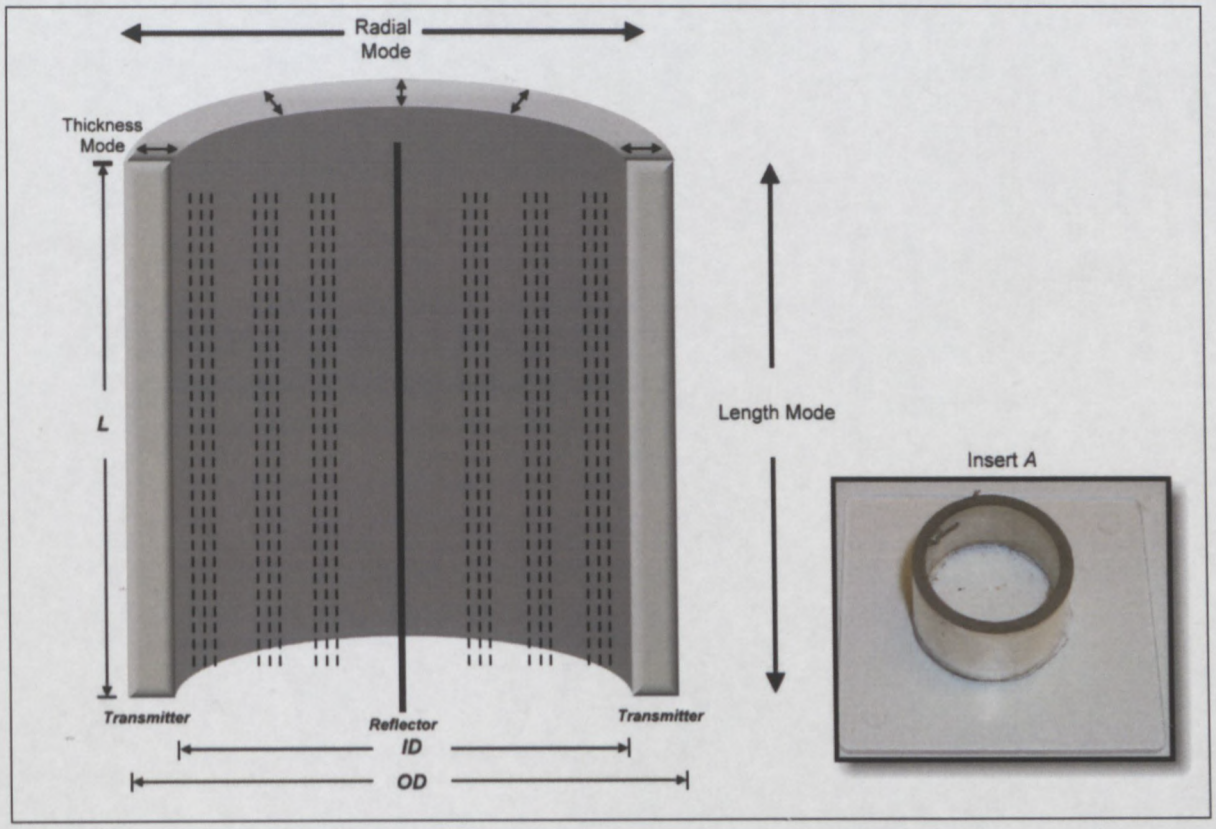

Figure 3-1: The photograph (see *Insert A)* depicts a piezoelectric cylinder poled in wall thickness. A schematic showing a sectional view of the piezoelectric tube with arrows indicates the displacements associated with radial, length and thickness modes. The wall of the transducer acts as a transmitter whilst the centre axis represents the reflector. The dotted lines represent the propagation of the acoustic wave. L, ID and OD represent the length, inner diameter and outer diameter of the transducer respectively

Radial Mode:

$$f_R = \frac{2N}{OD + ID} \tag{3.1}$$

Length Mode:

$$f_L = \frac{N}{L} \tag{3.2}$$

Thickness Mode:

$$f_T = \frac{2N}{OD - ID} \tag{3.3}$$

where

OD = Outer diameter;

ID = Inner diameter;

L = Length of the cylinder and,

N = Mode number.

This thesis focuses on the cylindrical geometry of a PZT tube as it easily enables the filling and retention of a liquid under test. An inline velocimeter is also possible using this method. Using a single cylinder for resonance velocimetery is much easier than with a double disk interferometer method of liquid velocity measurement, since the piezoelectric properties of both disks (Tx & Rx) need to be exactly matched. Furthermore, the alignment between the two disks is required to be precise, with both disks exactly parallel; misadjustment usually results in satellite resonance[9]. The aim of this chapter is to investigate different types of PZT cylinders on the piezoelectric resonances of the transducer. Consequently, the best transducer to be used in liquid property measurement (discussed in the following chapter) can be determined from these results.

3.1 Electro-Mechanical Spectral Response of a Piezoelectric Cylinder

The resonance frequency of a PZT cylinder was examined by attaching an empty piezoelectric cylinder to a coaxial cable and measuring admittance as a function of frequency using an impedance analyser (HP41942A). The admittance spectra were then used to examine the piezoelectric effect as discussed below.

3.1.1 Admittance Diagram

The admittance spectrum was typically used for observing the real and imaginary parts of the current flowing into the network, which were measured by sweeping the unit voltage over a predefined frequency range[16]. The electrical admittance, Y, is composed of a real part, conductance (G) and an imaginary part, its susceptance (B). The equivalent expression is thus:

$$Y = G + jB \tag{3.4}$$

The measured admittance of a transducer over a broad frequency sweep showed a clearly defined piezoelectric resonance. The absolute admittance spectrum of a PZT-4 cylinder ($OD \times ID \times L = 38 \times 32 \times 38\ mm$) is detailed in Fig.3-2. This spectrum consisted of three fundamental resonance modes as described earlier namely: radial, length and thickness mode. Each mode was characterised by two piezoelectric resonances; the peak rising to a maximum (f_{max}) is the series resonance, followed by a trough indicating a local minimum (f_{min}), which is the anti-resonance or parallel resonance. The thickness mode created by the vibration through the wall thickness of the cylinder, had the largest piezoelectric effect compared to the radial and length mode. This result is from the ceramic been polarised in the radial direction[2].

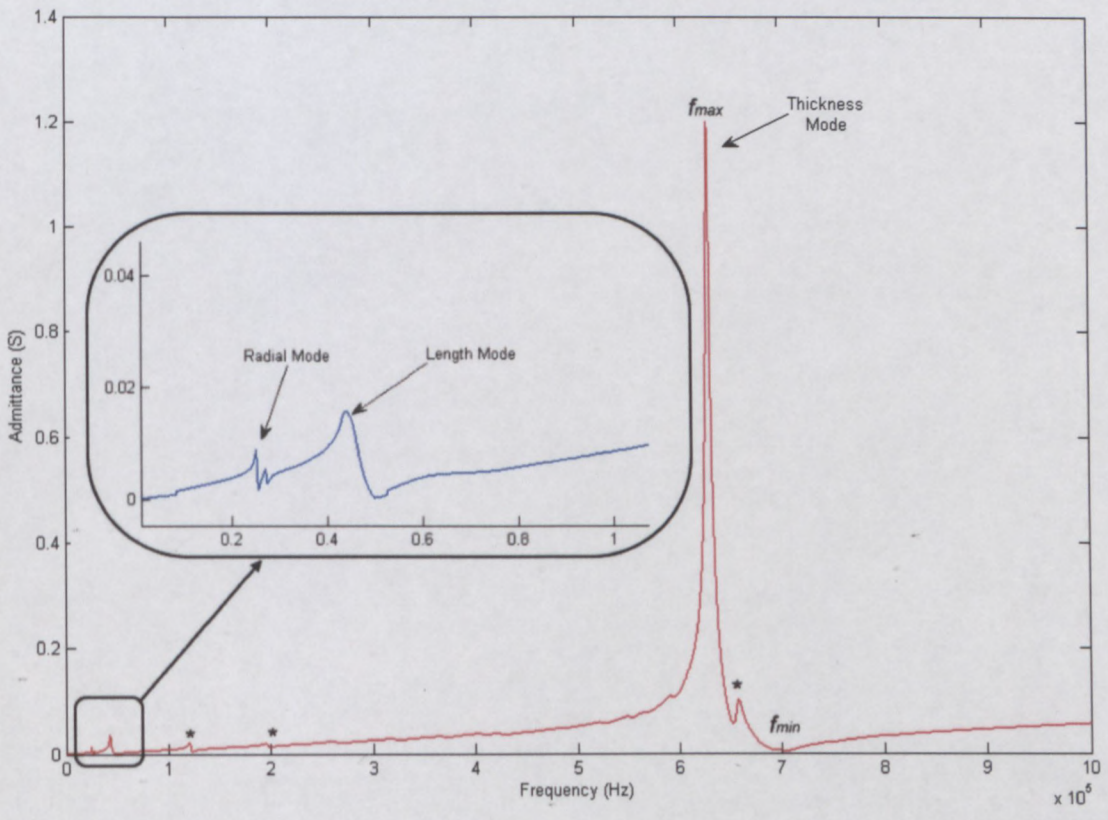

Figure 3-2: Typical admittance response of an empty PZT-4 tube. Three fundamental vibration modes are shown: radial, length and thickness. The thickness mode has the largest piezoelectric effect which occurred at 6.3×10^5Hz at admittance of 1.25 S, where the radial and length mode are situated at 2.5×10^4Hz ($Y = 9 \times 10^{-3}$ S) and 4.2×10^4Hz ($Y = 16 \times 10^{-3}$ S) respectively. Satellite resonances are marked with '*' and indicate overtones of the fundamental resonant modes

3.1.2 The Complex Vector Diagram

The behaviour of a piezoelectric transducer may be described in more detail using an admittance vector diagram where susceptance (B) was plotted against conductance (G) for each frequency point as shown in Fig.3-3[48]. This diagram could be used for analysing the performance of a piezoelectric transducer. As frequency was increased, the graph moved clockwise for a particular resonance. The vector diagram which follows a circle in the complex admittance plane is usually referred to as a transadmittance circle[48].

The vertical offset of the circle in susceptance was because of the amount of clamped capacitance C_o[16]. This circle characterises a single piezoelectric mode and had a diameter of $1/R$ which can be measured by the absolute admittance difference. The half power points f_{3dB} are shown at angle $\pi/4$ from the horizontal diameter. The admittance vector diagram allowed understanding of a piezoelectric behaviour. Each additional circle represented a unique superimposed resonance and the radius indicated its magnitude and quality factor. The admittance vector circle of an empty PZT-4 cylinder with three fundamental modes is illustrated in Fig.3-4.

where

f_n =frequency of minimum admittance;

f_m =frequency of maximum admittance;

f_s =series resonance frequency;

f_p =parallel resonance frequency;

f_{3dB} =the half power point and,

ω =angular frequency.

The equation for the admittance Y of the equivalent electric circuit of a piezoelectric transducer is defined as the following complex expression[16][27][48]:

$$Y = \frac{R}{R^2 + X^2} + j\left[\omega C_o - \frac{X}{R^2 + X^2}\right] \tag{3.5}$$

The reactance X is defined by:

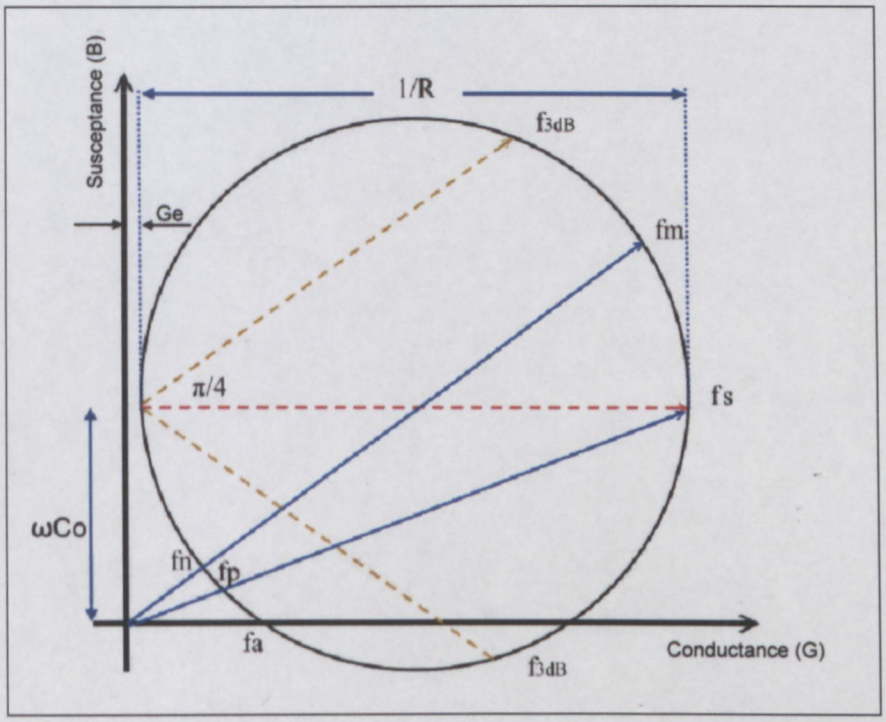

Figure 3-3: The admittance vector diagram for a piezoelectric vibrator. The maximum and minimum absolute admittance are shown as f_m and f_n together with series and parallel mechanical resonances f_s and f_p. R represents the mechanical damping of the resonance. G_e is the dielectric loss conductance which determines the offset between the circle and the imaginary axes[48]

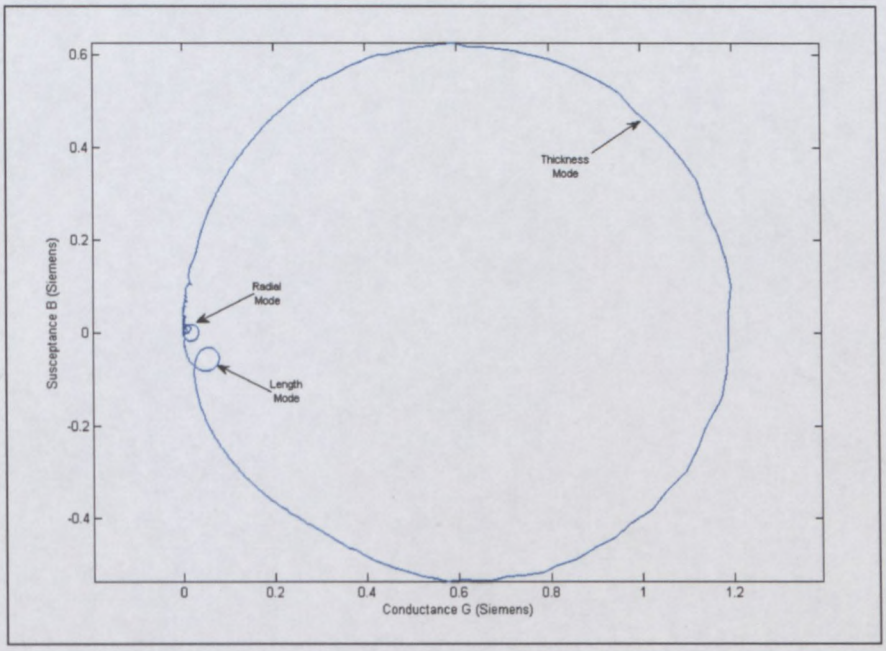

Figure 3-4: The admittance circle of an empty PZT-4 cylinder. The susceptance(B) is plotted against the conductance(G). Each circle indicated by an arrow line represents a different resonances mode at a different frequency

$$X = 2\pi f_s L - \frac{1}{2\pi f_s C} \tag{3.6}$$

Observing the absolute and complex admittance spectra enables the modelling of the behaviour of piezoelectric resonance as an equivalent electrical circuit and estimation of the electro-mechanical equivalent circuit parameters.

Electromechanical coupling factor

The absolute admittance spectrum could display both mechanical and electrical resonance behaviour through its maxima and minima. The magnitude plot of these points provided information on the electromechanical coupling of the transducer, k_{eff}, which is calculated by:

$$k_{eff} = \sqrt{1 - \frac{f_s^2}{f_p^2}} \approx \sqrt{1 - \frac{f_m^2}{f_n^2}} \tag{3.7}$$

where

f_s =the series resonance frequency from the conductance curve;

f_m =the maxima, series resonances and,

f_n =the minima, represents parallel resonances from absolute admittance spectrum.

Quality factor

The mechanical quality factor Q_m can be determined by measuring the series resonance f_s and half power point Δf_{3dB} of the conductance curve:

$$Q_m = \frac{f_s}{\Delta f_{3dB}} \tag{3.8}$$

or may be approximated from the absolute admittance curve:

$$Q_m \approx \frac{\omega_m}{2(\omega_n - \omega_m)} \left[\frac{|Y_{fm}|}{|Y_{fn}|}\right] \tag{3.9}$$

3.1.3 Basic Piezoelectric modelling using Butterworth-Van Dyke (BVD) circuit

The electromechanical relationship for a piezoelectric device is frequently shown in terms of a lumped element circuit also known as the BVD electrical equivalent circuit. Butterworth and Van Dyke[11][18] derived an equivalent circuit for a quartz resonator. They proposed that an electromechanical system could be represented by an electric network. The resonance of the circuit behaves like an electric series RLC oscillating circuit shunted by an electrical capacitor C_o. This model is, however, valid only at frequencies near the fundamental resonance frequency of the device. It is also important to note that C_o introduces a current with a phase shift in quadrature with the applied voltage[30]. The resonance presented using the BVD circuit is distorted by this shunt capacitance C_o (as shown in Fig.3-5). The additional phase shift changes the magnitude and frequency. At this point the series resonance frequency of the motional arm does not accurately describe the resonance frequency of the piezoelectric transducer and C_o needs to be removed

adequately (discussed in Section 3.1.5).

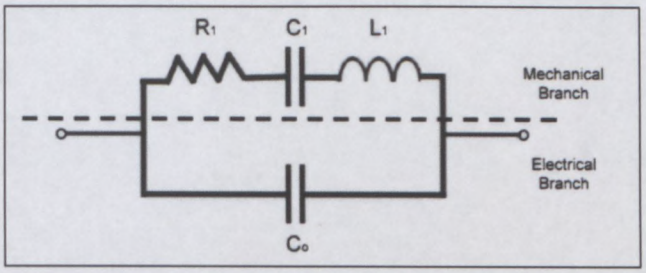

Figure 3-5: Piezoelectric equivalent circuit, also known as the Butterworth-Van Dyke (BVD) equivalent circuit. C_o =shunt capacitance, C_1 =motional capacitor, L_1 =motional inductance and R_1 = motional resistance

Parameters of a Piezoelectric Transducer

The four fundamental electrical parameters for modeling a piezoelectric transducer are R_1, L_1, C_1 and C_o. These define the network completely and other parameters may be derived thereafter. Once Q_m is calculated, the following parameters can be determined[16]:

$$R_1 = \frac{1}{|Y_{fm} - Y_{fn}|} \tag{3.10}$$

$$L_1 = \frac{Q_m R_1}{\omega_s} \tag{3.11}$$

$$C_1 = \frac{1}{\omega_s Q_m R_1} \tag{3.12}$$

The clamped electrical capacitance C_o is easily measured by a capacitance bridge circuit or using a Q-meter. The alternative method is to use the electromechanical coupling factor, k_{eff}, derived from equation 3.7. This is given by equation 3.13:

$$C_o = C_1 \left(\frac{1}{k_{eff}^2} - 1 \right) \tag{3.13}$$

Using formulas described by equations 3.10-3.13, an electrical equivalent BVD circuit was modelled to approximate the measured values of a PZT cylinder. A comparison of admittance spectrum between measured and theoretical calculations is shown in Fig.3-6.

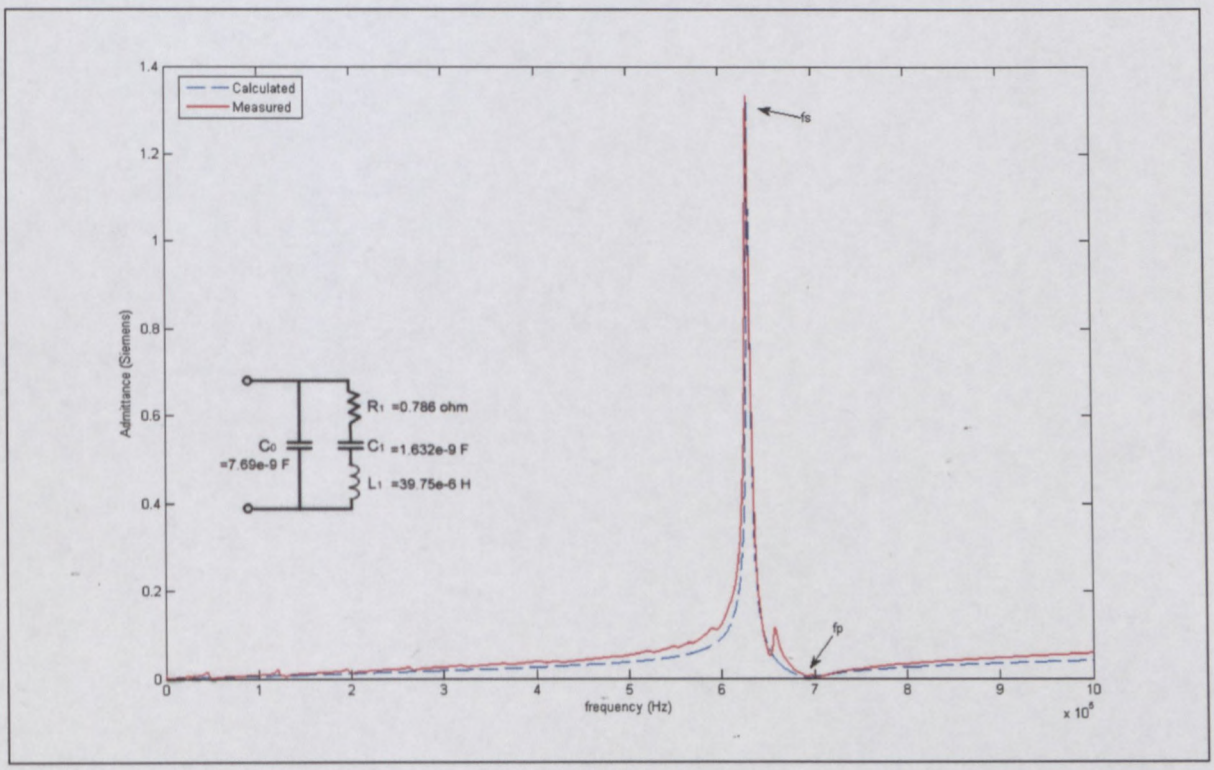

Figure 3-6: A comparison between measured and theoretically calculated (using a BVD/ Mason's equivalent electromechanical circuit) admittance spectra. The theoretical circuit parameters, whilst not highly accurate, are often sufficient for modelling a measured system operating under identical conditions over a limited frequency band

3.1.4 Coaxial Cable Problem (and Solutions)

A short length of coaxial cable was soldered to a piezoelectric cylinder to transmit signals, as shown in Fig.3-7. Since the sweeping frequency operated in megahertz, the coaxial cable acted as a resonant circuit. Multiple reflected waves were present because of impedance mismatching. These standing waves were caused by the load impedance Z_L which was mismatched with the characteristic impedance Z_o of the cable. Z_o was the ratio of E to I at every point along the line. However, in this section, interest was only in the first resonance mode of the coaxial cable. The equivalent circuit of a transmission line could be obtained with a distributed series of inductance L_T, resistance R_T, shunt capacitance C_T, and conductance G_T[30].

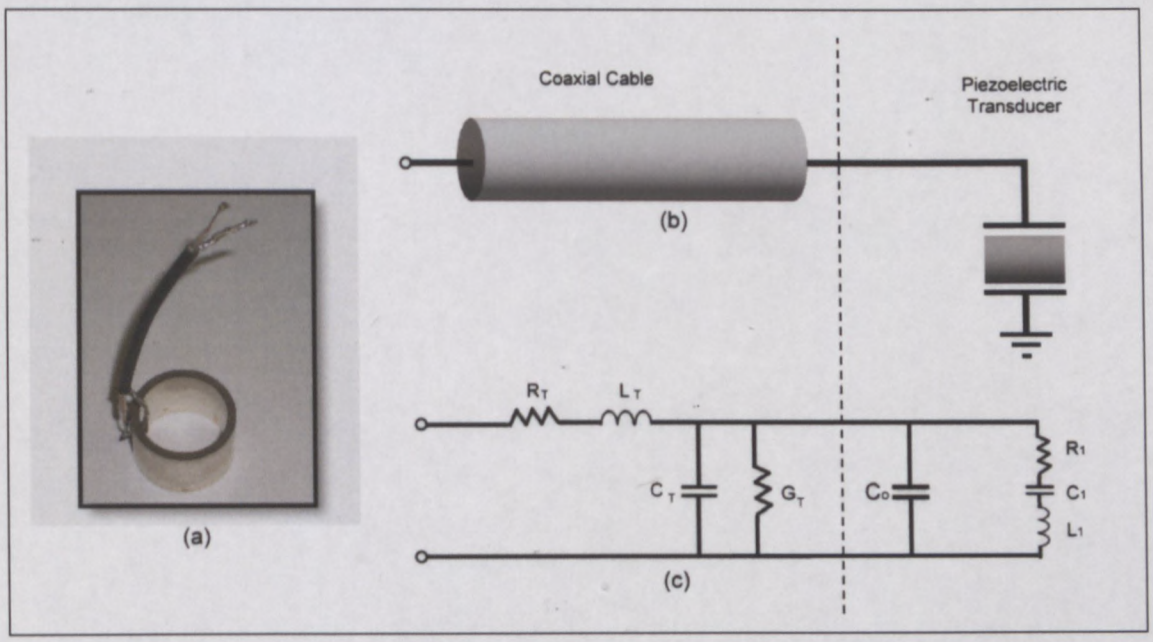

Figure 3-7: (a) and (b) shows a connection of coaxial cable attached to a piezoelectric cylinder and (c) illustrates the equivalent circuit of coaxial cable coupled to a electromechanical equivalent circuit. Note, the series resonance frequency was dropped to much lower frequency due to the lumped shunt C_T and C_o in series with L_T.

The transmission line can be represented by the equivalent circuit as shown in Fig.3-

8(a). The characteristic impedance, Z_o can, therefore, be calculated by:

$$Z_o = \sqrt{\frac{R_T + j\omega L_T}{G_T + j\omega C_T}} \tag{3.14}$$

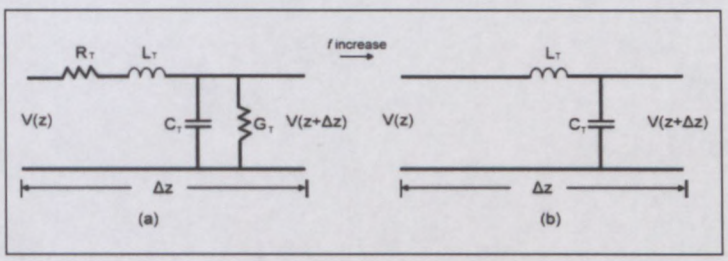

Figure 3-8: (a) Lumped parameter equivalent circuit of a general transmission line and (b) the equivalent circuit operating at high frequency, where R_T and G_T are so small when compared to $j\omega L_T$ and $j\omega C_T$ and, therefore, can be ignored[13]

As the operational frequencies increased, the impedance of the inductance ($Z_{L_T} = j\omega L_T$) and capacitance ($Z_{C_T} = \frac{1}{j\omega C_T}$) also increased. Therefore, $R << j\omega L_T$ and $G_T << j\omega C_T$. The lumped parameters circuit could be simplified to Fig.3-8(b) and the Z_o at high frequency is given by:

$$Z_o = \sqrt{\frac{L_T}{C_T}} \tag{3.15}$$

Consequently, as the length of the coaxial cable connected to the piezoelectric cylinder was increased, the cable's own resonant mode fell closer to that of the cylinder's. Fig.3-9 shows the absolute admittance plotted with frequency over a wide range frequency spectrum, for an empty piezoelectric cylinder connected with different lengths of coaxial cable.

3.1.5 Eliminating the Cable Mode

It was important to remove the cable mode from the spectrum of a PZT cylinder. In order to be able to analyse the simulation results in later a chapter, and to determine the precise piezoelectric resonance frequency to accurately measure sound speed. The

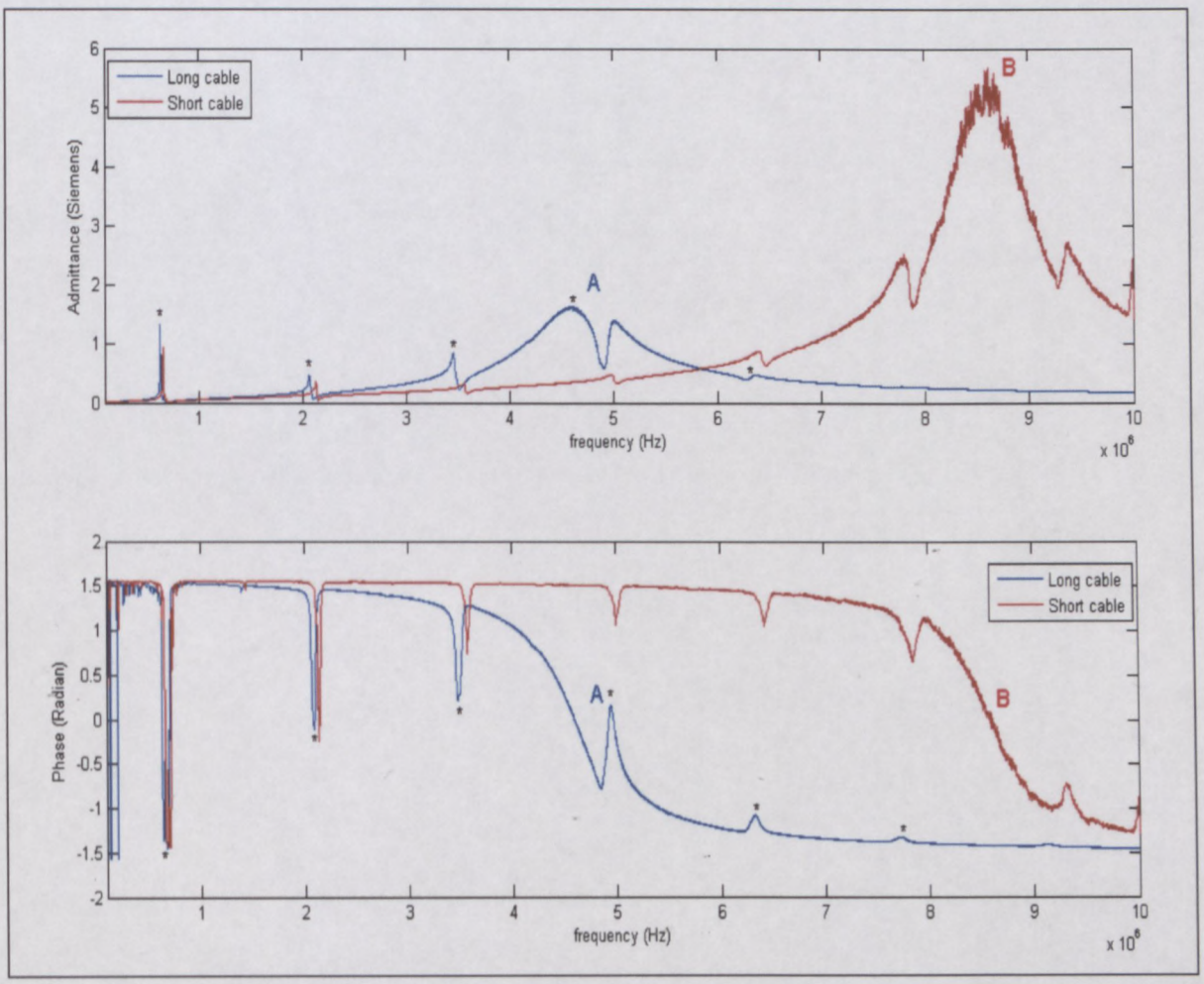

Figure 3-9: Absolute impedance spectra of an empty PZT-4 tube connected with different lengths of coaxial cables. The shorter cable has cable mode occurring at 8.6MHz as indicated with mark 'B'. As the cable length increased, the cable mode decreased to 4.8MHz where its indicated with mark 'A'. Note the piezoelectric resonances superimposed on the spectra '*'

removal of the cable mode could be approached by mathematically subtracting the total admittance using the calculated cable mode lumped element's parameters (R_T, L_T and C_T) as shown in equations (3.18) and (3.19). The value of R_T can be determined easily by using the admittance circle since $G = 1/R_T$.

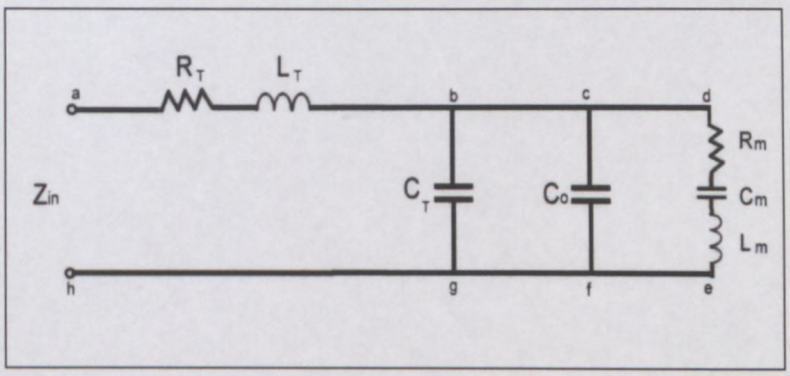

Figure 3-10: The cascaded equivalent circuit for admittance calculations

As shown in Fig.3-10, Z_{ab} is the impedance calculated by R_T in series with inductive reactance $j\omega L_T$. Y_{bcfg} is the admittance calculated using the capacitive susceptance of the coaxial cable element $j\omega C_T$ in parallel with the susceptance of PZT clamped capacitive $j\omega C_o$.

The series impedance (Z_{ab}):

$$Z_{ab} = R_T + j\omega L_T \tag{3.16}$$

The parallel admittance (Y_{bcfg}):

$$Y_{bcfg} = j\omega C_T + j\omega C_o \tag{3.17}$$

$$= j\omega(C_T + C_o)$$

By subtracting the cable mode parameters and clamped capacitance, one can calculate the admittance of the mechanical port of a PZT cylinder (Y_{de}):

$$Z_{bg} = Z_{in} - Z_{ab} \tag{3.18}$$

$$Y_{bg} = \frac{1}{Z_{in} - Z_{ab}}$$

$$Y_{de} = Y_{bg} - Y_{bcfg} \tag{3.19}$$

$$= \frac{1}{Z_{in} - Z_{ab}} - j\omega(C_T + C_o)$$

$$= \frac{1}{Z_{in} - (j\omega L_T + R_T)} - j\omega(C_T + C_o)$$

The result of the piezoelectric electrical admittance spectrum with cable mode removed is shown in Fig.3-11(b). The admittance circle of the simulated cable mode is supposed to be fully encircled by the piezoelectric's admittance circle. However, in this spectrum, the PZT resonance modes were interfered with the cable mode because of the frequency pulling. Therefore, the simulated admittance circle should be adjusted slightly larger than the average of measured admittance circle as shown in Fig.3-12.

3.1.6 Materials of Piezoelectric Ceramics

A variety of PZT ceramics exist for different applications such as instrumentation, power ultrasound and transducers. These can be grouped as "hard" and "soft" ceramics. For this study PZT-26 (hard) and PZT-27 (soft) cylinders manufactured by Ferroperm[2], each with dimensions of $6.35 \times 5.2 \times 6.35$ mm were selected. Each material has different advantages and applications[2]. The hard type PZT material has a large mechanical value and low sensitivity of piezoelectric effect, suitable for high power transmission. The higher order overtones often interacted with the fundamental mode and caused the splitting resonance as exhibited in Fig.3-13. The hard type material gave long ringing because of the high Q_m value and interfered with the fundamental thickness resonance. For this thesis PZT-27 soft ceramic were used. The soft material was suitable for sensor applications and had higher sensitivity and a low mechanical Q_m value, showing clear and undisturbed resonances with quick deterioration of overtones.

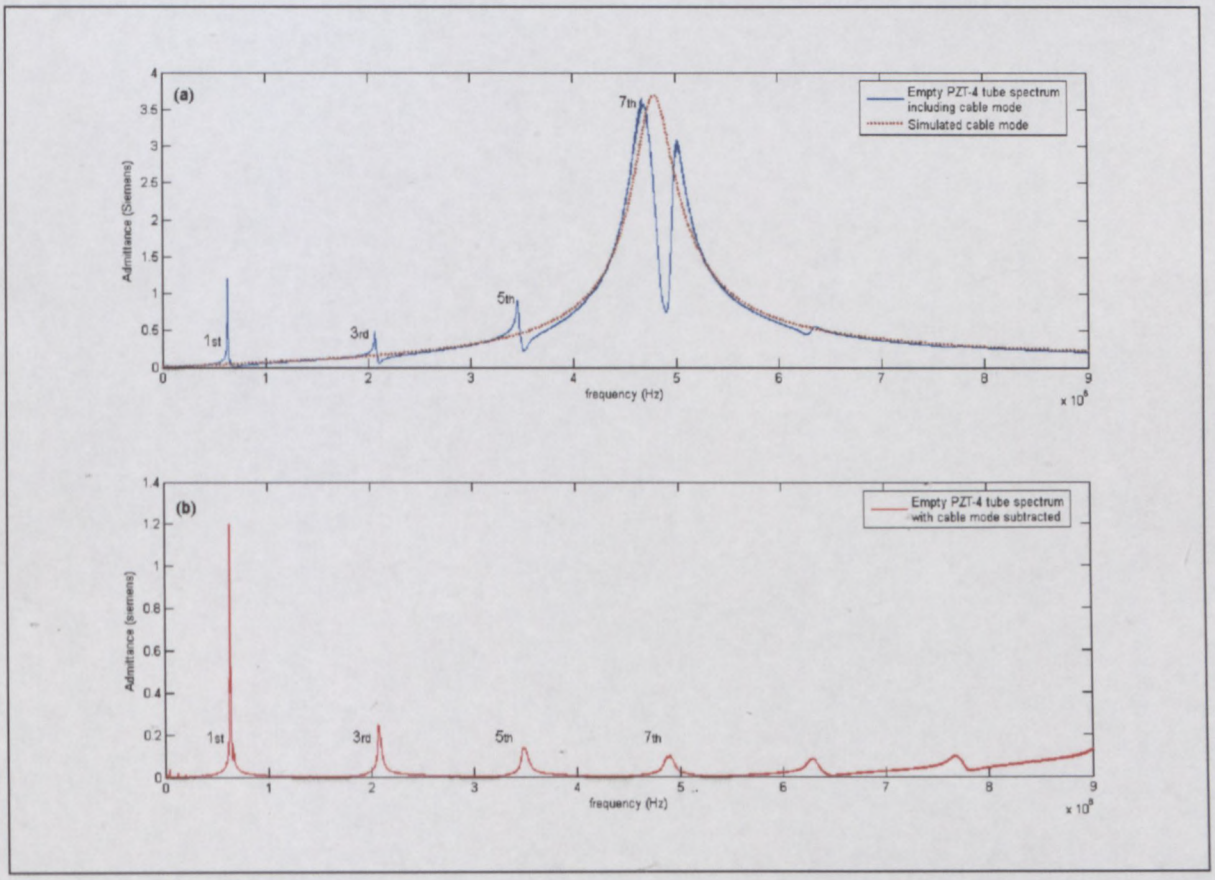

Figure 3-11: Spectrum (a) shows an empty PZT-4 tube connected with a coaxial cable, which was used for the demonstration of cable mode elimination. The dotted line shows the calculated cable mode. The spectrum (b), shows the pure piezoelectric spectrum with the cable mode subtracted

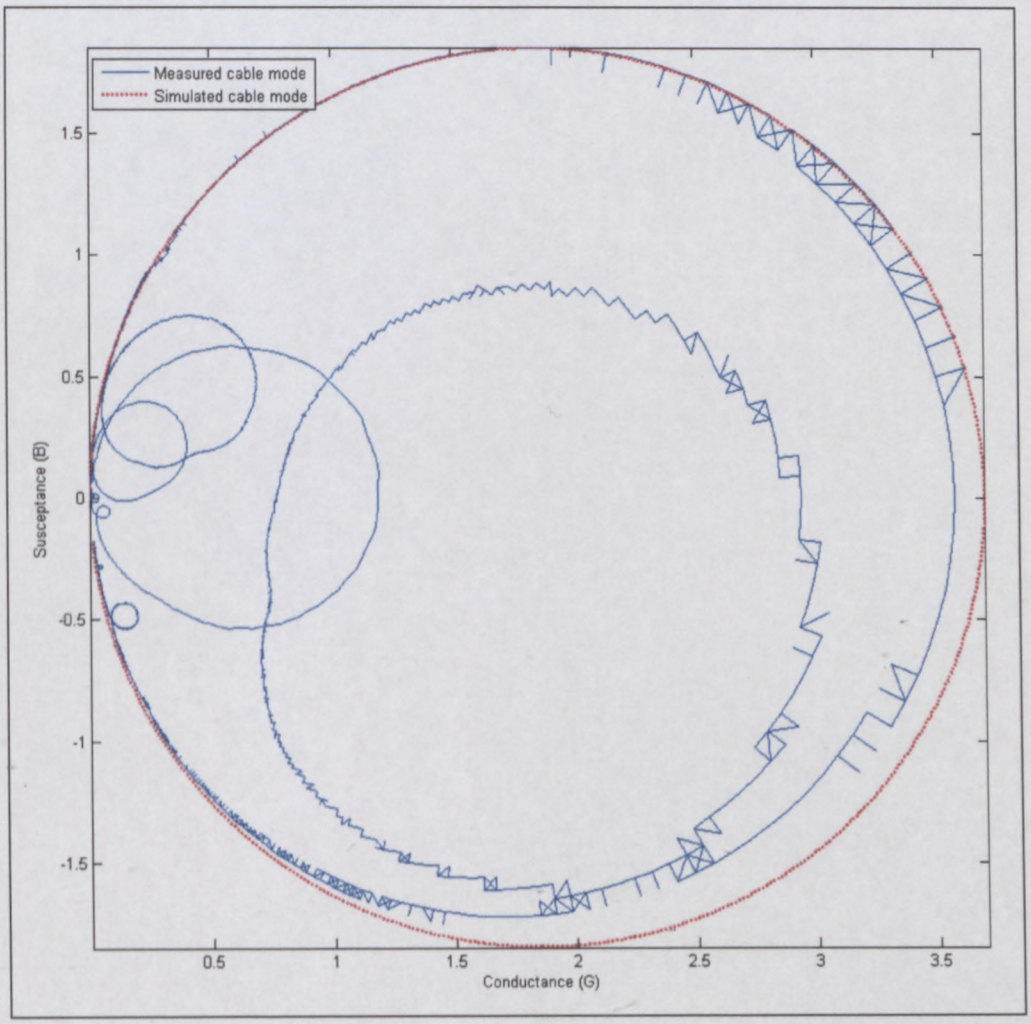

Figure 3-12: The admittance circles of measured and simulated cable mode. The largest admittance circle (blue) represents the measured cable mode. The dotted circle (red) illustrated the simulated cable mode. The simulated circle is hypothesized slightly larger than the average of the measured circle since the average of measured circle has been badly affected by the mode of a piezoelectric cylinder because of the frequency pulling. Quantisation error evident at measured mode is caused by lack of resolution from the impedance analyser (HP 1492A)

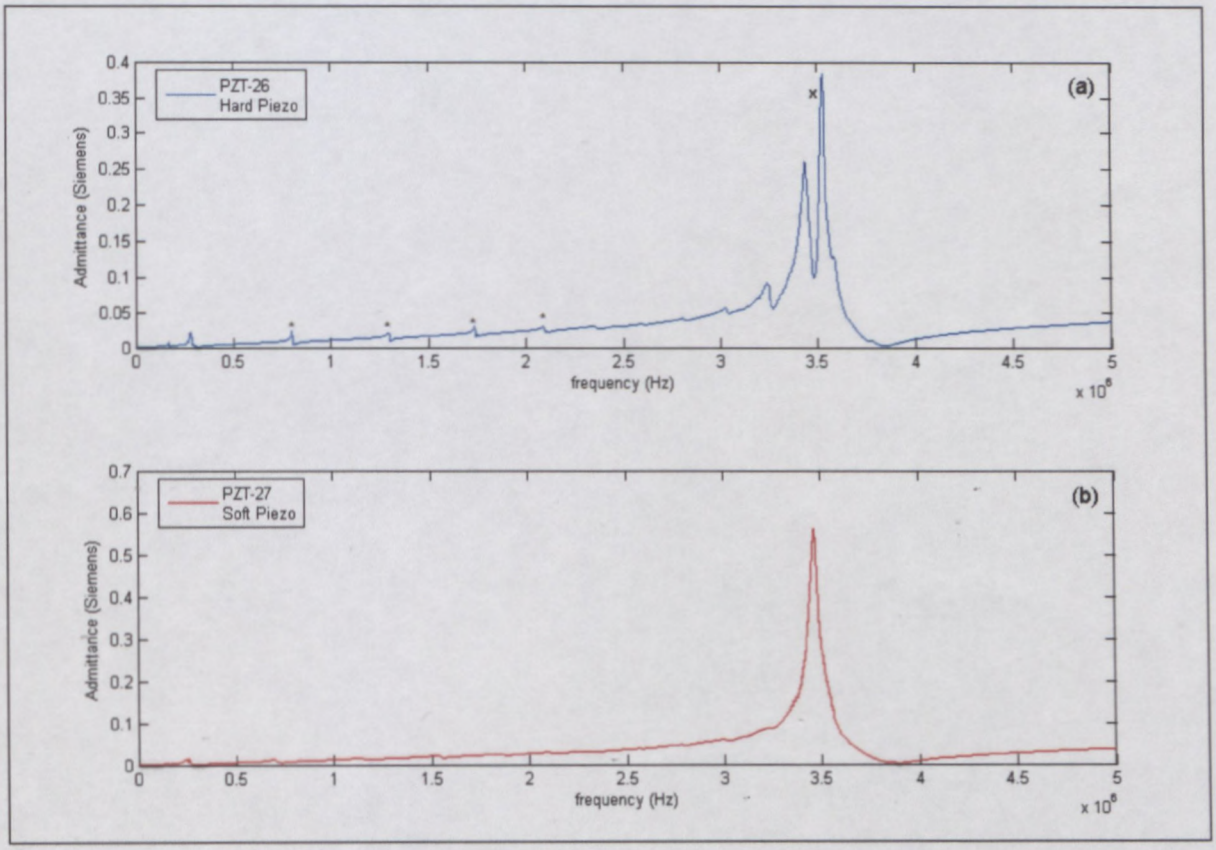

Figure 3-13: Admittance spectra for different type of PZT materials. Note the hard PZT cylinder (a) has high order overtones as indicated with '$*$', which interact with the fundamental thickness mode and causing the splitting resonance as indicated with an 'x'. The soft PZT cylinder (b), exhibits clear and undisturbed thickness resonance, with minimum disturbance from other modes

3.2 Liquid Coupled Modes

This section discusses the modes of vibration of distilled water in a PZT cylinder. The study characterises the behaviour of a PZT cylinder under empty and liquid filled conditions. The loading effect with liquid was observed. The experiment describes the wetting technique and the results of frequency pulling examined in detail in the second subsection.

3.2.1 Acoustic coupling (Wetting Phenomenon)

The existence of liquid modes within a PZT cylinder was discovered unexpectedly. The admittance spectrum determined for a water filled PZT cylinder had a strong resemblance to an empty cylinder. However, an unanticipated result appeared after a PZT cylinder was rinsed with soapy water (at least 15-20 minute periods were required for the excitation). The soapy water on the wall of the cylinder was left to dry and refilled with sample liquid. An acoustic series of resonant piezoelectric responses appeared as shown in Fig.3-14. This phenomenon was repeatable for several hours. This effect, however, vanished after the cylinder had been left to stand to dry overnight and returned to its "unwet" state [16]. There was better coupling between the piezoelectric transducer and the sample liquid as the soap acted as a coupling agent. The spectra that compare a liquid filled piezoelectric cylinder, before and after wetting, are shown in Fig.3-14 (a) and Fig.3-14 (d). The spectrum of the wetting phenomenon exhibits a unique set of acoustic modes, with sharp quality factors (Q_s) forming an extensive harmonic series.

3.2.2 Frequency Pulling

The phenomenon of frequency pulling occurs when two resonant systems approach each other in frequency, so that energy can be transferred from one to another. This is often demonstrated in two coupled electrically tuned circuits where the inductance from both circuits is mutually coupled[16]. The individual resonance frequency is pushed or pulled by an amount associated with the energy coupling of each resonance system. By differentiating equation $f = \frac{VN}{\lambda}$, the velocity of sound of a liquid filled PZT cylinder is

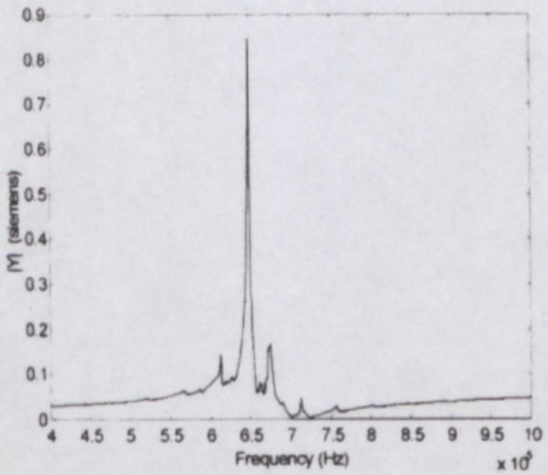

(a) Time = 5 minutes

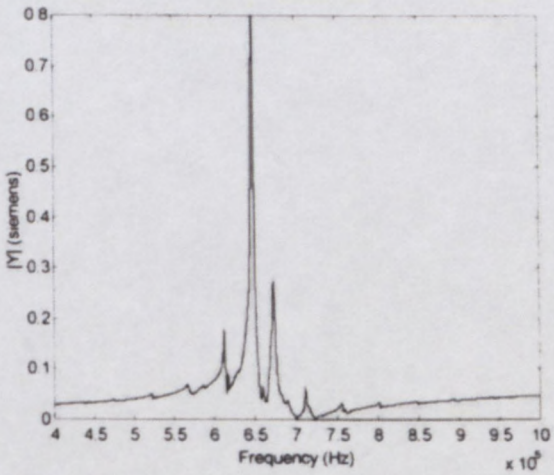

(b) Time = 10 minutes

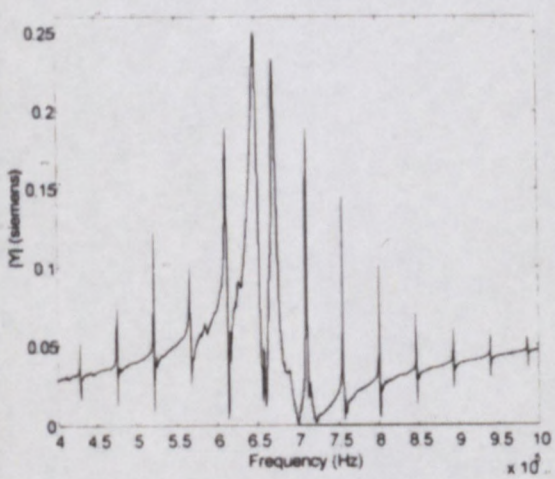

(c) Time = 15 minutes

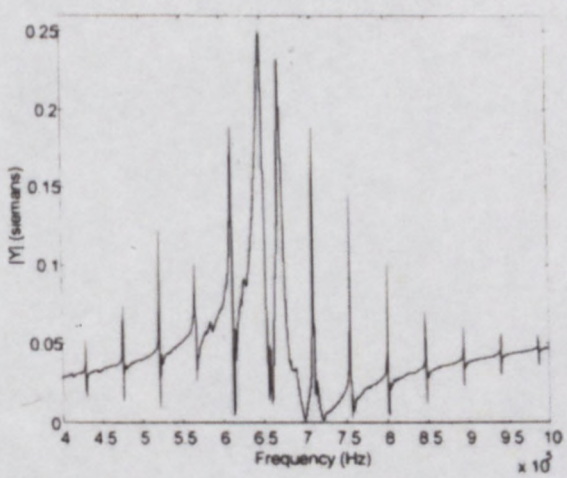

(d) Time = 20 minutes

Figure 3-14: A time sequence capturing the wetting phenomenon associated with a water filled PZT cylinder. The time interval between each spectrum is 5 minutes. Note, after wetting for 20 minutes, the fundamental PZT resonance is dumped and uncharacteristically sharp Qs associated with the liquid modes are harmonically spaced.[16]

calculated by:

$$\frac{df}{dN} = \frac{V}{\lambda} \tag{3.20}$$

$$V = \lambda \frac{df}{dN} \tag{3.21}$$

Since the velocity of sound, V and the wavelength, λ are constant, the changing resonance frequency with mode number should be expected to be linear. For a water filled PZT cylinder with inner diameter of 32cm, the $df/dN = 4.74 \times 10^4$Hz. Evidence of frequency pulling can be seen in Fig.3-15 (b), where the resonance frequency of liquid modes are precisely linear as a function of mode number. An exception was the bandwidth inclosed the PZT thickness resonance (mode number 8, 9, 11 and 12). These modes were the liquid resonance modes interfered with the thickness resonance of a PZT cylinder and resulting in frequency pulling between one another.

3.2.3 Temperature Effects and Drifting of Modes

The effect of temperature fluctuation on the frequency drifting was studied by Prenzlow[38]. A phase locked loop (PLL) technique was used to lock a liquid mode at resonance frequency and the temperature recorded as a function of frequency. As shown in Fig.??, although the temperature risen only less then 0.1 °C (30.0934 °C to 30.166 °C), the change of frequency fluctuation was captured (2387.9kHz to 2388.3kHz). The significance of thermal effects on resonance frequency drifting necessitated the design of an isothermal bath and rig for the velocimeter. This was to prevent the frequency changes from ambient temperature fluctuation which will be discussed in Chapter 6.

3.3 Conclusions

The behaviour of an empty PZT cylinder and its fundamental resonances were examined. The interfering of the cable mode was successfully removed from the piezoelectric spectrum. Soft and hard types of PZT materials were investigated. The soft material (PZT-27) was selected for study, showing clear and undisturbed resonances with quick deterioration of overtones. A liquid filled PZT cylinder with soap as coupling agent led to

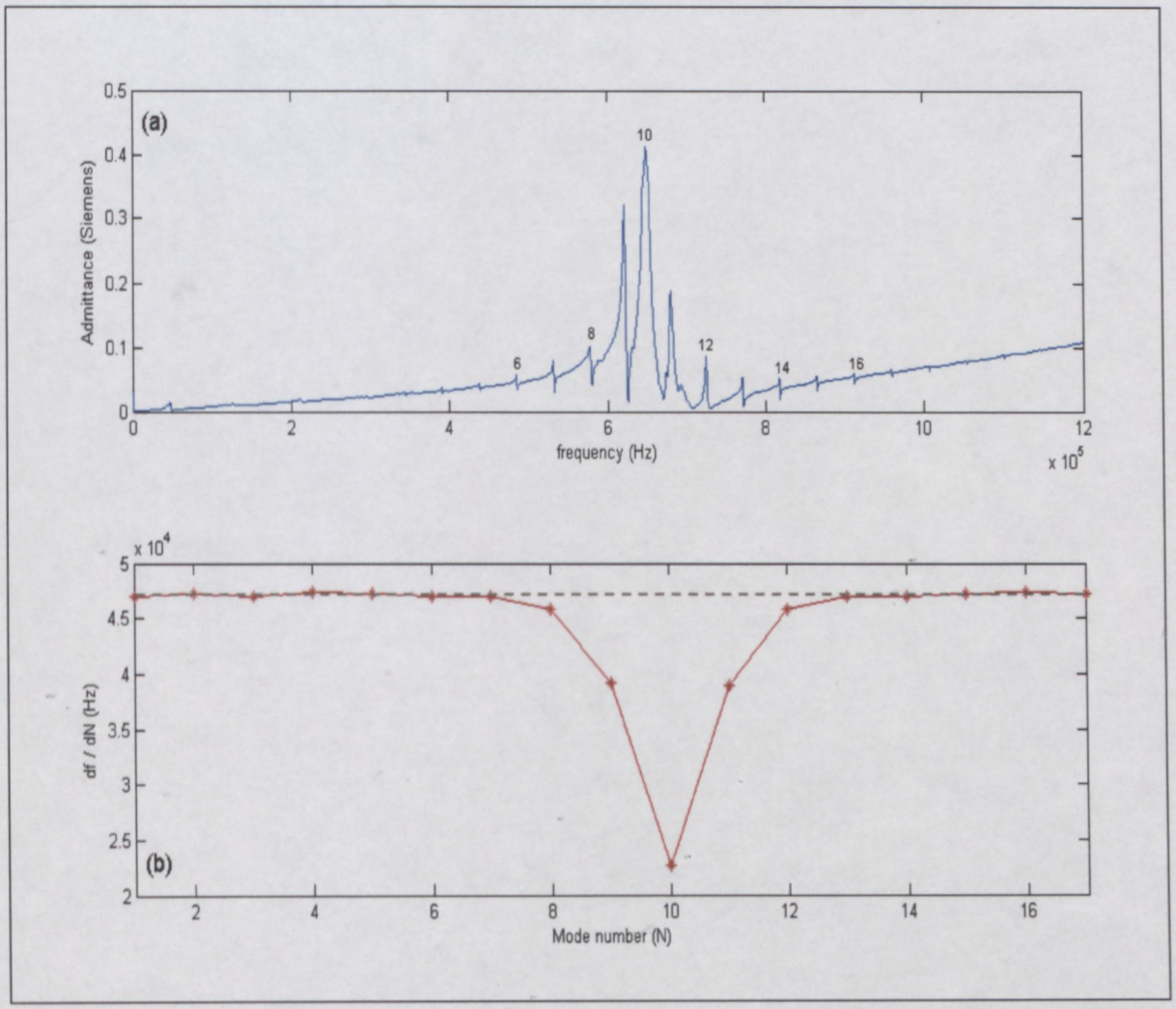

Figure 3-15: (a) PZT-4 spectrum of admittance against frequency for water at 30 °C and (b) the plot of change in frequency against mode numbers. The dotted line indicates the velocity of sound in water at 30 °C. The dip (mode number 10) in the vicinity of the thickness mode demonstrates the phenomenon of frequency pulling

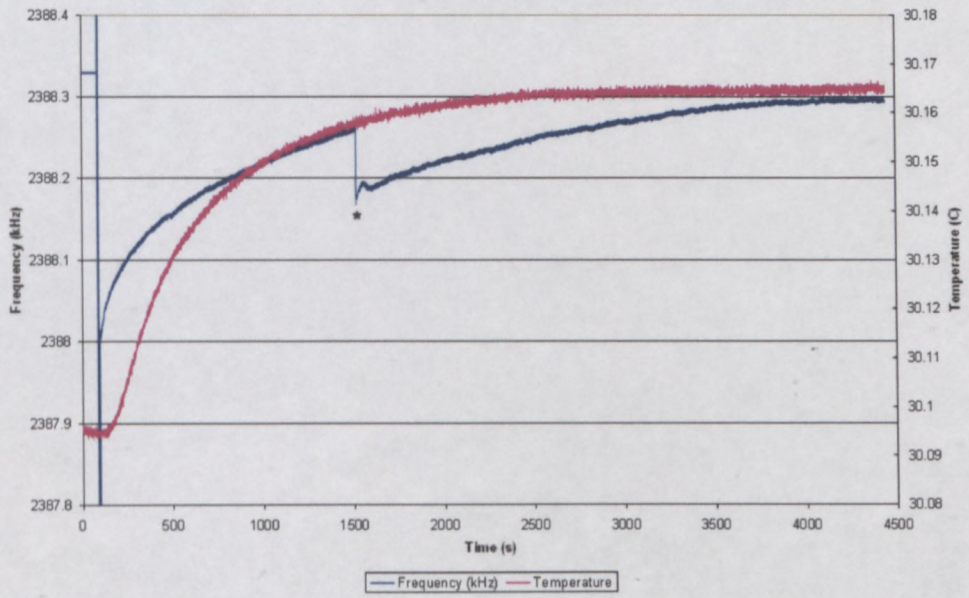

Figure 3-16: The graph of locked frequency and temperature inside the test rig (which will be discussed in a later chapter). At 1500s (marked with '*'), the phase reference signal of the PLL was changed to test whether it would have an influence on the temperature change[38]. Note the frequency increase from the thermal changes.

the discovery of a loosely coupled series of acoustic modes[16]. The resonance frequencies were precisely linear as a function of mode number except in the bandwidth inclosed the PZT thickness resonance caused by frequency pulling. In order to measure the velocity of sound, it was a requirement that liquid resonance be independent of frequency pulling. The thickness mode of a piezoelectric cylinder had to be divorced from the liquid modes. Unfortunately, Mason's electro-mechanical model, although employed to represent many PZT transducers, did not account for all aspects of liquid mode superposition and frequency pulling between the modes. This caused traditional theories to become increasingly complex in predicting equivalent circuit parameters. A new "electro-acoustic" model was proposed and is described in the next chapter.

Chapter 4

Electro-Acoustic Modelling Techniques

This chapter introduces the basic concepts and equations of electromechanical equivalent circuits and the general transmission line theory that, although well-known to those in the field, are necessary to understand subsequent analysis in later chapters. The piezoelectric transducer is important in ultrasonic and acoustic studies, since it converts electrical signals into mechanical waves, and vice versa[42]. The interaction of the physical processes between electrical and mechanical energy can be achieved by manipulating the piezoelectric equations of the states, or experimentally modelling the piezoelectric behaviour as equivalent electrical or mechanical circuits[22][30]. The most common electromechanical models used to represent a piezoelectric transducer are those of Mason[30], KLM[39] and Redwood[41]. Each model has its own advantages and disadvantages[45]. The most popular method for analysis and design of a piezoelectric transducer, however, is Mason's equivalent circuit and that model is adopted throughout this thesis. A new equivalent circuit was proposed to model the behaviour of an electro-acoustic system for the measurement of the liquid velocity behaviour. The liquid parameters further enabled derivation of Bulk modulus and density (this, however is not the subject of this thesis).

4.1 Mason's Electro-Mechanical Model

Analysis of a piezoelectric transducer operating at resonance is usually determined through an equivalent BVD electromechanical network (see Chapter 3). For understanding the operation over a wider frequency spectrum, or at frequency other than that of resonance, a more exact equivalent circuit model was necessary (see Fig.4-1(a)). Warren Mason's model achieves this by implementing two mechanical ports (which represents the mechanical motion of the transducer at each face) and one electrical port. The ideal electromechanical transformer of ratio N provides the coupling between electrical and mechanical variables. On the electrical port, all circuit variables are standard electrical elements. The voltage E is related to the current through Ohm's Law. On the mechanical or acoustical port, the force, F which is related to velocity ν via $F = \nu Z_o$, where Z_o is the characteristic acoustic impedance and $Z_o \propto \rho A v$. Represented are ρ which is the density, A is the surface area of the piezoelectric transducer, I is current, v is the velocity of the piezoelectric material and Y_b is the blocked electrical admittance. The fundamental equations of Mason's two-port electromechanical circuit are, therefore, defined [29][32]:

$$F = NE + Z_o\nu \tag{4.1}$$

$$I = Y_b - N\nu \tag{4.2}$$

By using equations 4.1 and 4.2 co-operatively with the wave equation and the piezoelectric equations of the state, one could further extend and derive electrical circuit parameters. The mathematical derivation for this has been shown in detail in the literature[22][30]. The circuit parameters for Mason's equivalent electromechanical circuit (shown in Fig.4-1(a)) are defined by the following equations[30]:

$$Z_T = jZ_o \tan(\frac{kt}{2}) \tag{4.3}$$

$$Z_S = j\frac{Z_o}{\sin(kt)} \tag{4.4}$$

where

$k = \frac{2\pi}{\lambda}$ or $\frac{\omega}{v}$; k is wave number, λ is the wavelength, ν is velocity of sound in the PZT cylinder and ω is the angular frequency;

Z_o =characteristic acoustic impedance and,

t =thickness of the transducer.

The electrical capacitance C_o and the electromechanical transformer ratio N are calculated by:

$$C_o = \frac{\varepsilon^s_{33} A}{t} \tag{4.5}$$

$$N = h_{33} C_o \tag{4.6}$$

where

C_o =electrical capacitance;

N =electromechanical transformer ratio;

ε^s_{33} =clamped permittivity;

A = surface area of the transducer;

t =thickness of the transducer and,

h_{33} =piezoelectric constant.

The negative capacitor, $-C_o$, presented in the circuit shown in the Fig.4-1(a) indicates the excitation of a piezoelectric cylinder when an applied electrical field is parallel to the wave propagation direction (thickness excitation). On the other hand, when the resonant mode is excited by a field which is transverse to the wave propagation direction, it is known as lateral excitation, in which case, the negative capacitor can be disregarded[10].

Furthermore, if the equivalent electromechanical circuit is free on one end and drives an acoustic load on the other end, the transmission line can be reduced to a lumped element network resulting in the simplified circuit depicted in Fig.4-1(b). The ideal transformer is coupled to the electrical terminals on the primary side and a mechanical arm on the secondary side of the transformer. The variable C_o stems from the electrodes

on the transducer plus the stray capacitance from the cables[50]. The series motional branch consists of three components: (1) a motional capacitance, C_m, representing the compliance of the oscillating body, (2) a motional inductance, M, which gives a measure of the mass and (3) R_m, corresponding to the mechanical energy losses due to the mechanical impedance.

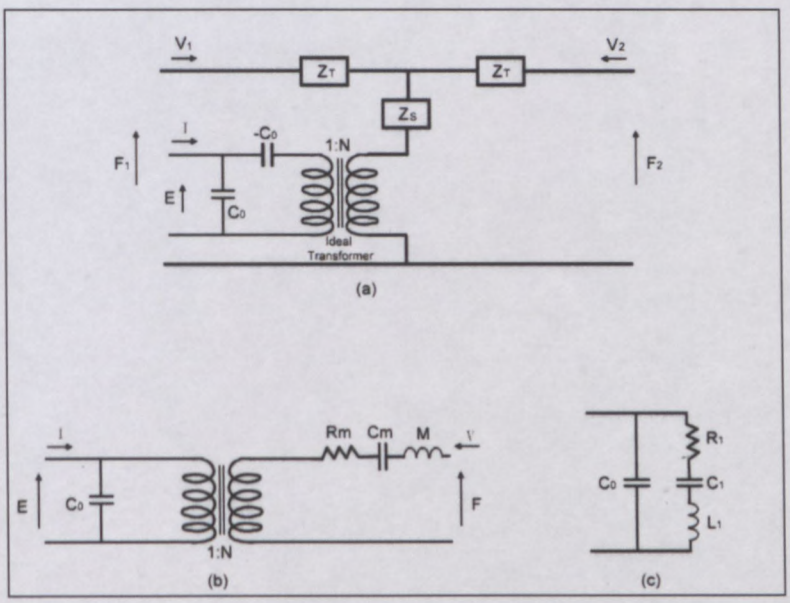

Figure 4-1: Shows the equivalent electromechanical circuit used to represent the behaviour of a PZT transducer. (a) Mason's transmission line model. (b) simplified model where oscillator is free on the one end and drives a load on the other; and (c) the Butterworth-Van Dyke (BVD) one-port equivalent electromechanical circuit, valid only in a vicinity of single piezoelectric resonance

The electromechanical relationship is frequently shown in terms of the lumped element circuit, also known as the Butterworth-Van Dyke (BVD) electrical equivalent circuit, shown in Fig.4-1(c). Butterworth and Van Dyke[18][11] derived an equivalent circuit for a quartz resonator, considering the electromechanical system to be represented by an electric network. The resonance of the circuit behaves like an electric series RLC oscillating circuit shunted by an electrical capacitor C_o. This model is, however, only valid at frequencies near the fundamental resonance frequency of the device.

4.2 Redwood and KLM Models

4.2.1 Redwood's Model

Redwood [41],[40] altered Mason's equivalent circuit by replacing the impedances Z_T and Z_S in Mason's circuit with a piece of coaxial cable or transmission line as shown in Fig.4-2. Redwood's model is mostly identical to Mason's model, save that negative capacitance, $-C_o$, which has been transferred to the acoustic side of the network. The negative value of the capacitance has no electrical equivalence and its magnitude is equal to that of the static capacitance C_o[40]. The transmission line at the acoustic port represents the mechanical properties of the transducer.

Redwood further distinguished the model by using a graphic form representation of the T-form of the distributed network as illustrated in Fig.4-3. The transformer which represents the electromechanical coupling is removed from the two boundaries[41].

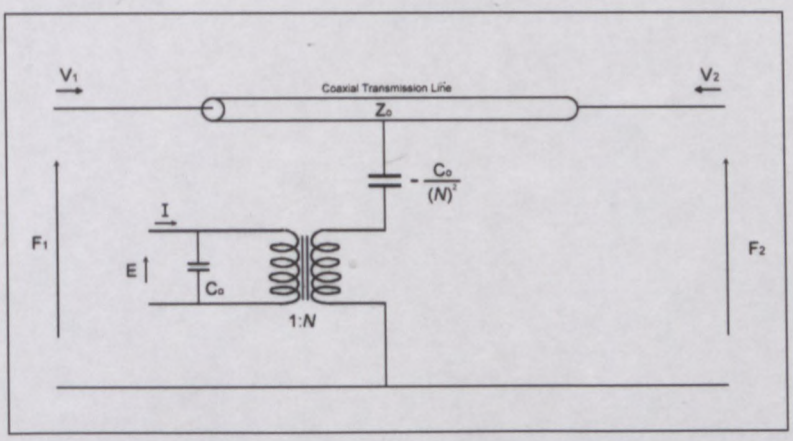

Figure 4-2: Redwood's model, redrawn from the Mason's equivalent electro-mechanical circuit

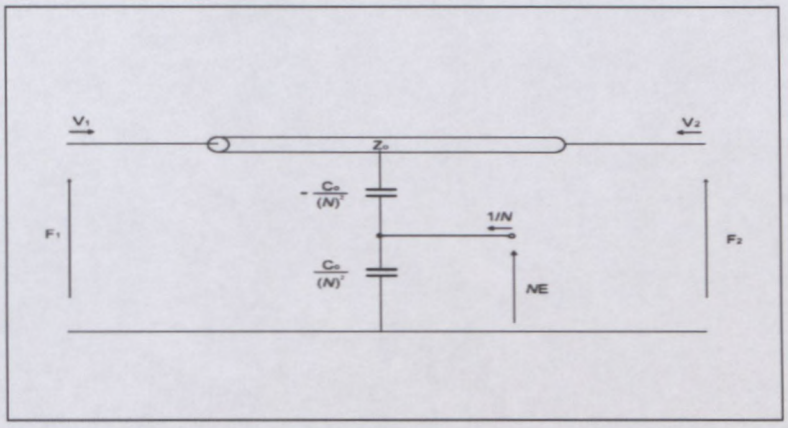

Figure 4-3: Redwood's transformed model which is shown in coaxial transmission line format to investigate the schematic explicitly with a physical length

4.2.2 KLM's Model

Although Mason's model is well-known and widely used for analysing both free and mass loaded resonators, and transient response [30][41], the negative capacitance at the electrical port is impractical. In an effort to remove the negative capacitance element between the electrical port and the node of the acoustic transmission line, KLM, the acronym for Krimholtz, Leedom and Matthae[39][45] published an alternative equivalent model for solving such a problem.

KLM's model uses a transmission line to represent the mechanical port. A motivation for the development of KLM's model is the fact that Mason's and Redwood's model showed the acoustic force acting on the transducer surface as developed not only across the transmission line, but partially across the secondary of the piezoelectric transformer. The acoustic forces in KLM's model were directly across the transmission line terminals. This was physically more reasonable and depicted a clear distinction between the lumped element electrical behaviour and the acoustic wave behaviour of the transducer[8][39].

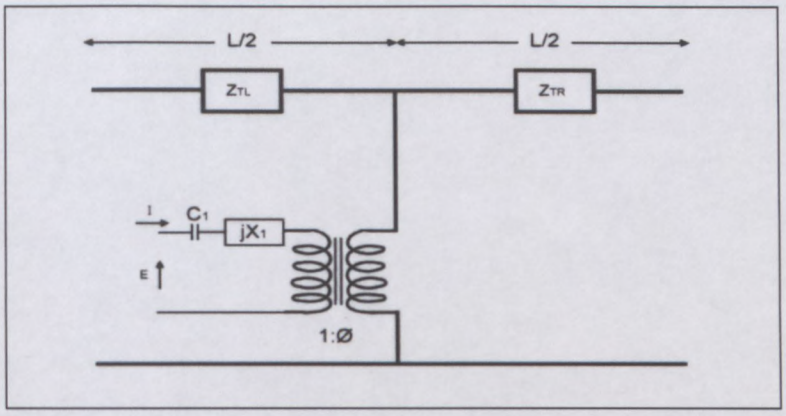

Figure 4-4: KLM equivalent model of a thickness mode piezoelectric transducer. L represents the length of a PZT cylinder, E and I are the voltage and current. Z_{TL} and Z_{TR} represent the load impedance on left and right side of acoustic ports

The length L is equal to the transducer dimension in the direction of the acoustic wave propagated. Z_o represents the characteristic acoustic impedance of the transducer. The acoustic energy which is radiated to the acoustic ports depends mainly on the load impedance of the media on left and right side of the transducer. The electrical port is tapped to the centre of the transmission line through a transformer with a turns ratio of ϕ. The KLM model's parameters and material constants can be calculated using the following equations:

$$Z_{TR} = Zo\left[\frac{Z_R\cos(\frac{kt}{2}) + jZ_o\sin(\frac{kt}{2})}{Z_o\cos(\frac{kt}{2}) + jZ_R\sin(\frac{kt}{2})}\right] \tag{4.7}$$

$$Z_{TR} = Zo\left[\frac{Z_L\cos(\frac{kt}{2}) + jZ_o\sin(\frac{kt}{2})}{Z_o\cos(\frac{kt}{2}) + jZ_L\sin(\frac{kt}{2})}\right] \tag{4.8}$$

$$X_1 = jZ_oM^2\sin(\frac{kt}{2}) \tag{4.9}$$

$$\phi = \frac{1}{2M}\csc(\frac{kt}{2}) \tag{4.10}$$

where

Z_o =characteristic acoustic impedance;

Z_L and Z_R represent the load impedance on left and right side of the acoustic ports;

k =wave number;

t =thickness of the transducer;

ϕ =the transformer ratio of the KLM's model and,

$M = \frac{h_{33}}{\omega Z_o}$.

4.3 Electro-Acoustic Modelling

An equivalent circuit was required to represent the acoustic (or liquid) modes of a liquid filled PZT cylinder. Neither Mason, KLM nor Redwood's models (although employed to represent multiple PZT transducers) took that into account. The "electro-acoustic" model proposed provids an extension to Mason's original electromechanical circuit. The hypothesis behind this was to couple a liquid resonance mode to an equivalent piezoelectric circuit model by implementing a "mechanical-acoustic" transformer. The standing wave behaviour of a liquid enclosed by a piezoelectric cylinder could be represented by a liquid transmission line (see Fig.4-5). The liquid transmission line was terminated by impedance Z_r and had a series reactance $X_{(LIQ)}$. The $R_{(LIQ)}$ corresponded to viscus effects present in the liquid. M_a represented the "mechanical-acoustic" transformer ratio which coupled the mechanical and acoustic system. The coupling ratio of the transformer was scaled to the inner area of the PZT cylinder.

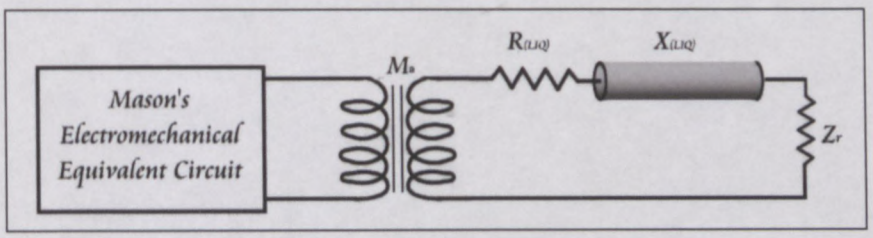

Figure 4-5: The proposed liquid acoustic network utilising Mason's electromechanical equivalent circuit model

In an attempt to quantify the behaviour of this model, it was simplified to its lumped element equivalence as seen in Fig.4-6. Each individual liquid mode was represented

by a series LCR circuit, which is treated as an isolated acoustic response coupled to the "mechanical-acoustic" transformer. It was proposed that the superposition of the liquid modes with the piezoelectric equivalent circuit would provide the total frequency characteristic of the "electro-acoustic" system.

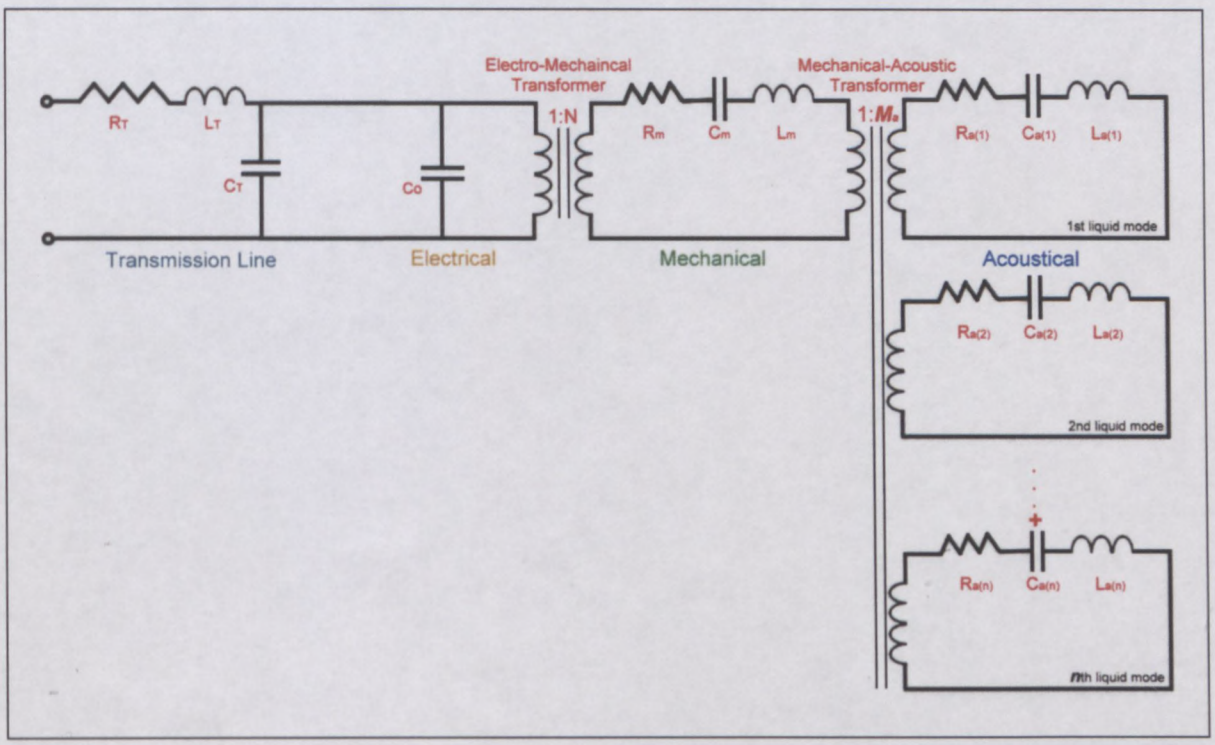

Figure 4-6: A representation of the electro-acoustic model. Mason's electromechanical equivalent circuit is coupled to individual liquid resonances through a mechanical-acoustic transformer. Each liquid mode is defined by a series of LCR circuits which are coupled to the motional inductance of the PZT

4.4 Simulations

To verify the "electro-acoustic" model described in the Section 4.3, the liquid mode parameters L_a, C_a and R_a were calculated. A list of liquid modes calculated is given in table 4.1. A simulation of liquid modes coupled with an electromechanical equivalent model was achieved by using Matlab and comparing them with the experimental observation.

Once the liquid mode parameters were extracted from the spectrum, the values were

Table 4.1: A table of calculated L, C and R parameters for 13 equivalent liquid modes. The values are calculated by equations 3.10-3.14. The circuit simulated is based on the PZT-27 cylinder with dimensions ID = 5.2, OD = 6.35 and L = 6.35 (mm). Note the Mode number 5 is the fundamental thickness mode of the PZT cylinder

Mode No.(n)	f_r (MHz)	$L_{\mathbf{a}}$ (μH)	$C_{\mathbf{a}}$ (pF)	$R_{\mathbf{a}}$ (Ω)
1	2.38	137	32.8	0.45
2	2.66	126	28.3	0.22
3	2.95	43.8	66.5	0.31
4	3.23	33.2	73.3	0.11
5*	3.44	1.59	1350	0.09
6	3.59	2.83	696	0.1
7	3.84	10.3	168	0.16
8	4.12	26.2	56.9	0.21
9	4.41	115	11.3	0.33
10	4.69	224	5.16	0.57
11	4.98	88.4	11.6	0.9
12	5.26	96.7	9.46	1.51
13	5.55	262	3.14	2.55

substituted into the following set of equations to calculate the total input admittance of a piezoelectric cylinder. The impedance looking into the acoustic port is calculated as:

$$Z_{ac(n)} = R_{a(n)} + j\omega L_{a(n)} - \frac{j}{\omega C_{a(n)}} \tag{4.11}$$

The admittance looking into the mechanical-acoustic transformer is described as:

$$Y_{ac\_mac} = \frac{(M_a)^2}{Z_{ac(n)}} \tag{4.12}$$

$$Z_{ac\_mac} = \frac{1}{Y_{ac\_mac}}$$

The "mechanical-acoustic" transformer ratio is calculated by inner area of PZT cylinder. This is the conversion of pressure to force and volume flow rate to velocity. This occurs for the outside of the liquid at the inner diameter of the cylinder. Thus the equations are:

$$P = \frac{F}{A} \tag{4.13}$$

and

$$Q = vA \tag{4.14}$$

Thus P and F are equivalent to voltages and v and Q are related to current. Then the transformer ratio (M_a) for such a conversion is:

$$M_a = A \tag{4.15}$$

The mechanical port impedance is calculated by:

$$Z_{mec} = R_m + j\omega L_m - \frac{j}{\omega C_m} \tag{4.16}$$

$$Z_{mec\_tot} = Z_{mec} + Z_{ac\_mac} \tag{4.17}$$

The admittance looking into the electromechanical transformer is described as:

$$Z_{mec\_elec} = (\frac{Z_{mec\_tot}}{N^2}) \tag{4.18}$$

$$Y_{mec\_elec} = \frac{1}{Z_{mec\_elec}}$$

The electromechanical transformer ratio is calculated by:

$$N = h_{33} \times C_o \tag{4.19}$$

The electrical port impedance is determined by:

$$Z_{Co} = -\frac{j}{\omega C_o} \tag{4.20}$$

$$Y_{Co} = \frac{1}{Z_{Co}}$$

The total impedance of an electro-acoustic circuit model is, therefore:

$$Y_{total} = Y_{mec\_elec} + Y_{Co} \tag{4.21}$$

The input of absolute admittance is examined over the frequency spectrum up to

7MHz. Several simulations are computed with different M_a values (see graphs shown in Fig.4-7). Although the simulation has a resemblance to the measured spectrum, the result is unsatisfactory.

4.5 Discussion and Results

A new equivalent circuit is proposed to model the behaviour of an "electro-acoustic" system for the measurement of liquid velocity behaviour. Mason's model was adapted by coupling a "mechanical-acoustic" transformer to the mechanical port of the piezoelectric. The transformer accounts for both frequency pulling and the wetting phenomenon. This analysis is novel and contributes toward the understanding of the resonance of a liquid filled PZT cylinder. The measured and simulated absolute admittance spectra of a PZT-27 cylinder is shown in Fig.4-7. From the spectra, the simulation result of an "electro-acoustic" model and measured values, although unsatisfactory, yet seemed to agree with each other. Therefore, the "electro-acoustic" model described in the Section 4.3 appears to explain the behaviours of the resonance characteristics of the PZT cylinder.

The calculation of each liquid mode parameter using traditional methods was however, time-consuming. A more accurate coefficient of M_a was yet to be determined (hypothesis equation (4.15) was used for the simulation) to be able to couple the mechanical and acoustic systems. As a solution, a stochastic search optimiser was utilised as a means of predicting multiple resonance modes that interact with one another. By utilising the AMBA (Adaptive Mutation Breeder Algorithm) with a variation of the Mason's transmission line model, one can easily resolve equivalent circuit parameters for L_a, C_a, R_a and further estimate the value of the 'mechanical-acoustic' transformer ratio (M_a).

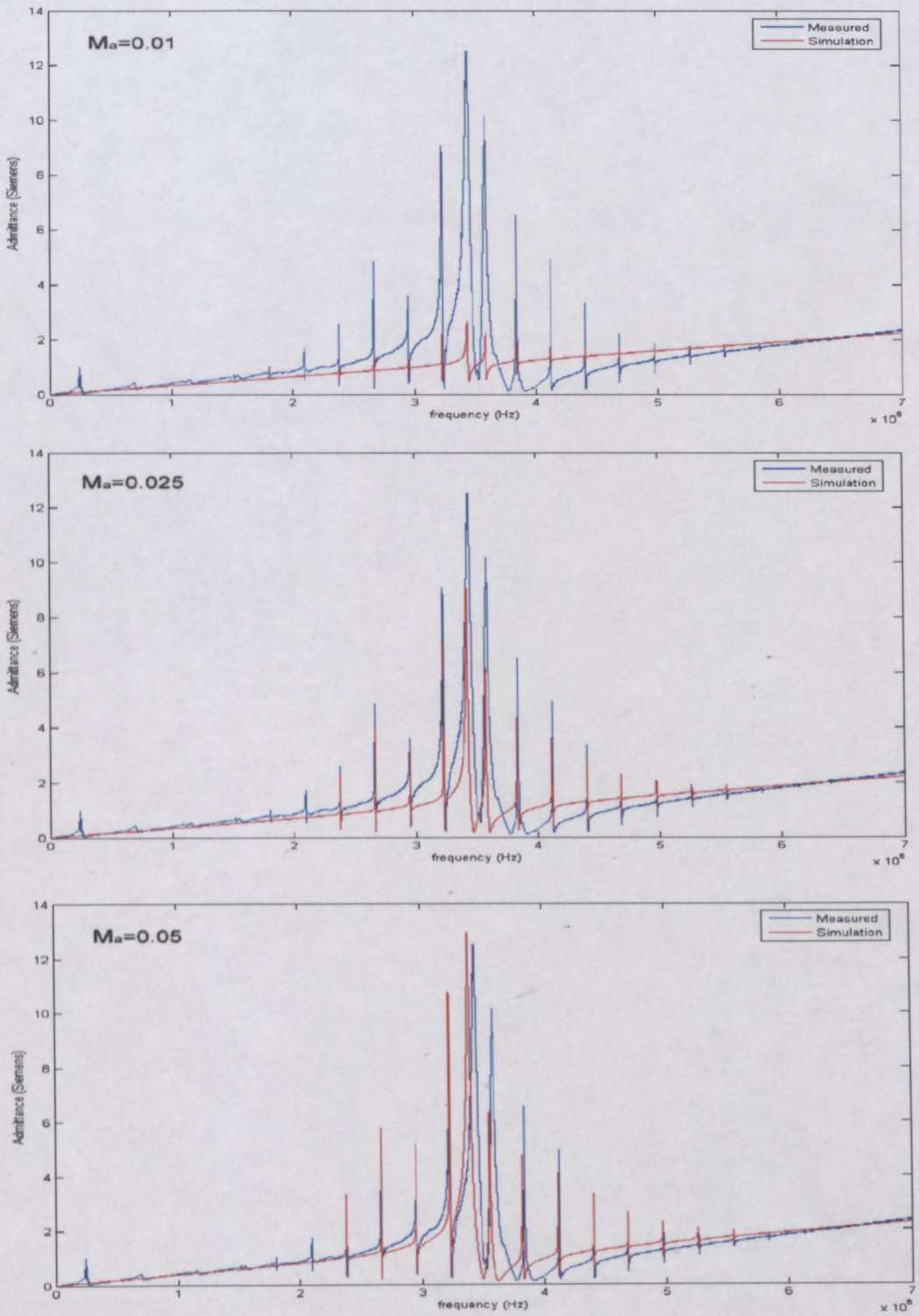

Figure 4-7: Simulation of an electro-acoustic model with absolute admittance versus frequency. Each of the graphs is simulated with a different M_a coefficient. The value of M_a was tweaked until a preferred spectrum is achieved

Chapter 5

Adaptive Mutating Breeder Algorithm (AMBA)

Many acoustic systems require an equivalent electro-mechanical model to describe their behaviour. Thus, a variety of models are described in the literature and outlined in previous chapters. Although such models describe complex acoustic systems, it is often difficult to determine circuit parameters for such systems using traditional theory. Aspects of mode superposition, and frequency pulling between modes cause traditional theories to become increasingly complex for prediction of equivalent circuit parameters. As a solution, a stochastic search optimiser was proposed as a means of predicting multiple resonance modes interacting with one another. A liquid filled piezoelectric cylinder was used as an acoustic system to represent coupled piezoelectric and liquid vibrational modes. By utilising AMBA with a variation of the Mason's transmission line model, one could predict the spectral response measured by an impedance analyser.

5.1 Fundamentals of Genetic Algorithms

Stochastic search and optimisation techniques are used in many areas, including aerospace, medicine, transportation, and finance. Stochastic algorithms cover a broad range of today's most widely used algorithms, including: simulated annealing, genetic algorithms,

local search methods, gradient-based methods and hill-climbing[47]. Stochastic search and optimisation is a procedure of finding and comparing feasible solutions until an ultimate solution is found. Most traditional approaches to stochastic optimisation involve local optimisers. The advantage of local optimisers are time efficiency, and often simplicity of implementation. A disadvantage is that they do not provide a mechanism for the search to escape from a local optimum (see Fig.5-1), thereby not producing a global optimal solution. Moreover they cannot detect whether a given problem has no feasible solution.

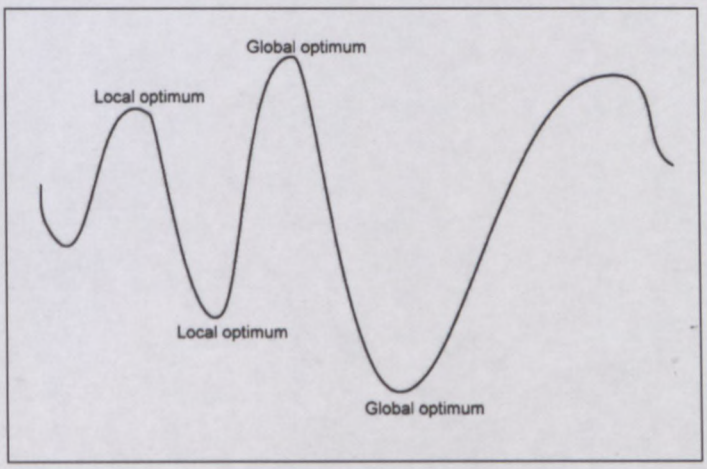

Figure 5-1: Illustration of global optimum and local optimum

Genetic Algorithms (GAs) are known to be a particularly good approach for multimodal optimisation[34], whose search methods model the natural phenomena of genetic inheritance and Darwin's "survival of the fittest"[7]. What makes GAs so beneficial when compared to other approaches is the most significant advantages lie in the gain of their flexibility and adaptability to a task at hand, as well as robust performance and "global search" characteristics[7]. However, the solution quality is a trade-off with the computing time.

Although many different methods are proposed by an AMBA, these variants are inspired by the spirit which underlies Holland's original genetic algorithms. GAs were originally proposed by John Holland in 1975[26]. They play an important role in pattern

recognition, planning and statistics by using randomised decisions while searching for solutions to a given problem. The GA works by performing a stochastic global search through the solution space by sweeping information between potential solutions. The solutions are encoded in bitstrings, real value variables, or in a matrix for easy, random generation. The trial solutions form a population and are uniformly randomly generated over the search space. During each generation, the solutions are evaluated and the better results are retained. A small additional amount of "randomness component" (mutation) is added to the trial solutions to prevent premature convergence[26].

5.2 Adaptive Mutation Breeder Algorithm

AMBA is an advanced GA which works under a similar evolution process. There are several features which distinguish GAs from AMBA:

- The representation uses–real-valued vectors;
- the method of selection–rank selection;
- the use of recombination–line or volume crossover and,
- a unique adaptive mutation is applied.

The uniqueness of AMBA is that it is equipped with a new technique for dynamically tracking the optimal mutation rate[24]. This method controls the convergence rate, which tracks optimum values without the need of a user's control or external intervention. It results in significant improvement in the performance of AMBA as an optimiser.

5.2.1 Advantages and Limitations Over Other Search Techniques

The principle of AMBA is simple. Variations on the basic theme can be used in a variety of scientific and engineering problems and models. The comparison of AMBA over other

search optimisers are summarised in the following[7][24][34][51]:

- AMBA is robust and almost universally applicable (optimisation, machine learning, economics and automatic programming); unfortunately, results are generally unpredictable;
- AMBA benefits from an effective use of parallelism, in which several possibilities are efficiently explored simultaneously, rather than one solution being evaluated at a time;
- the user can interpret the solution in the form of a bitstring, real-vector, integers or indices/pointers. The real-vector is used in this simulation because the large amount of matrices (although bitstring generated better mutation offsprings, but resulted in excessive time in encoding/decoding);
- any recombination operator can be adopted to generate new trial solutions from the survivors of the previous generation. The results will be at worst equal to classical approaches;
- AMBA is simple to describe and programme; using fewer than 50 lines of Matlab code;
- due to the randomness included, there are no guarantees of successful optimisation; several attempts are recommended and,
- AMBA requires considerable individual evaluation to obtain a solution and hence may be slow.

The aim of AMBA is to seek for the best solution to a problem by randomly generating a collected population of potential solutions. In order to achieve convergence, the AMBA requires a large population, yet a low mutation rate[43]. The population size is a critical parameter, too small and the AMBA converges to sub-optimal solutions, too large and the AMBA devours unnecessary computation resources[43]. Initially, a total population (for example 100) of trial solutions were randomly generated and inserted to evaluate

the function. Of the results, the top 15% fittest solutions (elastic seeds) were ranked and selected, those whose values most satisfied the requirements for optimisation, and the rest discarded from the solution pool. Next, the genetic operators such as recombination and adaptive mutation were applied to the individual to produce offspring. The offspring created by the genetic operators needed to be merged to form the next generation. In each successive generation the population was restored to 100. Gradually the fitness of the population rose and eventually the performance of the best solution met requirements. The flow diagram of AMBA is illustrated in Fig.5-2.

5.2.2 Recombination

Recombination is the process of using two individual solutions which are highly fit (satisfactory solutions), but would still create a superior individual with the best characteristics from each parent. Depending on the representation of the variables (bitstrings, real value number or matrix) different methods need to be applied. In the case of real value variable representations, recombination must be adopted with either uniform, volume, line or extended line crossover.

As shown in Fig.5-3, the volume crossover is more aggressive and exploratory in comparison to the line crossover as illustrated in Fig.5-4. The advantage of line crossover is it has a good approximation to uniform sampling of the convex hull of a set of points[24].

The offspring V_{ar} are produced by the following equation:

$$V_{ar_i} = V_{ar_i^{P1}}\alpha_i + V_{ar_i^{P2}}(1-\alpha_i) \tag{5.1}$$

where

$i \in \mathbb{Z}$;

$V_{ar_i^{P1}}$ and $V_{ar_i^{P2}}$ are random valuables (parents) selected from the genetic pool and,

α = a uniformly random scaling factor. In the case of line recombination, α is set to be $0 < \alpha < 1$ (Line recombination is similar to volume crossover, except that *only one* value of α is used for all variables).

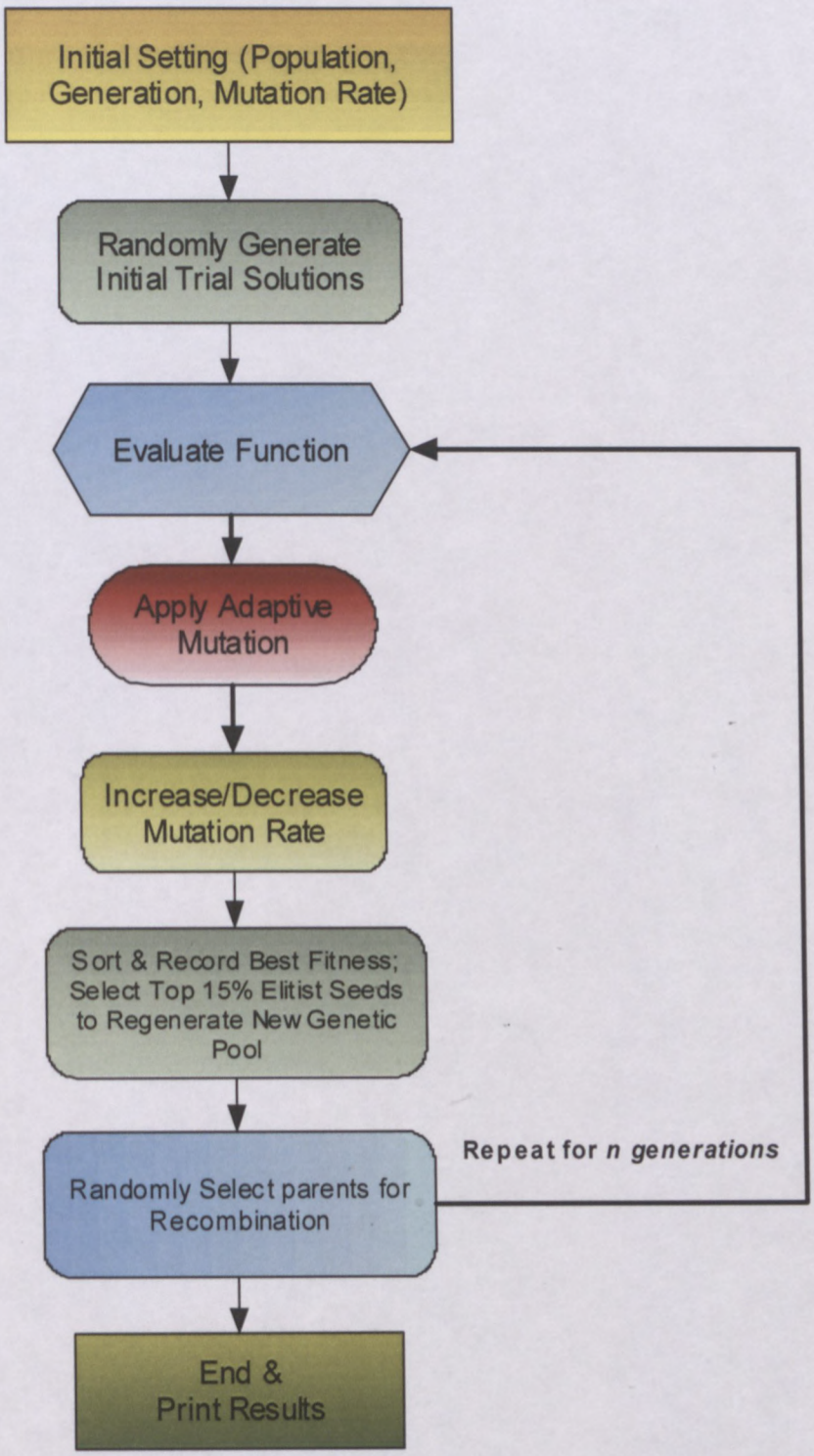

Figure 5-2: A flow chart diagram showing the execution routines for AMBA

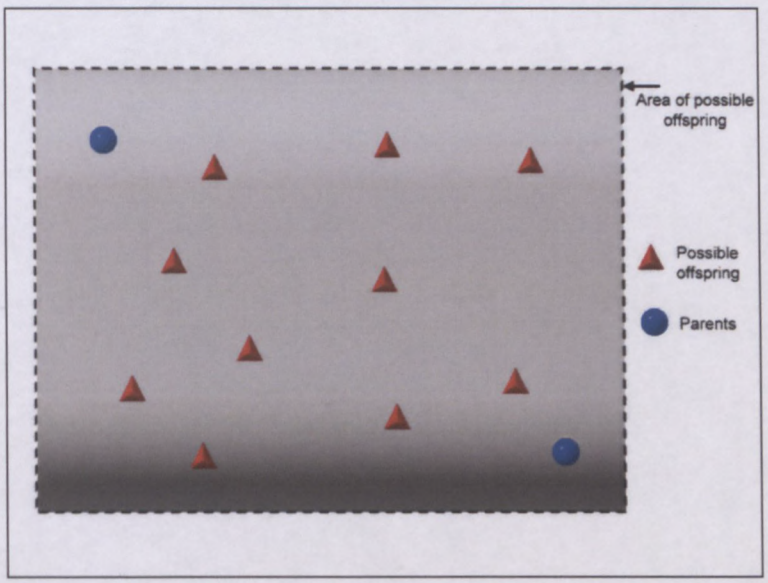

Figure 5-3: Volume recombination is capable of reproducing offspring at any point within a hyperbox defined by the parents. This method is more aggressive and exploratory than line recombination

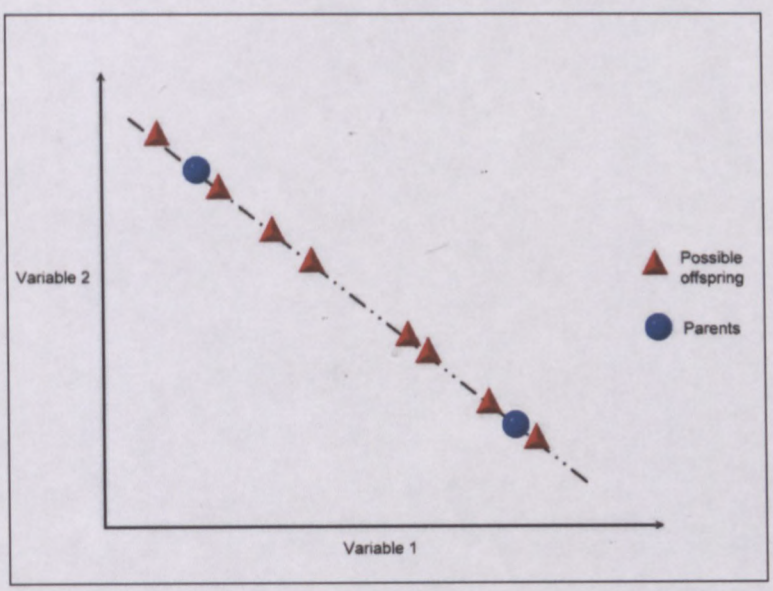

Figure 5-4: Possible offspring using line recombination can be generated at any point along the line which is defined by the parents

5.2.3 Adaptive Mutation Rate

Mutation was achieved by introducing small random changes in the representation of prior trial solutions to ensure that the entire space was accessible and converged to the global optimum, rather than to a local optimum (which occurred in some cases and dominated the population, which is undesirable). In AMBA, the rate at which mutation was applied was an implementation decision. If the rate is too low, there was a likely chance the offspring would be identical to their parents. On the other hand, if the mutation was set too high, the valuable information in the individual might be destroyed. Greene[24] proposed that a vector of small random numbers (R) be added to each trial (child) solution created by recombination. This is achieved by dividing the entire population into two groups: X (higher mutation rate) and Y (lower mutation rate). To X was applied double the mutation rate ($2 \times R$), and to Y, half the normal rate ($R/2$). The fitness of the solutions and adjustment of the R were continuously tracked to see which strategy won. If X generated a trial solution which on average was fitter than those from Y, then the amount of mutation rate was increased by 10%. If the result turned out Y was winning, R was reduced by a similar amount. By using such a method the mutation rate approached the optimum at all times.

5.2.4 Error Calculation

A standard deviation was calculated to determine a measure of the amount of variation or deviation that might be expected between the actual indicator value and the forecasted value[35]. It was used in an AMBA as a means to track and minimise the error between the measured and simulation data. The standard deviation (σ) is measured by:

$$\sigma = \sqrt{\frac{\sum_{i=1}^{n} (X_i - Y_i)^2}{n-1}} \tag{5.2}$$

where

n =number of sample points;

X_i =individual data point (experimental data) and,

Y_i =individual data point (AMBA simulation data).

5.3 Computing and Predicting Circuit Parameters using AMBA

AMBA code was written in Matlab to predict the parameters of a radial shear mode admittance spectrum. The value of R_m, L_m and C_m were initially given randomly for the LCR equivalent circuit. The value of these parameters were then used and multiplied by the size of the population (defined by the user) to form a new genetic pool. The first generation of trial vector solutions were inserted into the function which calculated the total admittance of the resonance modes. The simulated absolute admittance was compared with the measured admittance data. The top 15% of the population was selected, with values resemblance between the measured result. The selected solutions are used to form a second generation of genetic pool by means of recombination and mutation. The same procedure was repeated until the condition was satisfied, or when a defined number of generations was reached.

Figure 5-5 shows the measured spectra of conductance over frequency of the shear modes (indicated in blue) compared with the AMBA simulation. The results of the simulation after 10, 50 and 100 generations is shown respectively. The percentage error over a number of generations also presented. Note the simulation result is dramatically improved between 30-35 generations and reaches the optimal after 60 generations.

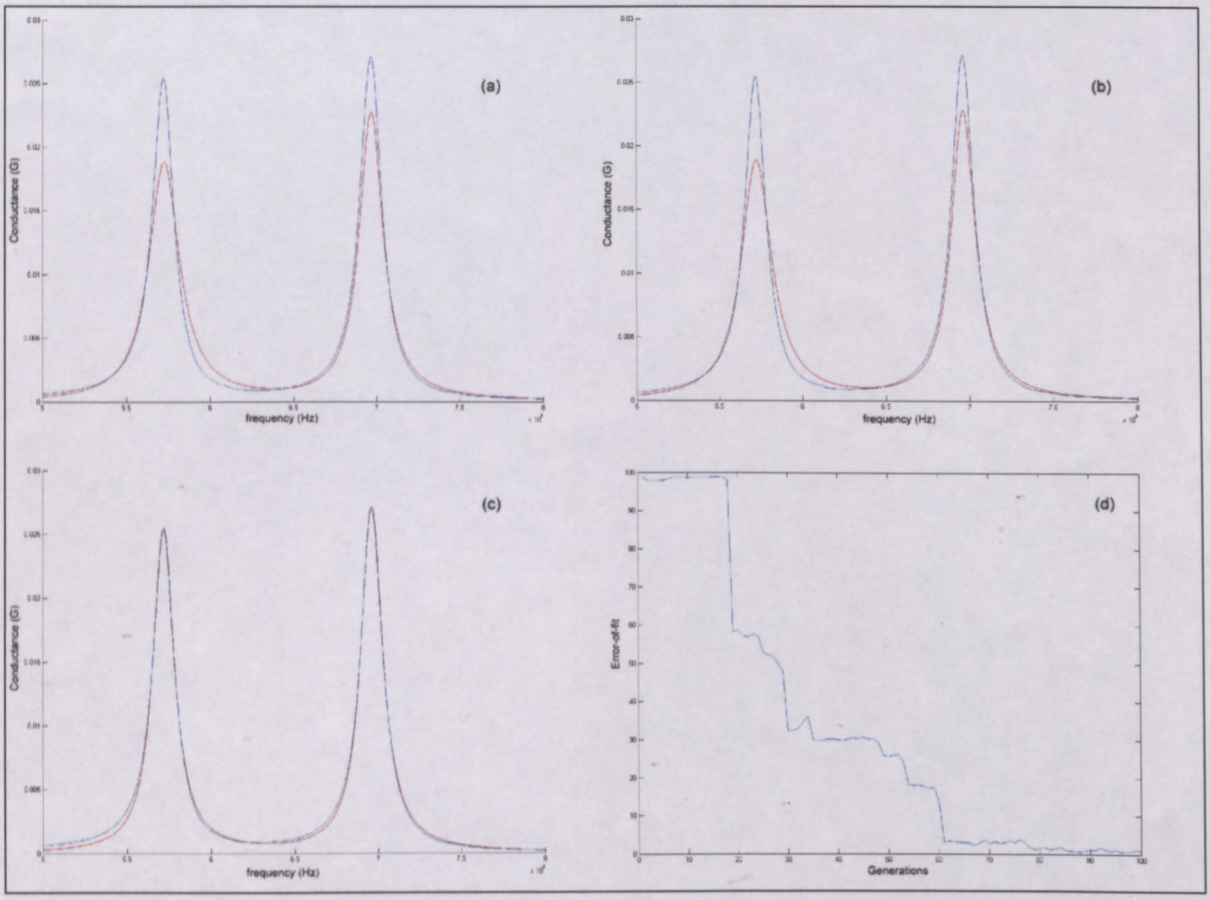

Figure 5-5: Performance of AMBA using random numbers to simulate radial shear resonant modes. (a) shows the simulation after 10 generations interval, blue spectrum represents the measured data and red spectrum is the AMBA simulation (b) 50 generations interval and (c) 100 generation interval; the measured and simulated values agree to each other well and (d) error-of-fit as against the number of generations

5.4 Modelling an Electro-Acoustic Equivalent Circuit Using AMBA

A liquid filled piezoelectric cylinder was used as an acoustic system to represent coupled piezoelectric and liquid resonance modes. An "electro-acoustic" model was chosen which as a variation of the Mason's transmission line model and coupled to multiple acoustical circuits (described in Chapter 4). Based on the consideration of complexities from extracting the equivalent circuit parameters, the AMBA code used in the previous section was modified in order to evaluate the "electro-acoustic" model more efficiently (see Appendix E).

AMBA was used as a means of predicting component values for an equivalent "electro-acoustic" model as described above. These values represent the behaviour and properties of a liquid under tests. The admittance spectrum from a liquid filled PZT cylinder was used as an input reference for AMBA to determine the equivalent circuit parameters. AMBA was used specifically to optimise and predict a value for the mutual "mechanical-acoustic" coupling coefficient M_a (see Fig.4-6) together with associated liquid resonance modes. Although the coefficient of M_a can be approximated by calculating the inner surface area of a PZT cylinder, it was important to use AMBA to optimise this value. Several factors including surface finish, solder joints, accurate diameter of the cylinders and different types of liquids can affect this value.

A graphic user interface (GUI) using Matlab was designed as shown in Fig.5-6 , which allowed the user to easily modify the AMBA parameters. The user was able to tweak the genetic parameters such as number of generations, size of genetic pool and mutation rate, which helped obtain an optimum result. A simulation result was compared to the measured data in the main window. The result of the acoustic model simulation is shown to fit almost identically over the measured spectra, as shown in Fig.5-7 and Fig.5-8.

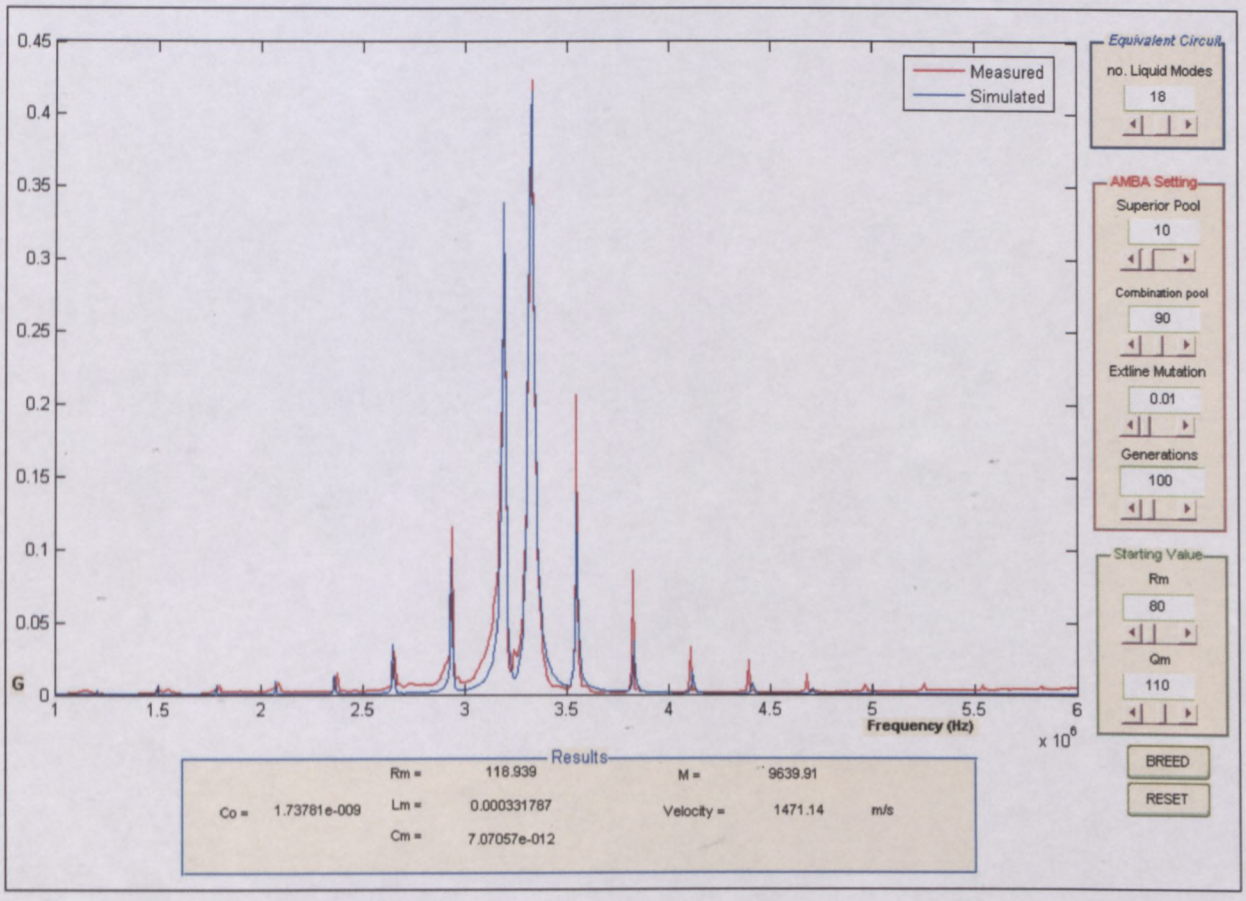

Figure 5-6: The Matlab GUI for AMBA which allows the user to initialise and configure the genetic operands. The results of measured and simulation of the distilled water spectrum (at 30 °C) is displayed in the main window. The piezoelectric circuit parameters and the velocity of sound are also calculated at the bottom

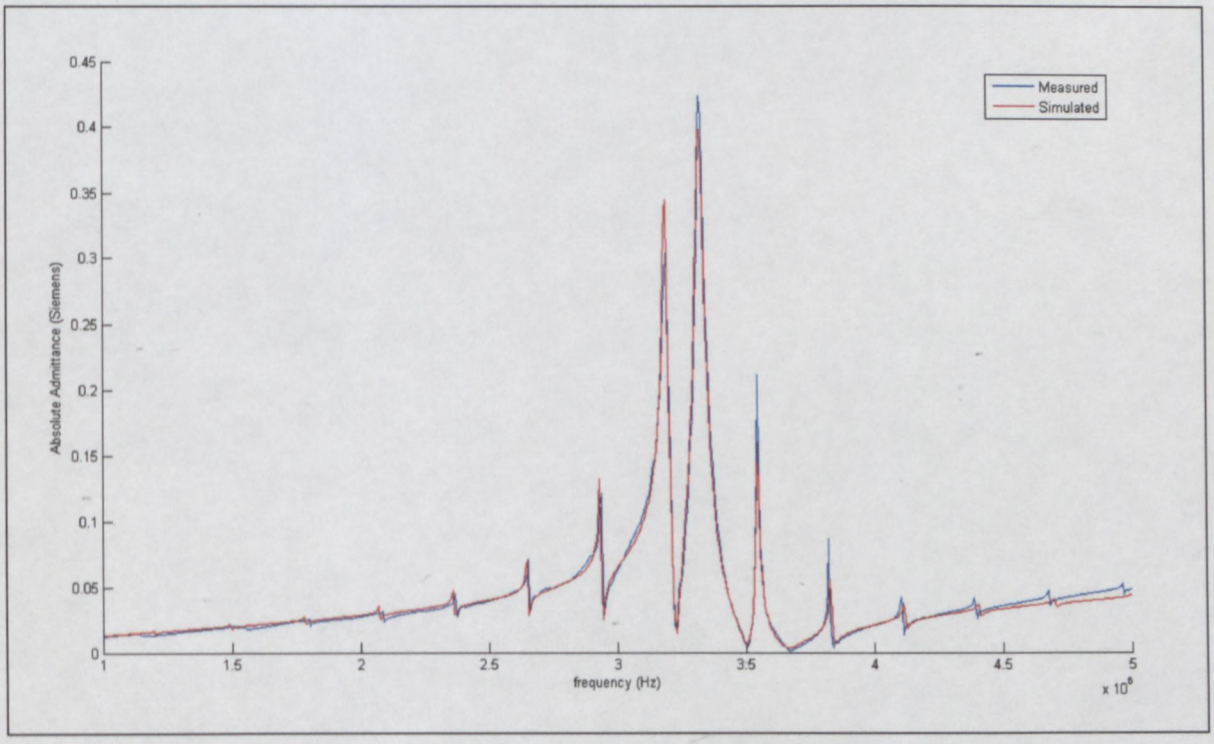

Figure 5-7: Demonstration of absolute admittance of experimental versus simulation spectrum. The simulation of electro-acoustic model using AMBA is shown to fit well with the measured result

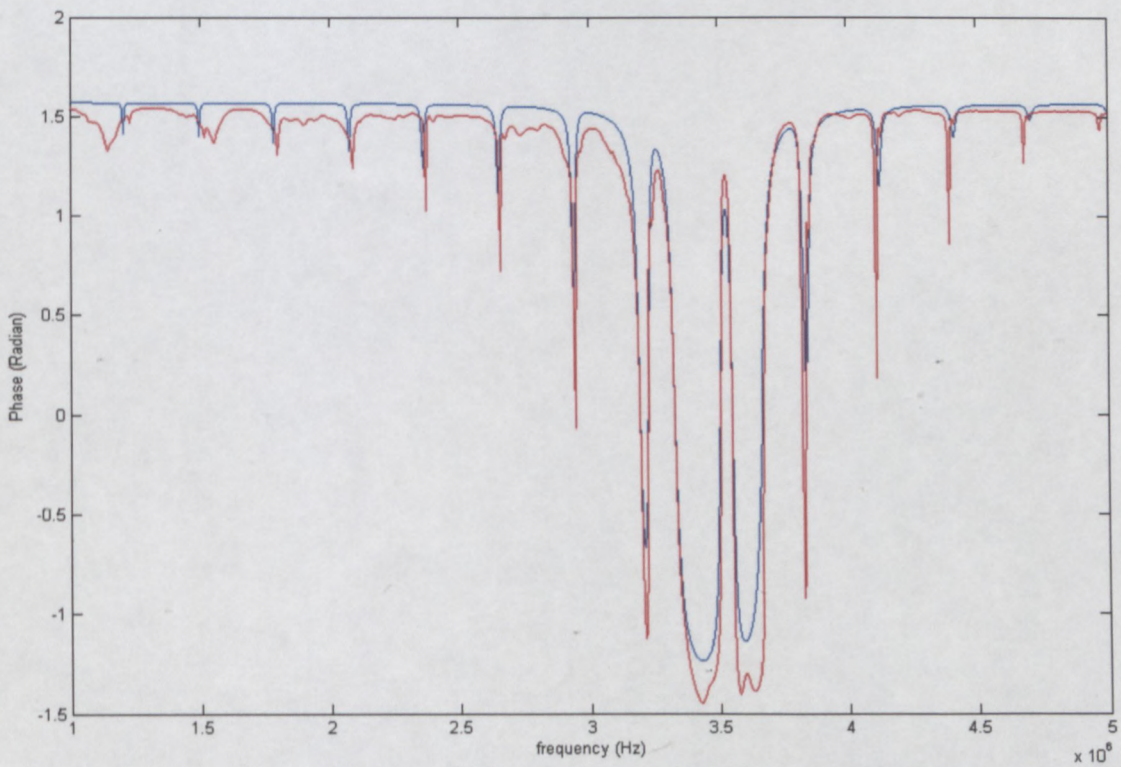

Figure 5-8: A comparison of the analytical solutions. The phase is measured against the function of frequency. The red curve represents the measured spectrum and blue represents an AMBA simulation

5.5 Phase Velocity Calculation

An adaptive mutation breeder algorithm was used to predict the spectral response measured by an impedance analyser. Each liquid mode parameter was successfully extracted from the formulae and its values used for simulation, then compared with the experimental spectrum. The comparison verified that the AMBA simulation matched the measured result.

It further showed that breeder algorithms could be utilised to calculate liquid velocity by inserting liquid mode circuit parameters (C_a and L_a) into the following equations:

$$f_{req\_a} = \frac{1}{2\pi\sqrt{L_a \times C_a}} \tag{5.3}$$

$$V_{(liq)} = \Delta f_{req\_a} \times ID \tag{5.4}$$

where

n = Mode number ($n \in 1, 2, 3..$);

L_a = Inductance of liquid mode;

C_a = Capacitance of liquid mode;

f_{req_a} = Resonance frequency of liquid mode;

Δf_{req_a} = Changing frequency and,

ID = Inside diameter of a PZT cylinder.

The results of the phase velocity measurements of different test liquids are shown in Fig.??-Fig.5-12. The brown line ('▲') depicts the literature report of the velocity of sound in water at 30 °C (1509.1 m/s[16]). The blue curve ('♦') is the experimental measurement. Although the velocity is close to the literature measurement, it is badly influenced by the frequency pulling (mode number 5-8). The AMBA simulation is shown (pink line, marked with '■'), where the liquid modes are harmonically spaced and are not influenced by the transducer coupling. The simulated result has a 2.43% difference when compared with the literature measurement. Although temperature fluctuation

plays an important role in the velocity measurement (as mentioned in Section 3.2.3) it is speculated that the error might arise from other factors. Since the measurement system was carefully designed to ensure the reduction of errors caused by temperature changes, it was therefore hypothesised that the inaccuracy of the velocimeter reading was caused by the inaccurate dimensions of the PZT cylinder. The cylinder's diameter was therefore carefully re-examined and measured with the vernier and the simulation was performed with rectified cylinder dimension (inner diameter +0.1mm). The result showed the error dropped to 0.5% (see Fig.5-10). The result of different test liquids FC43 and FC 75 are shown in Fig.5-11 and Fig.5-12 respectively.

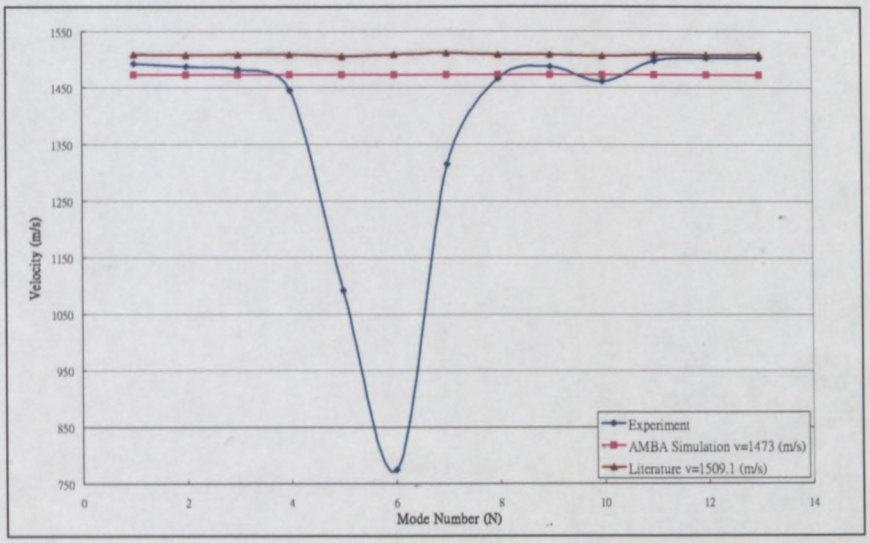

Figure 5-9: A comparison of phase velocity of distilled water between literature, experimental measurement and AMBA simulation at 30 °C. The literature measurement of sound velocity is 1509 m/s where AMBA simulation is 1473 m/s

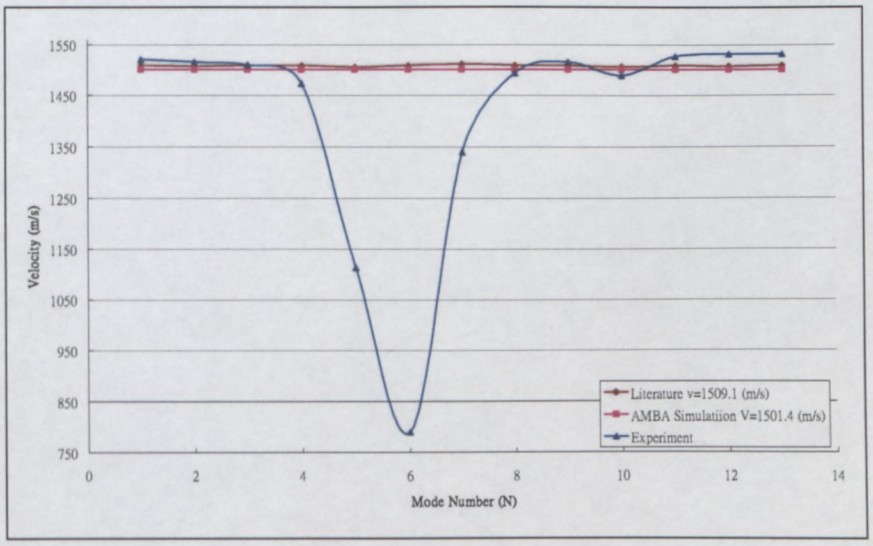

Figure 5-10: A spectrum after calibration by rectifying the dimension of the PZT cylinder (inner diameter +0.1mm). The AMBA calculated the velocity of sound equal to 1501 m/s, where literature measurement is 1509 m/s

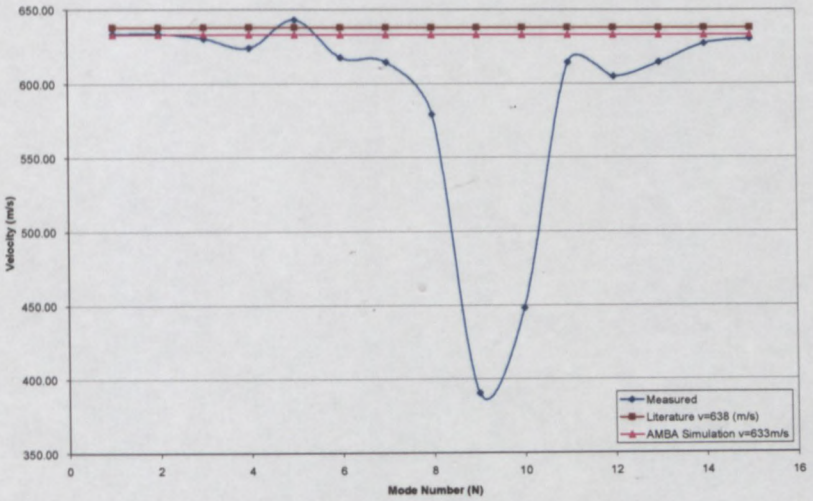

Figure 5-11: A comparison of phase velocity of FC43 between literature, experimental measurement and AMBA simulation at 30 °C. The literature measurement of sound velocity is 638 m/s where AMBA simulation is 633 m/s

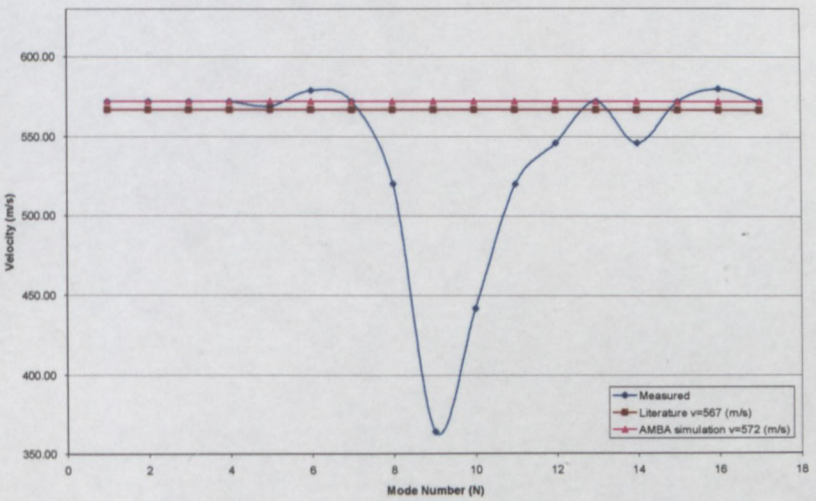

Figure 5-12: A comparison of phase velocity of FC75 between literature, experimental measurement and AMBA simulation at 30 °C. The literature measurement of sound velocity is 567 m/s where AMBA simulation is 572 m/s

Chapter 6

Design of a Liquid Velocity Measurement Rig

Several measurement apparatus and control modules were coupled to form a complete velocity measurement system. This chapter provides an understanding of the design and development of these modules. Fig.6-1 shows a block diagram of the set up for investigating liquid velocity measurement. The system consisted of the following modules:

(a) Temperature control system;

(b) test rig and,

(c) data capture and analysis.

The temperature control system consisted of a water bath, PID temperature control unit, PT100 sensor and an immersion heater. The Gefrane 600 temperature controller facilitated an accurate temperature control process. It relied upon a platinum resistive temperature sensor (PT100) as input and compared the bath's temperature with the desired set temperature. The LCD display on the controller provided a constant readout so a change in temperature in the bath could be observed. The output to a control element was also provided, in this case a 1500W immersion heater, used to heat up the bath. The primary function of the test rig was to hold the PZT cylinder inside a brass jacket for thermal stability. This was critical to velocity measurement as emphasised in Chapter 3. Once the test liquid was placed into the PZT cylinder the test rig was

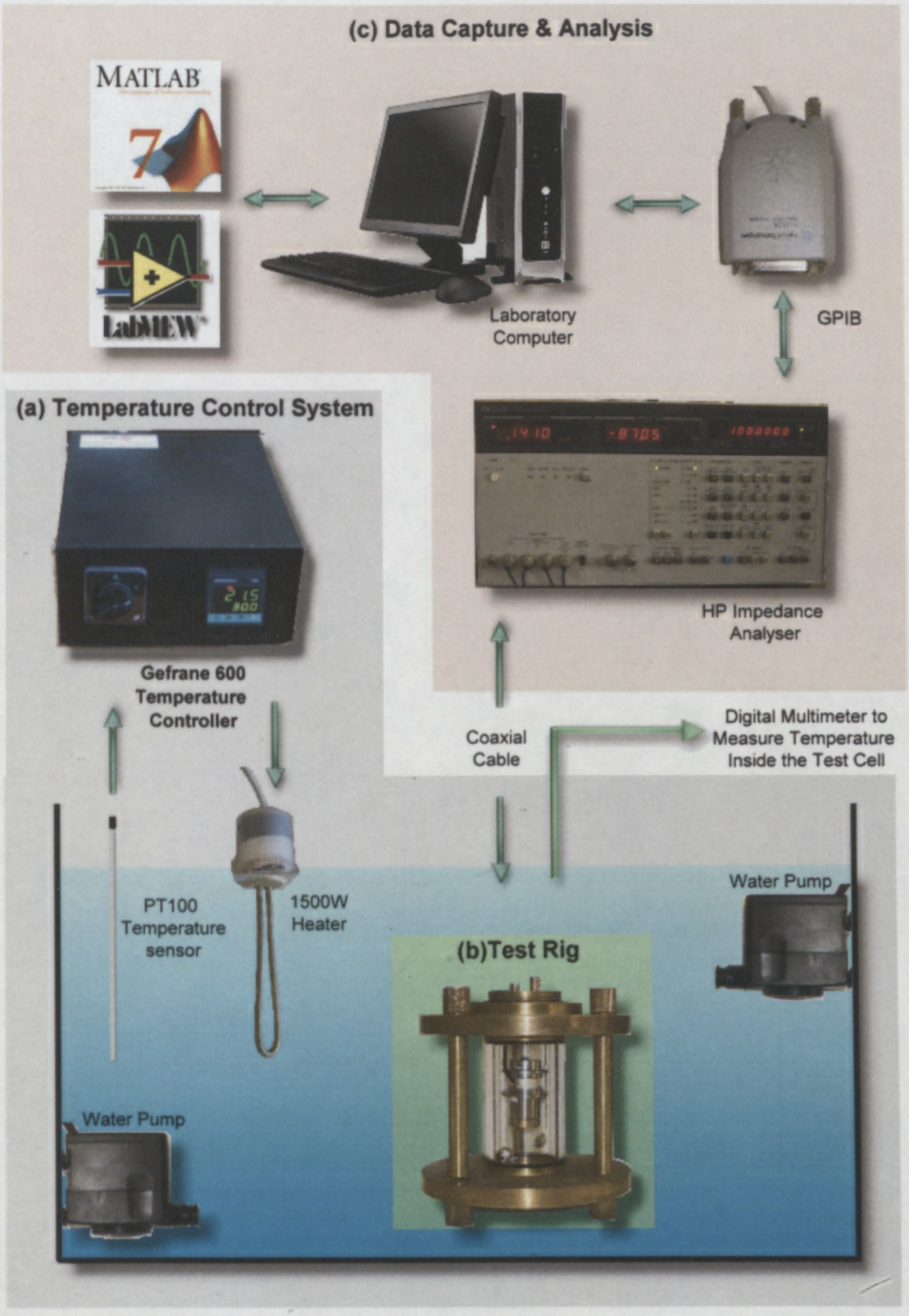

Figure 6-1: A block diagram for the interconnection of individual modules to form a complete velocity measurement system

sealed and immersed in the bath to allow the temperature inside the rig to reach thermal equilibrium (30 °C). When the temperature inside the test rig had reached the set point, LabVIEW was launched to automate the admittance and phase measurement of 100 Hz/sample. A process scan using AMBA (written in Matlab) was performed to calculate the velocity of sound in the test liquid. Insight into the design problems encountered and the solutions are discussed in subsequent sections.

6.1 Temperature Control System

Temperature control plays an important role in sound velocity measurement. A slight fluctuation in temperature (0.0024 °C) results in a change in the speed of sound in water by 0.001m/s[20]. Thermal fluctuation of the sample liquid introduced significant changes in the sound velocity which subsequently reduced the accuracy of the measurement. A temperature control system was designed to ensure that the velocity measurement was taken at a constant temperature and without changing more than ±0.01 °C during the measurement procedure.

6.1.1 Isothermal Water Bath

A water bath was constructed using 6 *mm* thick perspex, to form a rectangular tank. The perspex was selected for the low thermal conduction. The dimensions of the tank were $29(W) \times 61(L) \times 35(H)$ *cm* with a maximum capacity of 60 liter. The dimensions were chosen to accommodate a test rig and to provide a sufficient heat capacity effect. Once the bath had been filled, the test rig was immersed. Polystyrene chips were placed on top of the water to act as thermal insulation and to reduce convection as well as minimising the evaporation. The tank was insulated with 2cm thick polystyrene boards placed on all sides to prevent loss from conduction. Two water pumps were placed on each corner of the bath to circulate and agitate the water so as to reduce any thermal "hot spots" within the tank.

6.1.2 Temperature Control Unit

A Gefran 600 temperature controller[21] was used for controlling the temperature of the water to within $\pm 0.1\,^{\circ}C$. A cooling system was unnecessary and, therefore, not included in this study. The PID control unit was set to minimise temperature overshoot of the set point temperature. There was however, a trade-off between rapid response to deviation from the set point, elimination of overshoot and the stability of the process. The input was connected to a PT100 platinum sensor. When the water temperature dropped below the set point temperature, the controller turned on a 1500W immersion heater to elevate the waster temperature.

The absolute temperature of the bath and sample liquid inside the test cell was measured with a separate PT100 $\frac{1}{10}$th Din, 4 wire temperature sensor from *Unitemp Co*[6]. The sensor is made of a pure platinum element with which the resistance changes proportionally with temperature. The resistance was measured with a HP digital multimeter, where the conversion to temperature could be confirmed by the table included in Appendix C.

6.2 Test Rig

The focal point of this study was to investigate acoustic modes within a liquid filled PZT cylinder for determining liquid velocity. A test rig made of brass was designed and built for the purpose. The function of such a device was to house the PZT cylinder inside a brass jacket, which acted as a thermal low pass filter to ensure insulation from external temperature variation. Two rigs were used for the sound velocity measurement in this study.

6.2.1 Large Volume Test Rig

The first rig was developed by Davies for the study of the nonlinearity parameter B/A [16]. The rig as shown in Fig.6-2 was specifically designed for the measurement of a PZT-

4 cylinder and results measured from such a device were promising for this application. Several experiments were performed using this rig and the results used to compare with a small volume test rig described subsequently. The thermal jacket and sensor housing were both made from brass. The thermal jacket encased a PZT cylinder was secured to the bottom of the jacket by isobutylene glue. The electronic housing included a pressure sensor, temperature sensor and electrical feeds through to the cylindrical cavity. The sensor housing was attached to the thermal jacket using cap screws, clamped with O-ring seals to provide a pressurised, watertight cavity.

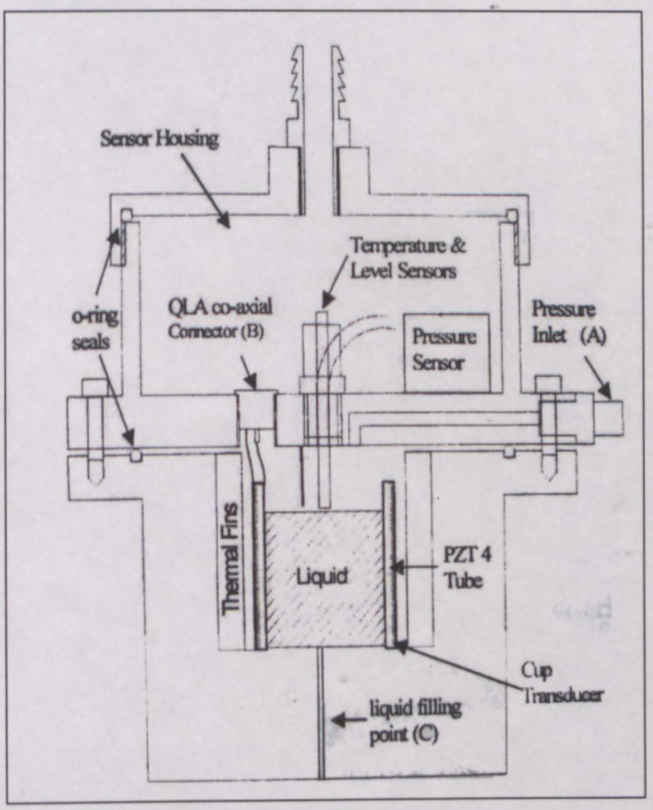

Figure 6-2: A schematic diagram of a test rig designed to house a PZT-4 cylinder[16]

6.2.2 Small Volume Test Rig

A second test rig was designed to house cylinders with small volumes. A distinguishing feature between the first (Fig.6-2) and second rig, was, in the former, the PZT cylinder was situated inside an air chamber, whereas in the second rig, the entire resonator assembly with the PZT cylinder was immersed within a perspex cylinder filled with silicon oil. In this case, the silicon oil acted as a thermal insulator and further minimised temperature fluctuation. A detailed design schematic is shown in Fig.6-3.

The resonator was assembled with an electrical and mechanical system composed of a vibrating PZT cylinder situated in the centre core of the rig. The silicon oil was filled into the perspex cylinder as shown in Fig.6-4. The following design criteria is described in detail for constructing a test rig to accommodate these requirements. A test resonator as shown in Fig.6-3 was developed to hold and excite the sample liquid enclosed within a PZT cylinder. The PZT cylinder was rigidly attached to a transducer housing to prevent leakage, yet not too tight, as resonance might appreciably be reduced by mechanical damping. Electrical contact was made to the outer and inner surfaces of the piezoelectric cylinder, without introducing any contact resistance or mechanical damping. It was recommended to connect the leads to the electrodes using conductive exproxy, since exceeding a specific soldering temperature might dissolve the electrode and immediately depolarize the piezoelectric phase[2]. The test cell needed to be impermeable, yet permit effortless exchange of the sample liquid. Interchanging of piezoelectric transducers of

Table 6.1: Parts of a resonator

Item Number	Title
1	Pressure window
2	Water chamber
3	PZT cylinder
4	O-ring seal
5	Transducer housing
6	Liquid injection hole
7	Screw to clamp the holding device with PZT cylinder
8	Coaxial cable
9	BNC connector sealed with glue
10	PT100 temperature sensor holder

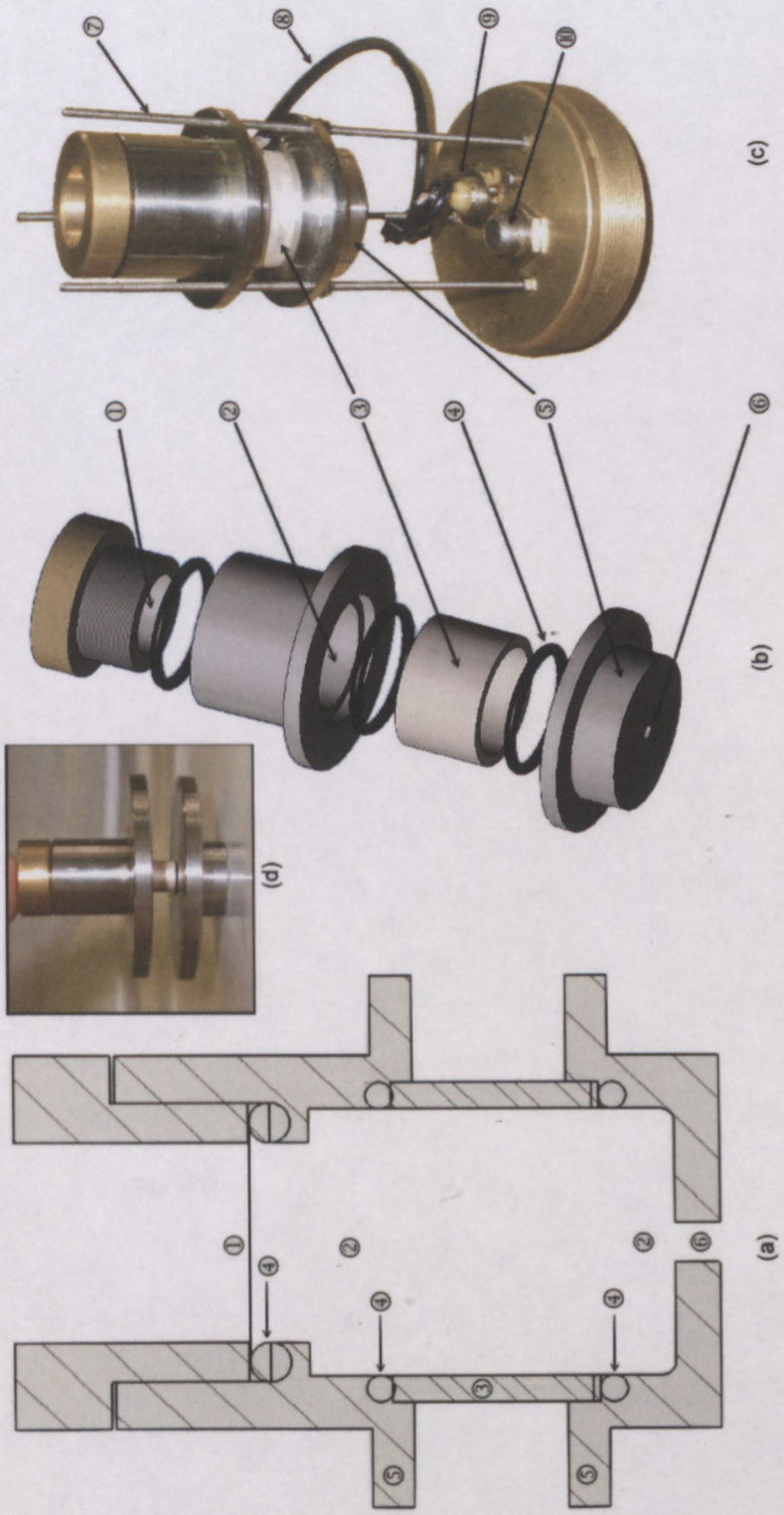

Figure 6-3: (a) cross-section drawing of the resonator, (b) CAD drawing showing the resonator design, (c) photograph of a resonator framework clamped with transducer housing (medium cylinder) and (d) small volume transducer housing

Figure 6-4: A photograph of a test rig with resonator assembled into the centre. The perspex cylinder is designed to hold silicon oil for electrical and thermal insulation

various sizes should have also been permitted. The test cell was designed to accommodate measurements of temperature and pressure inside the chamber (although pressure measurement was not critical to this study, but could be used for future research). The water chamber was designed for the liquid height to exceed that of the tube to avoid edge effects. The resonator framework consisted of three stainless steel threaded rods attached to a brass base. The transducer housing was securely assembled and clamped with stainless steel nuts threaded through the rod framework.

An acoustic wave, originally generated from the outer section of a PZT cylinder travelled through the silicon oil and reflected back to the transmitter when it reached the wall of the perspex cylinder. Although the emission wave causes the distortion to measurement, but in this study, any distortion was assumed to be small enough to be neglected (especially for small tube measurements, where the wave travelling from the PZT cylinder was remote to the wall of the perspex cylinder). A layer of neoprene surrounded the inner diameter of the perspex cylinder to ensure absorption of any excessive acoustic energy transmitted from the outer section of the PZT cylinder.

6.3 Data Capture and Analysis

Velocity measurement required data acquisition, which was recorded from the HP impedance analyser. An Intel Pentium 4 laboratory PC with a 3.2GHz processor and 1GB of RAM was used to capture data from the impedance analyser and to improve the performance of the AMBA simulation. All data collection was controlled from and performed in a LabVIEW environment. Data was subsequently analysed in Matlab. A flow chart diagram of the measurement procedure is shown in Fig.6-5

6.3.1 Data Acquisition Using LabVIEW

Data acquisition was controlled and accomplished using a PC running LabVIEW software. LabVIEW[5] is a software programming environment designed to enable the creation of "virtual instruments" for data acquisition and process-control purposes. LabVIEW is a graphical programming environment for creating a block diagram consisting of linked subroutines. The additional benefit of using LabVIEW over other development languages was the extensive support (drivers) for accessing instrumentation hardware. LabVIEW was interfaced with the impedance analyser using GPIB (General Purpose Interface Bus). This made it simple for real time data acquisition and provided an interface to make ease communicating with the instrument. An Agilent 82857A GPIB interface supporting all IEEE-488 compatible interfaces[3] was used. GPIB provided a standard interface for communication between instruments from different sources and a personal computer with the transfer rate over 750 kb/s. The GPIB allowed the bus controller to tell the interface what to do. In this manner, the PC directly controlled the HP impedance analyser, accessed data and automated measurement procedures. When the impedance scan setup was configured, the user easily selected the settings by choosing the configuration from a drop down menu. A designed interface in LabVIEW is depicted in Fig.6-6.

The LabVIEW program was designed to match the exact specifications of the HP 4192A instrument[25]. It allows the user to configure the following settings:

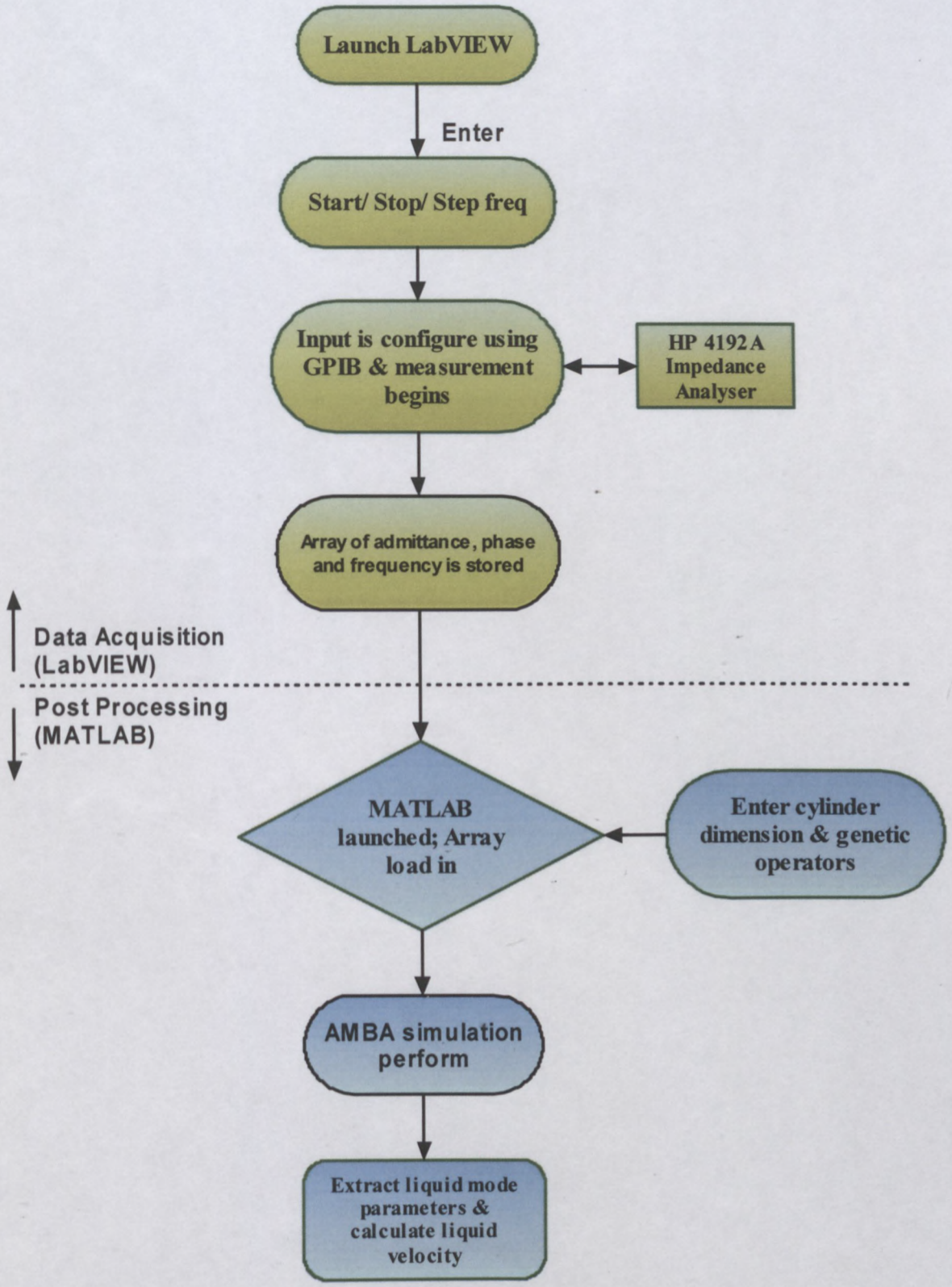

Figure 6-5: A flow chart illustrating the velocity measurement procedure

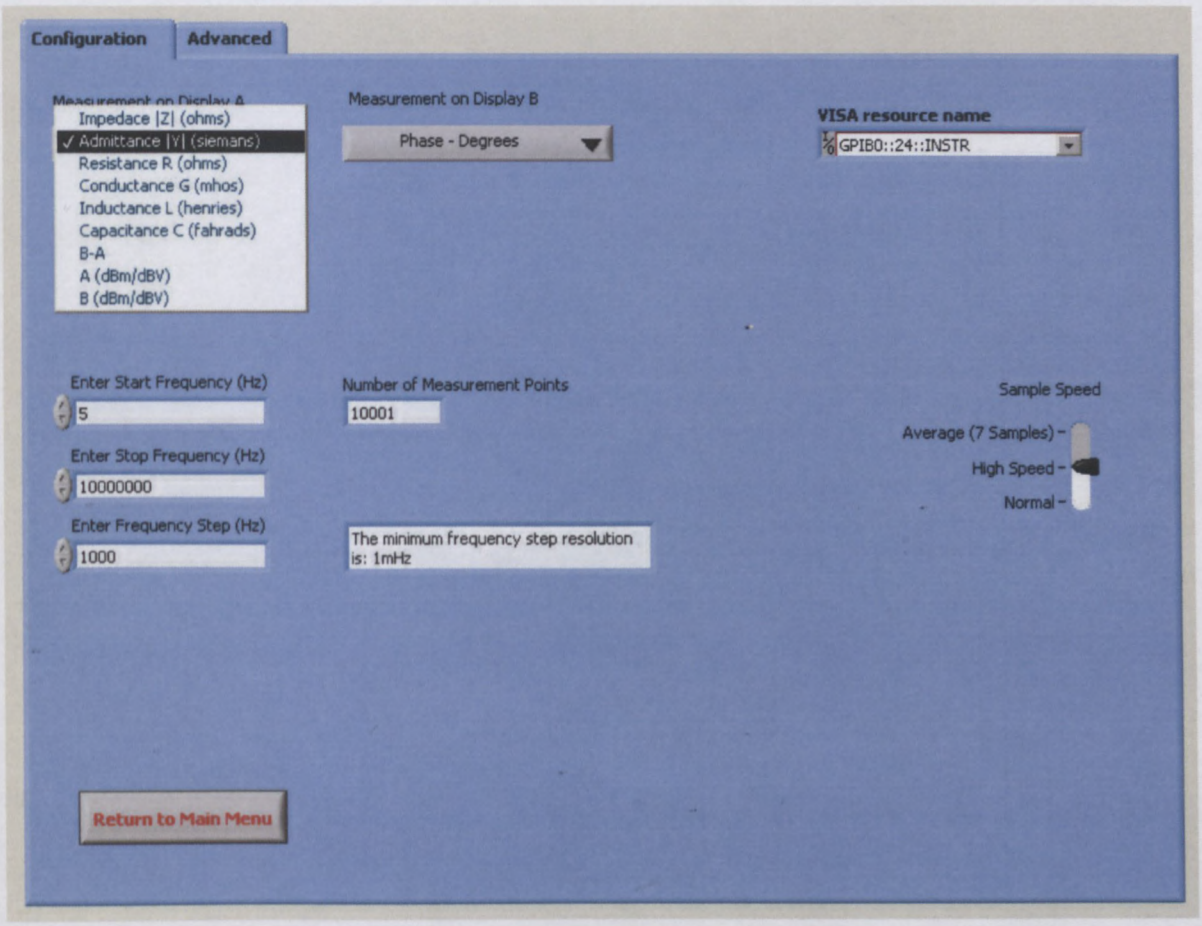

Figure 6-6: The design of user-friendly interface in LabVIEW. Users can easily choose the configuration from the drop down menu. The program required a user to enter the start/stop/step frequency before launching scan

Table 6.2: Operation instructions and descriptions for instrument's basic capabilities

Function	Descriptions
Measurement on display A	measure different types of parameters such as impedance, admittance, resistance, conductance, inductance or capacitance
Measurement on display B	measure different types of parameters to be displayed on display B such as phase angle, reactance, susceptance, quality factor, resistance or conductance
Maximum/Minimum sweep frequency	5Hz -13MHz
Minimum stepping frequency	1Hz
VISA source	different sets of output connection such as COM, GPIB or LPT
Sample Speed	this sets the measurement mode to high resolution and repeatability such as AVERAGE (7 samples) or HIGH speed mode in which the measurement time is approximately 1/2 shorter than the NORMAL speed. There is trade-off between the measurement speed and accuracy

The captured data consisted of defined (start to stop) frequencies, phase changes and admittances. After a set of timed-captures data were saved as a ".mat" (Matlab) file. All subsequent data processing was performed in Matlab.

6.3.2 Matlab (post processing)

The Matlab program was launched using the data captured by LabVIEW. The measured data was passed to the AMBA for simulation where the dimension of a PZT cylinder and genetic operators (number of generations, size of genetic pool and mutation rate) were required to be entered before the simulation began. AMBA returns the result with calculated liquid mode parameters and also computed the velocity of sound of the test liquid. The experimental result was plotted against simulation for comparison. Modification of genetic operators had to be adjusted for optimum results.

Chapter 7

Results and Conclusions

Based on the implementation of the system, the results and conclusions have been drawn and summarised as follows. It was decided to study the resonant behaviour of both an empty and a liquid filled piezoelectric cylinder. Different types of PZT materials (soft and hard) were investigated and results show the soft type material was adequate for the study. The soft material was suitable for sensor applications, as it had higher sensitivity and a low mechanical Q_s value. Most importantly, it showed that clear and undisturbed resonances with quick deterioration of overtones.

An "electro-acoustic" model was proposed which adopted Mason's electro-mechanical equivalent circuit with acoustic lumped circuit elements. The theory of this model included an understanding of the frequency pulling phenomenon caused by mutual inductance (M_a) of a coupled "mechanical-acoustic" transformer. This transformer was essential for defining the mutual coupled behaviour between liquid resonant series and the piezoelectric resonant series. An acoustic series was investigated in detail by analysing the electrical characteristics of admittance and phase using the HP impedance analyser. Acoustic equivalent circuit models were derived for each of the liquid modes. Each of individual liquid mode had extremely sharp quality factors (Q_s) and these were mostly harmonic, providing ideal conditions for velocity of sound measurement. A study of frequency pulling was confirmed and conclusively defined the coupled interaction between a piezoelectric cylinder and the liquid resonance series. A comparison between an ex-

perimental spectrum and a simulated "electro-acoustic" equivalent circuit model showed excellent agreement.

A cavity resonator was designed to encapsulate the PZT cylinder so the liquid modes could be utilised to measure velocity. The velocimeter test rig was constructed from brass and designed to measure temperature and velocity. The construction of a resonator was such that it was relatively simple to inject and remove test liquids without needing to disassemble the entire test rig system. Three test liquids were used for velocity measurement namely, distilled water, fluorocarbon FC43 and FC75. The fluorocarbon liquid had unusually slow sound speed which was used to generate a closely acoustic resonance (see Fig.7-1). This allowed comparison of the acoustic behaviour in terms of adjacent mode coupling and resonant interaction between liquid and PZT cylinder.

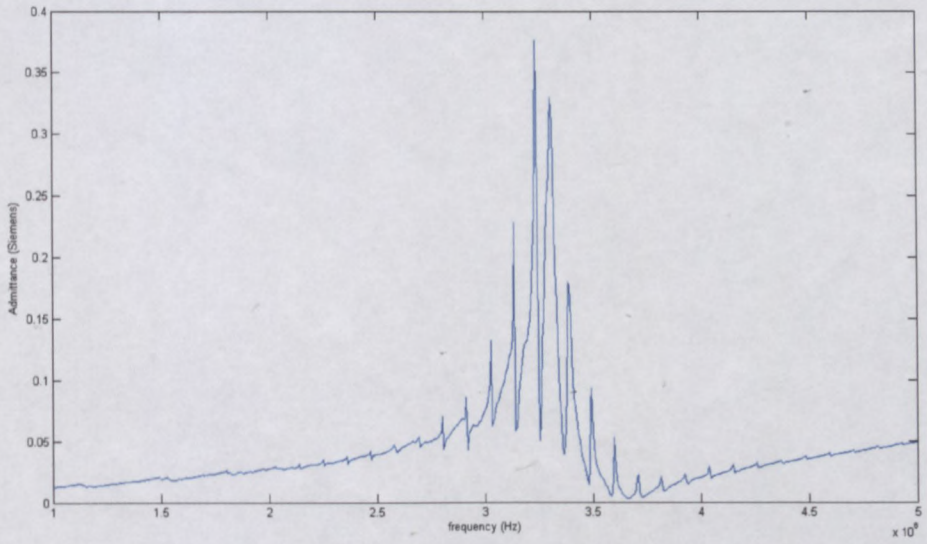

Figure 7-1: Spectrum of absolute admittance with frequency of a PZT-27 cylinder filled with FC75

The same test liquid (FC75) was also measured using a PZT-4 cylinder (inner diameter of 32mm). Note the number of liquid modes in Fig.7-2 was almost twice the amount when compared with Fig.7-1. This was because of the increased diameter of a PZT cylinder.

AMBA was utilised as a means of predicting multiple resonance liquid modes inter-

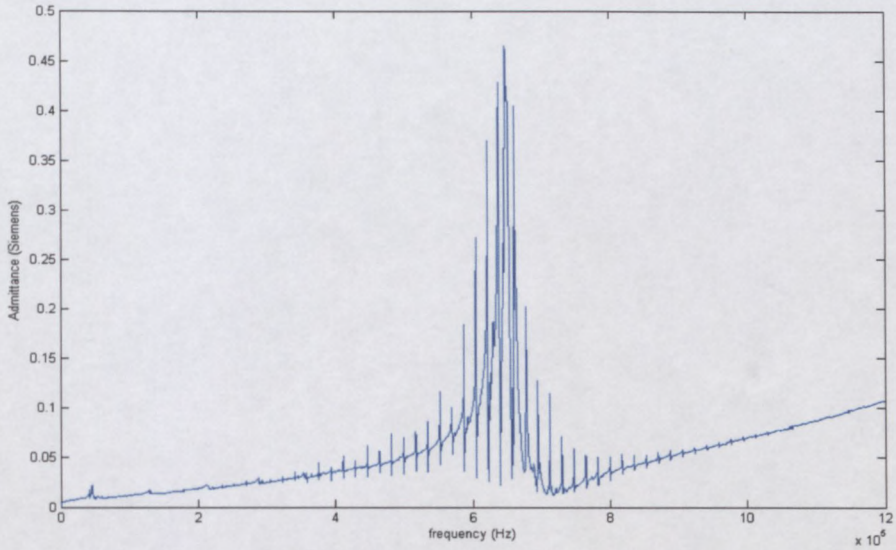

Figure 7-2: A comparison of FC75 admittance spectrum measured with a PZT4 cylinder ($38 \times 32 \times 38\ mm$). Note the increased number of modes due to the larger diameter of cylinder. The raised number of modes give better resolution

acting with one another. A liquid filled piezoelectric cylinder was used as an acoustic system to represent coupled piezoelectric and liquid vibrational modes. Using a variation of Mason's transmission line model, an AMBA was used to predict the spectral response measured by an impedance analyser. As shown in Fig.7-3, the acoustic model was shown to fit almost identically over the measured data for a distilled water spectrum. It was also proved the breeder algorithms could successfully be used to predict the sound velocity of the liquid inside the cylinder. But, because of a large amount (more than 25) of liquid modes in the FC43 and FC75 spectra, it increased the complexity and difficulty of the simulation and the prediction of liquid mode parameters using AMBA. The frequency range was narrowed to strike a balance between the complexity of the simulation and the resolution of the sample mode.

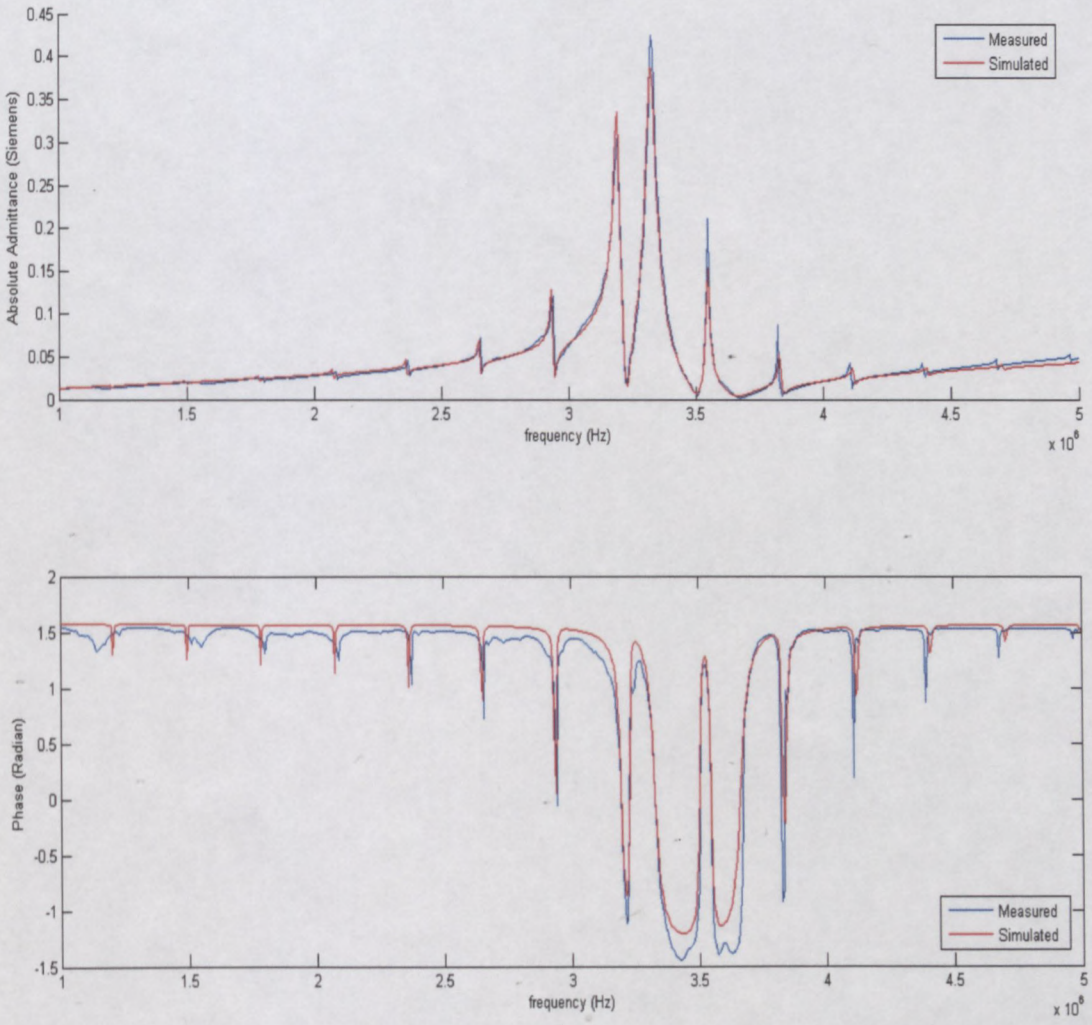

Figure 7-3: A comparion of measured and AMBA simulated admittance & phase spectrum of a PZT-27 cylinder filled with distilled water

Table 7.1: A comparison between literature results and velocimeter measurement in this study

Liquid	Temperature (°C)	Sound Speed (m/s)[16]	Sound Speed Measured $(m/s) \pm \sigma$
Distilled Water	30 °C	1509.1	1473±1.38
FC75	30 °C	567	572±2.95
FC43	30 °C	638	633±3.74

The velocimeter using a small volume PZT-27 cylinder in the measurement of sound speed produced accurate results. Table 7.1 shows a comparison between literature measurement[16] and velocimeter measurement used in this study. Each measurement is defined at 30 °C.

Chapter 8

Future Work

The following recommendations are made for future work on this project. The continuous wave technology using a PZT cylinder to measure the velocity of liquid was proved to be simple and accurate. This study, however, did not account for every possible technique. Some of the approaches include phase locking techniques to trap liquid modes within the test rig; an alternative method such as amplitude or admittance locking could also be considered to track changes in velocity. It is recommended the existing AMBA code be optimised and different mutation and recombination methods implemented to achieve better results. The existing AMBA code might also be used to extract liquid parameters such as bulk modulus, viscosity and density. The ultimate goal is to utilise the concept of this study and implement a PZT cylinder as an in-line pipe system for instant liquid velocity and acoustic concentration of particle measurement.

References

[1] Http://imaginis.com/ultrasound/, 18 May 2005.

[2] Ferroperm pty. Http://www.ferroperm-piezo.com/index.html, 04 September 2006.

[3] IEEE 488. Http://www.ieee.org, 14 December 2005.

[4] IVUS. Http://cvmed.stanford.edu/interventional/ivus.htm, 11 May 2005.

[5] National instruments. Http://www.ni.com/, 10 September 2006.

[6] Unitemp. Http://www.unitemp.co.za/frame.htm, 03 September 2006.

[7] T. Back, D. Fogel, and Z. Michalewiez. *Handbook of Evolutionary Computation.* Institute of Physics Publishing and Oxford University Press, 1997.

[8] A. Ballato. *Modelling Piezoelectric and Piezomagnetic Devices and Structures Via Equivalent Networks.* IEEE Transactions on Ultrasonics, Ferroelectrics and Frequency Control. 48 (5): pp. 1189-1240, 2001.

[9] J. Bell. *Satellite Resonances in Ultrasonic Interferometry.* Proc. Physical Society B. LXIII: 958-964, 1950.

[10] D. Berlincourt, D. Curran, and H. Jaffe. *Piezoelectric and Piezomagnetic Materials and their Function in Transducers.* Academic Press, New York, 1964.

[11] S. Butterworth. *On a Null Method of Testing Vibration Galvanometers.* Proc. Phy. Soc (London). 26: pp. 264-273, 1914.

[12] N. Cedrone and D. Curran. *Electronic Pulse Method for Measuring the Velocity of Sound in Liquids and Solids.* J. Acoust. Soc. Am. 26(6): pp. 963-966, 1954.

[13] W. Chen. *The Electrical Engineering Handbook.* Elsevier Academic Press. pp. 525-534, 2004.

[14] Y. Cohena, S. Sherrita, B. Dolgina, D. Palb, T. Petersonb, J. Krohb, and R. Kraheb. *Ultrasonic/Sonic Drilling/Coring (USDC) for in-Situ Planetary Applications.* SPIE Smart Structures 2000. pp. 3992, March 2000.

[15] L. Crum and W. Law. *The Use of High-Intensity Focused Ultrasound for Noninvasive Surgery.* J. Acous. Soc. Am. 97(5): pp 3325, May 1995.

[16] J. Davies. *Continuous Wave Mode Locking for the Determanation of the Acoustic Nonlinearity Parameter B/A.* PhD thesis, Electrical Engineering of University of Cape Town, 2002.

[17] J. Davies, J. Tapson, and B. Mortime. *Determination of the Acoustic Nonlinearity Parameter B/A Using a Phase Locked Ultrasonic Interferometer.* J. Acoust. Soc. Am. 103: pp. 3080, 1998.

[18] K. V. Dyke. *The Electric Network Equivalent of a Pizeoelectric Resonator*, volume 895A. Phys. Rev. 25, 1925.

[19] D. Ebenezer. *Three-Port Parameters and Equivalent Circuit of Radially Polarized Piezoelectric Ceramic Cylinders of Finite Length.* J. Acoust. Soc. Am. 99(5): pp. 2908-2912, 1996.

[20] E. Everbach. *Tissue Composition Determination Via Measurement of the Acoustic Nonlinearity Parameter.* PhD Thesis, Yale University, New Haven CT, 1989.

[21] Gefran. Gefran 600 user manual. http://www.gefranonline.com, 14 December 2005.

[22] A. Green. *The Design for High Power Ultrasonic Transducers.* Master's thesis, Electrical Engineering University of Cape Town, 2002.

[23] J. Greene. *AMBA-An Adaptively Mutating Breeder Algorithm for Global Stochastic Optimisation.* Classnote for Electrical Engineering, University of Cape Town, 2005.

[24] J. Greene. *Course EEE4096S, Neural Fuzzy and Evolving Systems, Electrical Engineering University of Cape Town.* 2005.

[25] Hewlett Packard. *4192A LF Impedance Analyser User Menu.*

[26] J. Holland. *Adaptation in Natural and Artificial Systems.* The University of Michign Press, 1975.

[27] A. Khazan. *Transducers and their Elements.* PTR Prentice Hall, 1994.

[28] S. Kwiatkowski and D. Sinha. *Single-Transducer Continuous-Wave Noninvasive Ultrasonic Characterization of Fluids (A).* J. Acoust. Soc. Am. 112: pp. 2440, 2002.

[29] W. Mason. *Piezoelectricity, It's History and Applications.* J. Acoust. Soc. Am. 70(6): pp. 1564-1566, 1981.

[30] W. Mason. *Electromechanical Transducer and Wave Filters.* D. Van Nostrand, 1st edition, 1942.

[31] W. Mason. *Piezoelectric Crystals and Their Application to Ultrasonics.* D. Van Nostrand, 1950.

[32] W. Mason and R. Thurston. *Physical Acoustics Vol XVI.* Academic Press, 1982.

[33] H. McSkimin. *Variations of the Ultrasonic Pulse-Superposition Method for Increasing the Senstivity of Delay-Time Measurements.* J. Acoust. Soc. Am. 37(5): pp. 864-871, 1965.

[34] M. Mitchell. *An Introduction to Genetic Algorithms.* The MIT Press Cambridge, Massachusetts, 1996.

[35] A. Morris. *Measurement and Instrumentation Principles.* Elsevier, 2005.

[36] E. Papadakis. *Ultrasonic Phase Velocity by the Pulse-Echo-Overlap Method Incorporating Diffraction Phase Correction.* J. Acoust. Soc. Am. 42(5): pp. 1045-1051, 1967.

[37] R. Pethrick. *The Swept Frequency Acoustic Resonant Interfermeter: Measurement of Acoustic Dispersion Parameters in Low Magahertz Frequency Range.* J. of Phys. E. Scientific Instr. 5: pp. 571-574, 1972.

[38] B. Prenzlow. *Design of Low Pressure System to Determine the Acoustic Nonliearity Parameter B/A for Small Volumes of Sample Liquids.* Master's thesis, Electrical Engineering University of Cape Town, 2002.

[39] D. L. R. Krimholtz and G. Matthaei. *New Equivalent Circuit for Elementary Piezoelectric Transducers.* Electron Letter. 6(13): pp. 398-399, 1970.

[40] M. Redwood. *Experiments with the Electrical Analog of a Piezoelectric Transducer.* J. Acoust. Soc. Am. 36: pp. 1872-1880, 1964.

[41] M. Redwood. *Transient Peformance of a Piezoelectric Transducer.* J. Acoust. Soc. Am. 33(4): pp. 527-536, 1961.

[42] W. Roth. *Piezoelectric Transducers.* Proceeding of the I.R.E. pp. 750-758.

[43] J. Schaffer, R. Caruana, L. Eshelman, and R. Das. *A Study of Control Parameters Affecting Online Performance of Genetic Algorithms for Function Optimisation.* Proceeding of the Third Inter. Conf on Genetic Algorithms, San Mateo, CA: Morgan Kaufman Publisher, 1989.

[44] C. Sehgal, R. Bahn, and J. Greenleaf. *Measurement of the Acoustic Nonlinearity Parameter B/A in Human Tissue by a Thermodynamic Method.* J. Acoust. Soc. Am. 76(4): pp. 1023-1029, 1984.

[45] S. Sherrit, S. Leary, and B. Dolgin. *Comparision of the Mason and KLM Equivalent Circuit for Piezoelectric Resonantors in the Thickness Mode.* IEEE Ultrasonics Symposium, 1999.

[46] B. Sinha and M. Gouilloud. *Surface Acoustic Wave Sensors.* J. Acoust. Soc. Am. 78(5): pp. 1932, 1985.

[47] J. Spall. *Introduction to Stochastic Search and Optimization.* Wiley, 2003.

[48] D. Stansfield. *Underwater Electroacoustic Transducer.* Bath University Press and Institute of Acoustic, 1990.

[49] F. Stremler. *Introduction to Communication Systems.* Addison-Wesley, New York, 3 edition, 1990.

[50] J. Vig. *Introduction to Quartz Frequency Standards.* US Army Communication-Electronics Command Research, Development and Engineering Center. http://www.ieee-uffc.org/freqcontrol/quartz/vig/vigquartz.htm.

[51] L. Whitley. *Fundations of Genetic Algorithms.2.* Morgan Kaufmann Publishers, 1993.

[52] W. Yost, J. Cantrell, and P. Kushnick. *Fundamental Aspects of Phase-Locking Loop Technology-Base Methods for Measurement of Ultrasonic Velocity.* J. Acoust. Soc. Am. 91(3): pp. 1456-1468, 1992.

Appendix A

PZT Cylinder Properties

Ferroperm Piezoceramics A/S

Material data based on typical values

Symbol	Unit	Pz21	Pz23	Pz24	Pz26	Pz27	Pz28	Pz29	Pz34	Pz35	Pz37	Pz46	Pz52	Pz54	Pz26, FEM use
$\varepsilon_{1,r}^{\sigma}$		3.24E+03	1.37E+03	8.10E+02	**1.19E+03**	**1.80E+03**	1.22E+03	2.44E+03	2.37E+02	2.47E+02		1.27E+02			
$\varepsilon_{3,r}^{\sigma}$		3.98E+03	1.50E+03	4.25E+02	**1.33E+03**	**1.80E+03**	9.90E+02	2.87E+03	2.08E+02	2.19E+02	9.12E+02	1.24E+02	1.86E+03	2.87E+03	1.08E+03
$\varepsilon_{1,r}^{S}$		2.12E+03	8.60E+02	7.23E+02	**8.28E+02**	**1.13E+03**	7.34E+02	1.34E+03	2.24E+02	2.39E+02		1.27E+02			
$\varepsilon_{3,r}^{S}$		1.98E+03	8.73E+02	2.39E+02	**7.00E+02**	**9.14E+02**	5.10E+02	1.22E+03	1.72E+02		5.93E+02	1.16E+02	8.63E+02	1.44E+03	5.18E+02
$\tan\delta$ ($_3^{\sigma}$)		0.016	0.013	0.002	**0.003**	**0.017**	0.004	0.016	0.014	0.006	0.017	0.004	0.003	0.003	
T_C >	°C	218	350	330	**330**	**350**	330	235	400	500	350	650	250	225	
k_p		0.603	0.522	0.494	**0.568**	**0.592**	0.579	0.643	0.074		0.256	0.033	0.599	0.585	-0.575
k_t		0.470	0.449	0.508	**0.471**	**0.469**	0.475	0.524	0.409	0.336	0.552	0.249	0.527	0.485	0.525
k_{31}		0.323	0.288	0.292	**0.327**	**0.327**	0.332	0.370	0.046		0.149	0.021	0.353	0.341	-0.310
k_{33}		0.691	0.646	0.659	**0.684**	**0.699**	0.687	0.752	0.397		0.579	0.087	0.711	0.698	0.707
k_{15}		0.590	0.612	0.327	**0.553**	**0.609**	0.631	0.671	0.228	0.169		0.045			
d_{31}	C/N	-2.59E-10	-1.28E-10	-5.80E-11	**-1.28E-10**	**-1.70E-10**	-1.14E-10	-2.43E-10	-5.33E-12		-8.16E-11	-2.26E-12	-1.74E-10	-2.01E-10	-1.06E-10
d_{33}	C/N	6.40E-10	3.28E-10	1.49E-10	**3.28E-10**	**4.25E-10**	2.75E-10	5.74E-10	4.60E-11	8.30E-11	3.91E-10	1.91E-11	3.70E-10	4.79E-10	2.77E-10
d_{15}	C/N	6.16E-10	4.21E-10	1.51E-10	**3.27E-10**	**5.06E-10**	4.03E-10	7.24E-10	4.33E-11	5.39E-11		7.79E-12			
d_h	C/N	1.22E-10	7.28E-11	3.34E-11	**7.24E-11**	**8.50E-11**	4.68E-11	8.82E-11	3.53E-11		2.28E-10	1.46E-11	2.24E-11	7.67E-11	
g_{31}	V m/N	-0.0074	-0.0096	-0.0154	**-0.0109**	**-0.0107**	-0.0130	-0.0096	-0.0029		-0.0101	-0.0021	-0.0106	-0.0079	-0.0111
g_{33}	V m/N	0.0156	0.0247	0.0397	**0.0280**	**0.0267**	0.0314	0.0226	0.0250	0.0428	0.0485	0.0174	0.0225	0.0189	0.0289
g_{15}	V m/N	0.0268	0.0343	0.0551	**0.0389**	**0.0373**	0.0373	0.0321	0.0279		0.0586	0.0195	0.0330	0.0268	
e_{31}	C/m^2	-2.92	-1.93	-1.45	**-2.80**	**-3.09**	-3.60	-5.06	-0.35		1.97	1.61			
e_{33}	C/m^2	23.4	15.5	9.9	**14.7**	**16.0**	12.4	21.2	6.5		8.0	2.6	17.6	21.6	13.6
e_{15}	C/m^2	16.19	10.81	6.55	**9.86**	**11.64**	10.67	13.40	2.52	1.16		0.30			
h_{31}	V/m	-1.67E+08	-2.50E+08	-6.88E+08	**-4.52E+08**	**-3.82E+08**	-7.99E+08	-4.68E+08	-2.27E+08		3.75E+08	1.56E+09			
h_{33}	V/m	1.34E+09	2.01E+09	4.70E+09	**2.37E+09**	**1.98E+09**	2.76E+09	1.96E+09	4.28E+09		1.53E+09	2.58E+09	2.31E+09	1.70E+09	
h_{15}	V/m	8.64E+08	1.42E+09	1.02E+09	**1.34E+09**	**1.16E+09**	1.64E+09	1.13E+09	1.27E+09	5.45E+08		2.64E+08			
N_p	m/s	1985	2159.61	2413.53	**2209.94**	**2011.08**	2187.56	1970.47	2771.62		1578	2468.17	2086	2124	
N_t	m/s	1928	2039	2146	**2038**	**1953**	1998	1966	2178	1.45E+03	1199	2002	1948	2004	
N_{31}	m/s	1375	1480	1670	**1500**	**1400**	1624	1410	2057			1905			
N_{33}	m/s	1328	1600	1600	**1800**	**1500**	1500	1500							
N_{15}	m/s	949.1	946.1	1201	**1018**	**896**	964	822	1394	972		1207			
$Q_{m,p}^{E}$		65	104	1.7E+03	**2.7E+03**	**89**	9.7E+02	76	7.0E+02		133	1.7E+03	1.2E+03	3.2E+03	
$Q_{m,t}^{E}$		59	69	3.6E+03	**3.3E+03**	**74**	1.1E+03	195	3.1E+02	1.7E+01	34	4.1E+03	9.8E+02	3.9E+03	

Ferroperm Piezoceramics A/S
Hejreskovvej 18A DK-3490 Kvistgaard Denmark Tel: +45 - 4912 7100 Fax: +45 - 4913 8188
Internet: www.ferroperm-piezo.com E-mail: pz@ferroperm-piezo.com

Ferroperm Piezoceramics A/S

Material data based on typical values

Symbol	Unit	Pz21	Pz23	Pz24	Pz26	Pz27	Pz28	Pz29	Pz34	Pz35	Pz37	Pz46	Pz52	Pz54	Pz26, FEM use
ρ	kg/m^3	7.78E+03	7.70E+03	7.70E+03	**7.70E+03**	**7.70E+03**	7.70E+03	7.46E+03	7.55E+03	5.72E+03	5.19E+03	6.53E+03	7.34E+03	7.76E+03	
ν_{12}^E		0.425	0.394	0.300	**0.334**	**0.389**	0.295	0.340	0.220	0,1985-1,1E-0	0.323	0.215	0.304	0.323	0.420
s_{11}^E	m^2/N	1.82E-11	1.48E-11	1.05E-11	**1.30E-11**	**1.70E-11**	1.26E-11	1.70E-11	7.33E-12	2,20552E-011	3.72E-11	1.06E-11	1.47E-11	1.38E-11	1.22E-11
s_{12}^E	m^2/N	-7.76E-12	-5.84E-12	-3.13E-12	**-4.35E-12**	**-6.60E-12**	-3.71E-12	-5.78E-12	-1.61E-12	-4,3755E-012	-1.20E-11	-2.28E-12	-4.46E-12	-4.45E-12	-5.13E-12
s_{13}^E	m^2/N	-6.85E-12	-7.12E-12	-4.77E-12	**-7.05E-12**	**-8.61E-12**	-6.60E-12	-8.79E-12	-5.36E-13		-1.63E-11	-1.20E-11	-5.99E-12	-6.89E-12	-5.13E-12
s_{33}^E	m^2/N	1.80E-11	1.94E-11	1.36E-11	**1.96E-11**	**2.32E-11**	1.83E-11	2.29E-11	7.31E-12		5.67E-11	4.42E-11	1.65E-11	1.86E-11	1.60E-11
$s_{44}^E = s_{55}^E$	m^2/N	3.80E-11	3.90E-11	2.30E-11	**3.32E-11**	**4.35E-11**	3.77E-11	5.41E-11	1.72E-11			2.62E-11			3.67E-11
s_{66}	m^2/N	5.20E-11	4.13E-11	2.72E-11	**3.47E-11**	**4.71E-11**	3.26E-11	4.56E-11	1.79E-11		9.85E-11	2.58E-11	3.83E-11	3.64E-11	
s_{11}^D	m^2/N	1.63E-11	1.36E-11	9.56E-12	**1.16E-11**	**1.51E-11**	1.11E-11	1.47E-11	7.31E-12	2,19919E-011	3.64E-11	1.06E-11	1.29E-11	1.22E-11	1.11E-11
s_{12}^D	m^2/N	-9.67E-12	-7.06E-12	-4.02E-12	**-5.74E-12**	**-8.41E-12**	-5.20E-12	-8.10E-12	-1.63E-12	-4,4388E-012	-1.28E-11	-2.29E-12	-6.30E-12	-6.04E-12	-6.31E-12
s_{13}^D	m^2/N	-2.80E-12	-3.97E-12	-2.46E-12	**-3.47E-12**	**-4.08E-12**	-3.01E-12	-3.30E-12	-4.03E-13		-1.24E-11	-1.20E-11	-2.08E-12	-3.09E-12	-6.31E-12
s_{33}^D	m^2/N	9.39E-12	1.13E-11	7.71E-12	**1.05E-11**	**1.19E-11**	9.65E-12	9.94E-12	6.16E-12		3.77E-11	4.39E-11	8.15E-12	9.54E-12	8.00E-12
$s_{44}^D = s_{55}^D$	m^2/N	2.48E-11	2.44E-11	2.05E-11	**2.31E-11**	**2.73E-11**	2.27E-11	2.98E-11	1.63E-11			2.62E-11			8.80E-13
c_{11}^E	N/m^2	1.14E+11	1.57E+11	1.62E+11	**1.68E+11**	**1.47E+11**	1.52E+11	1.34E+11	1.45E+11		4.18E+10	3.13E+11	1.11E+11	1.46E+11	
c_{12}^E	N/m^2	7.57E+10	1.09E+11	8.84E+10	**1.10E+11**	**1.05E+11**	9.05E+10	8.97E+10	3.28E+10		2.15E+10	2.36E+11	5.89E+10	9.15E+10	
c_{13}^E	N/m^2	7.24E+10	9.77E+10	8.75E+10	**9.99E+10**	**9.37E+10**	8.74E+10	8.57E+10	1.30E+10		1.82E+10	1.49E+11	6.18E+10	8.82E+10	
c_{33}^E	N/m^2	1.11E+11	1.23E+11	1.34E+11	**1.23E+11**	**1.13E+11**	1.18E+11	1.09E+11	1.39E+11	4.72E+10	2.82E+10	1.03E+11	1.06E+11	1.19E+11	
$c_{44}^E = c_{55}^E$	N/m^2	2.63E+10	2.57E+10	4.35E+10	**3.01E+10**	**2.30E+10**	2.65E+10	1.85E+10	5.81E+10	2.15E+10		3.82E+10			
c_{66}	N/m^2	1.92E+10	2.42E+10	3.68E+10	**2.88E+10**	**2.12E+10**	3.07E+10	2.20E+10	5.59E+10		1.02E+10	3.88E+10	2.61E+10	2.75E+10	
c_{11}^D	N/m^2	1.19E+11	1.58E+11	1.63E+11	**1.69E+11**	**1.49E+11**	1.55E+11	1.36E+11	1.45E+11		4.25E+10	3.16E+11	1.17E+11	1.49E+11	
c_{12}^D	N/m^2	8.08E+10	1.09E+11	8.94E+10	**1.12E+11**	**1.06E+11**	9.34E+10	9.21E+10	3.29E+10		2.22E+10	2.38E+11	6.47E+10	9.39E+10	
c_{13}^D	N/m^2	5.97E+10	9.38E+10	8.07E+10	**9.33E+10**	**8.75E+10**	7.75E+10	7.58E+10	1.16E+10		2.13E+10	1.51E+11	4.63E+10	7.87E+10	
c_{33}^D	N/m^2	1.42E+11	1.54E+11	1.81E+11	**1.58E+11**	**1.44E+11**	1.52E+11	1.51E+11	1.67E+11	5.32E+10	4.05E+10	1.10E+11	1.46E+11	1.56E+11	
$c_{44}^D = c_{55}^D$	N/m^2	4.03E+10	4.10E+10	4.87E+10	**4.34E+10**	**3.66E+10**	4.41E+10	3.36E+10	6.13E+10	* 2.21E+10		3.82E+10			
Y_{11}^E	GPa	5.48E+01	6.75E+01	9.56E+01	**7.69E+01**	**5.90E+01**	7.94E+01	5.88E+01	1.36E+02		2.69E+01	9.42E+01	6.80E+01	7.27E+01	8.18E+01
Y_{33}^E	GPa	5.56E+01	5.16E+01	7.33E+01	**5.09E+01**	**4.31E+01**	5.47E+01	4.37E+01	1.37E+02		1.76E+01	2.26E+01	6.07E+01	5.38E+01	6.25E+01
Y_{11}^D	GPa	6.12E+01	7.36E+01	1.05E+02	**8.62E+01**	**6.60E+01**	9.00E+01	6.81E+01	1.37E+02		2.75E+01	9.42E+01	7.77E+01	8.22E+01	9.05E+01
Y_{33}^D	GPa	1.07E+02	8.85E+01	1.30E+02	**9.56E+01**	**8.43E+01**	1.04E+02	1.01E+02	1.62E+02		2.65E+01	2.28E+01	1.23E+02	1.05E+02	1.25E+02

Ferroperm Piezoceramics A/S
Hejreskovvej 18A DK-3490 Kvistgaard Denmark Tel: +45 - 4912 7100 Fax: +45 - 4913 8188
Internet: www.ferroperm-piezo.com E-mail: pz@ferroperm-piezo.com

Appendix B

Schematic Diagram of Resonator

B.1 Medium Size Test Resonator

B.2 Small Size Test Resonator

part1.tif (993x768x24b tiff)

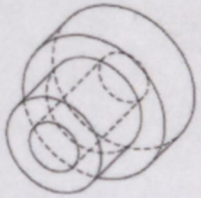

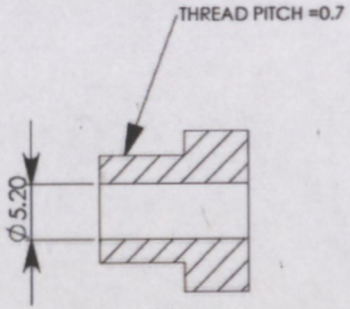

A-A

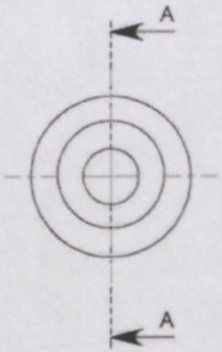

TOP VIEW

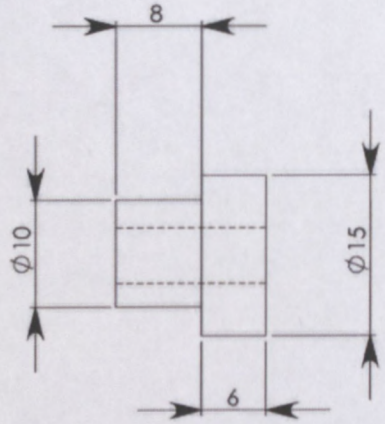

LEFT VIEW

DIMENSIONS ARE IN: mm	CIR
TOLERANCES: 0.02mm	Cape Peninsula University of Technology
MATERIAL: Brass	Tel: 4603606
QUANTITY: 1	Name: Lewis Chang
COMMENTS:	SIZE A | DWG. NO. | REV.
	SCALE 1:3 | WEIGHT: | SHEET 1 OF 1

part2.tif (993x768x24b tiff)

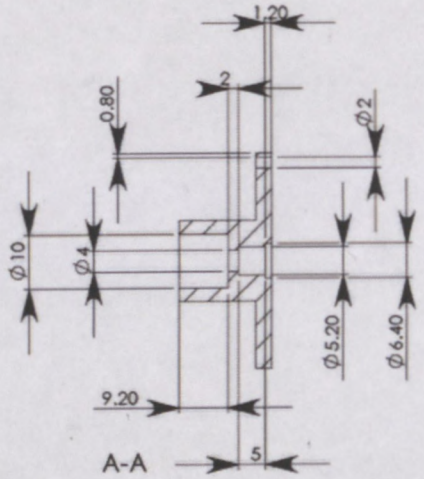

A-A

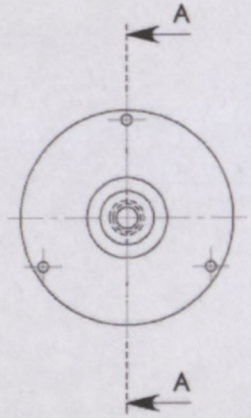

TOP VIEW

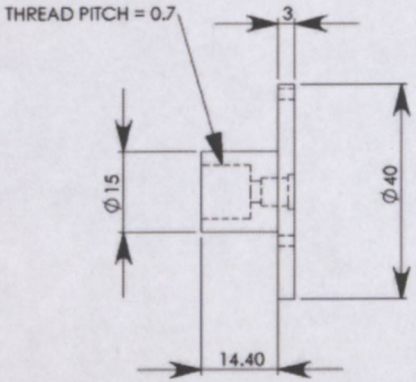

LEFT VIEW

ISOMETRIC VIEW

DIMENSIONS ARE IN: mm	CIR
TOLERANCES: 0.02mm	Cape Peninsula University of Technology
MATERIAL: STAINLESS STEEL	Tel: 4603606
QUANTITY: 1	Name: Lewis Chang
COMMENTS:	SIZE A | DWG. NO. | REV.
	SCALE 1:1 | WEIGHT: | SHEET 1 OF 1

part3.tif (993x768x24b tiff)

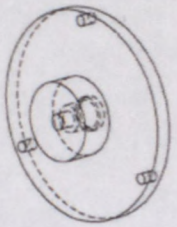

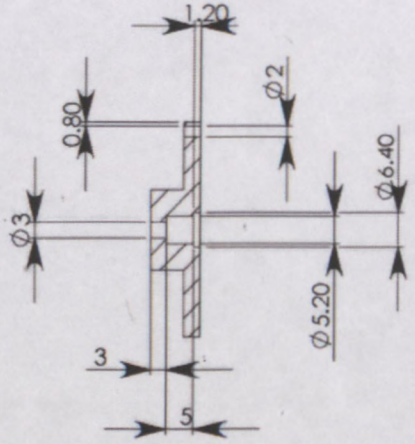

A-A

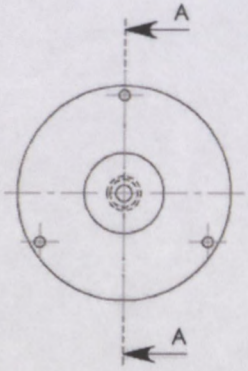

TOP VIEW

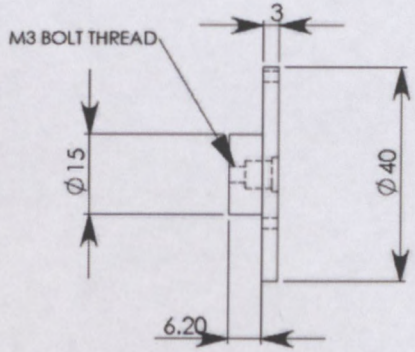

LEFT VIEW

DIMENSIONS ARE IN: mm	CIR
TOLERANCES: 0.02 mm	Cape Peninsula University of Technology
MATERIAL: STAINLESS STEEL	Tel: 4603606
QUANTITY : 1	Name: Lewis Chang
COMMENTS:	SIZE A | DWG. NO. | REV.
	SCALE 1:1 | WEIGHT: | SHEET 1 OF 1

part1.tif (993x768x24b tiff)

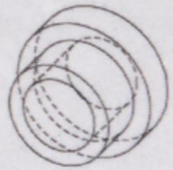

ISOMETRIC VIEW

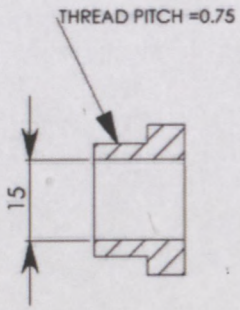

A-A

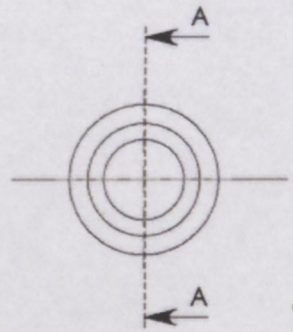

TOP VIEW

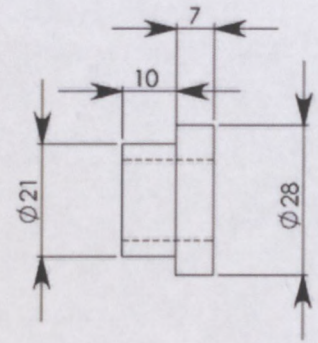

LEFT VIEW

DIMENSIONS ARE IN: mm TOLERANCES: ± 0.02mm MATERIAL: Brass QUANTITY: 1 COMMENTS:	CIR, Cape Peninsula University of Technology Tel: 4603606 Name: Lewis Chang
SIZE A | DWG. NO. | REV.	
SCALE 1:1 | WEIGHT: | SHEET 1 OF 1	

part 2.tif (993x768x24b tiff)

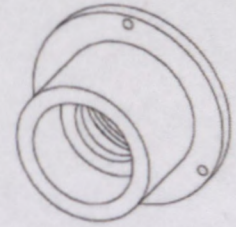

ISOMETRIC VIEW

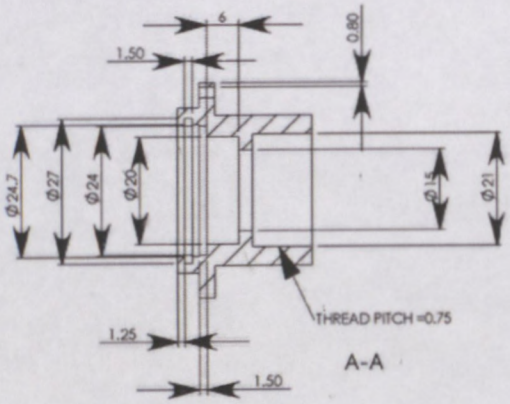

A-A

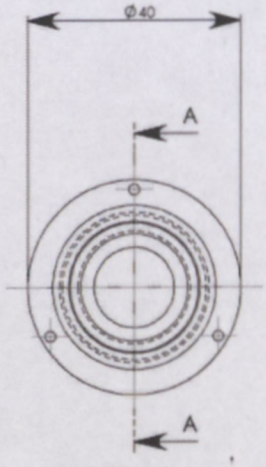

TOP VIEW

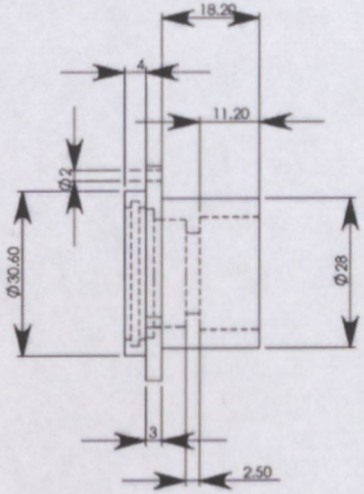

LEFT VIEW

DIMENSIONS ARE IN: mm TOLERANCES: 0.02mm MATERIAL: STAINLESS STEEL QUANTITY : 1 COMMENTS:	CIR Cape Peninsula University of Technology Tel: 4603606 Name: Lewis Chang
SIZE A	DWG. NO. REV.
SCALE 1:1	WEIGHT: SHEET 1 OF 1

part 3.tif (993x768x24b tiff)

ISOMETRIC VIEW

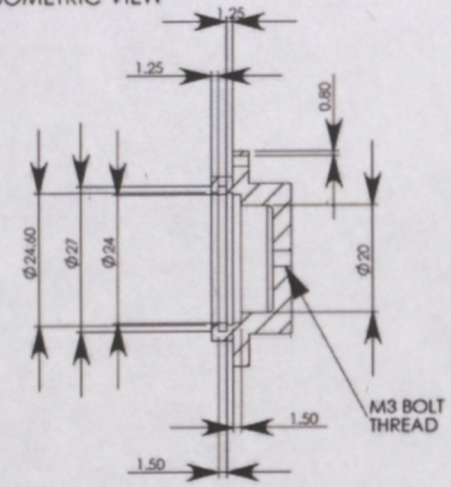

A-A

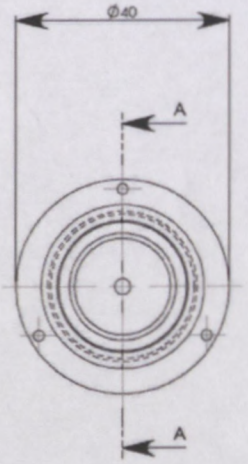

TOP VIEW

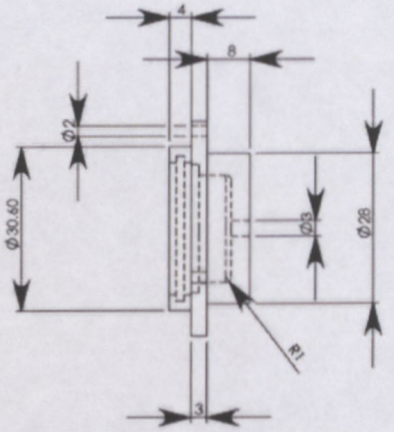

LEFT VIEW

DIMENSIONS ARE IN: mm	CIR
TOLERANCES: 0.02	Cape Peninsula University of Technology
MATERIAL: Stainless Steel	Tel: 4603606
QAUNTITY: 1	Name: Lewis Chang
COMMENTS:	SIZE A / DWG. NO. / REV.
	SCALE:1:1 / WEIGHT: / SHEET 1 OF 1

Appendix C

Lookup Table for PT100 Temperature Sensor

PT100 Resistance Table

°C	0	1	2	3	4	5	6	7	8	9	°C
-200.00	18.52										-200.00
-190.00	22.83	22.40	21.97	21.54	21.11	20.68	20.25	19.82	19.38	18.95	-190.00
-180.00	27.10	26.67	26.24	25.82	25.39	24.97	24.54	24.11	23.68	23.25	-180.00
-170.00	31.34	30.91	30.49	30.07	29.64	29.22	28.80	28.37	27.95	27.52	-170.00
-160.00	35.54	35.12	34.70	34.28	33.86	33.44	33.02	32.60	32.18	31.76	-160.00
-150.00	39.72	39.31	38.89	38.47	38.05	37.64	37.22	36.80	36.38	35.96	-150.00
-140.00	43.88	43.46	43.05	42.63	42.22	41.80	41.39	40.97	40.56	40.14	-140.00
-130.00	48.00	47.59	47.18	46.77	46.36	45.94	45.53	45.12	44.70	44.29	-130.00
-120.00	52.11	51.70	51.29	50.88	50.47	50.06	49.65	49.24	48.83	48.42	-120.00
-110.00	56.19	55.79	55.38	54.97	54.56	54.15	53.75	53.34	52.93	52.52	-110.00
-100.00	60.26	59.85	59.44	59.04	58.63	58.23	57.82	57.41	57.01	56.60	-100.00
-90.00	64.30	63.90	63.49	63.09	62.68	62.28	61.88	61.47	61.07	60.66	-90.00
-80.00	68.33	67.92	67.52	67.12	66.72	66.31	65.91	65.51	65.11	64.70	-80.00
-70.00	72.33	71.93	71.53	71.13	70.73	70.33	69.93	69.53	69.13	68.73	-70.00
-60.00	76.33	75.93	75.53	75.13	74.73	74.33	73.93	73.53	73.13	72.73	-60.00
-50.00	80.31	79.91	79.51	79.11	78.72	78.32	77.92	77.52	77.12	76.73	-50.00
-40.00	84.27	83.87	83.48	83.08	82.69	82.29	81.89	81.50	81.10	80.70	-40.00
-30.00	88.22	87.83	87.43	87.04	86.64	86.25	85.85	85.46	85.06	84.67	-30.00
-20.00	92.16	91.77	91.37	90.98	90.59	90.19	89.80	89.40	89.01	88.62	-20.00
-10.00	96.09	95.69	95.30	94.91	94.52	94.12	93.73	93.34	92.95	92.55	-10.00
0.00	100.00	99.61	99.22	98.83	98.44	98.04	97.65	97.26	96.87	96.48	0.00
0.00	100.00	100.39	100.78	101.17	101.56	101.95	102.34	102.73	103.12	103.51	0.00
10.00	103.90	104.29	104.68	105.07	105.46	105.85	106.24	106.63	107.02	107.40	10.00
20.00	107.79	108.18	108.57	108.96	109.35	109.73	110.12	110.51	110.90	111.29	20.00
30.00	111.67	112.06	112.45	112.83	113.22	113.61	114.00	114.38	114.77	115.15	30.00
40.00	115.54	115.93	116.31	116.70	117.08	117.47	117.86	118.24	118.63	119.01	40.00
50.00	119.40	119.78	120.17	120.55	120.94	121.32	121.71	122.09	122.47	122.86	50.00
60.00	123.24	123.63	124.01	124.39	124.78	125.16	125.54	125.93	126.31	126.69	60.00
70.00	127.08	127.46	127.84	128.22	128.61	128.99	129.37	129.75	130.13	130.52	70.00
80.00	130.90	131.28	131.66	132.04	132.42	132.80	133.18	133.57	133.95	134.33	80.00
90.00	134.71	135.09	135.47	135.85	136.23	136.61	136.99	137.37	137.75	138.13	90.00
100.00	138.51	138.88	139.26	139.64	140.02	140.40	140.78	141.16	141.54	141.91	100.00
110.00	142.29	142.67	143.05	143.43	143.80	144.18	144.56	144.94	145.31	145.69	110.00
120.00	146.07	146.44	146.82	147.20	147.57	147.95	148.33	148.70	149.08	149.46	120.00
130.00	149.83	150.21	150.58	150.96	151.33	151.71	152.08	152.46	152.83	153.21	130.00
140.00	153.58	153.96	154.33	154.71	155.08	155.46	155.83	156.20	156.58	156.95	140.00
150.00	157.33	157.70	158.07	158.45	158.82	159.19	159.56	159.94	160.31	160.68	150.00
160.00	161.05	161.43	161.80	162.17	162.54	162.91	163.29	163.66	164.03	164.40	160.00
170.00	164.77	165.14	165.51	165.89	166.26	166.63	167.00	167.37	167.74	168.11	170.00
180.00	168.48	168.85	169.22	169.59	169.96	170.33	170.70	171.07	171.43	171.80	180.00
190.00	172.17	172.54	172.91	173.28	173.65	174.02	174.38	174.75	175.12	175.49	190.00
200.00	175.86	176.22	176.59	176.96	177.33	177.69	178.06	178.43	178.79	179.16	200.00
210.00	179.53	179.89	180.26	180.63	180.99	181.36	181.72	182.09	182.46	182.82	210.00
220.00	183.19	183.55	183.92	184.28	184.65	185.01	185.38	185.74	186.11	186.47	220.00
230.00	186.84	187.20	187.56	187.93	188.29	188.66	189.02	189.38	189.75	190.11	230.00
240.00	190.47	190.84	191.20	191.56	191.92	192.29	192.65	193.01	193.37	193.74	240.00
250.00	194.10	194.46	194.82	195.18	195.55	195.91	196.27	196.63	196.99	197.35	250.00
260.00	197.71	198.07	198.43	198.79	199.15	199.51	199.87	200.23	200.59	200.95	260.00
270.00	201.31	201.67	202.03	202.39	202.75	203.11	203.47	203.83	204.19	204.55	270.00
280.00	204.90	205.26	205.62	205.98	206.34	206.70	207.05	207.41	207.77	208.13	280.00
290.00	208.48	208.84	209.20	209.56	209.91	210.27	210.63	210.98	211.34	211.70	290.00
300.00	212.05	212.41	212.76	213.12	213.48	213.83	214.19	214.54	214.90	215.25	300.00
310.00	215.61	215.96	216.32	216.67	217.03	217.38	217.74	218.09	218.44	218.80	310.00
320.00	219.15	219.51	219.86	220.21	220.57	220.92	221.27	221.63	221.98	222.33	320.00

°C	0	1	2	3	4	5	6	7	8	9	°C
330.00	222.68	223.04	223.39	223.74	224.09	224.45	224.80	225.15	225.50	225.85	330.00
340.00	226.21	226.56	226.91	227.26	227.61	227.96	228.31	228.66	229.02	229.37	340.00
350.00	229.72	230.07	230.42	230.77	231.12	231.47	231.82	232.17	232.52	232.87	350.00
360.00	233.21	233.56	233.91	234.26	234.61	234.96	235.31	235.66	236.00	236.35	360.00
370.00	236.70	237.05	237.40	237.74	238.09	238.44	238.79	239.13	239.48	239.83	370.00
380.00	240.18	240.52	240.87	241.22	241.56	241.91	242.26	242.60	242.95	243.29	380.00
390.00	243.64	243.99	244.33	244.68	245.02	245.37	245.71	246.06	246.40	246.75	390.00
400.00	247.09	247.44	247.78	248.13	248.47	248.81	249.16	249.50	249.85	250.19	400.00
410.00	250.53	250.88	251.22	251.56	251.91	252.25	252.59	252.93	253.28	253.62	410.00
420.00	253.96	254.30	254.65	254.99	255.33	255.67	256.01	256.35	256.70	257.04	420.00
430.00	257.38	257.72	258.06	258.40	258.74	259.08	259.42	259.76	260.10	260.44	430.00
440.00	260.78	261.12	261.46	261.80	262.14	262.48	262.82	263.16	263.50	263.84	440.00
450.00	264.18	264.52	264.86	265.20	265.53	265.87	266.21	266.55	266.89	267.22	450.00
460.00	267.56	267.90	268.24	268.57	268.91	269.25	269.59	269.92	270.26	270.60	460.00
470.00	270.93	271.27	271.61	271.94	272.28	272.61	272.95	273.29	273.62	273.96	470.00
480.00	274.29	274.63	274.96	275.30	275.63	275.97	276.30	276.64	276.97	277.31	480.00
490.00	277.64	277.98	278.31	278.64	278.98	279.31	279.64	279.98	280.31	280.64	490.00
500.00	280.98	281.31	281.64	281.98	282.31	282.64	282.97	283.31	283.64	283.97	500.00
510.00	284.30	284.63	284.97	285.30	285.63	285.96	286.29	286.62	286.95	287.29	510.00
520.00	287.62	287.95	288.28	288.61	288.94	289.27	289.60	289.93	290.26	290.59	520.00
530.00	290.92	291.25	291.58	291.91	292.24	292.56	292.89	293.22	293.55	293.88	530.00
540.00	294.21	294.54	294.86	295.19	295.52	295.85	296.18	296.50	296.83	297.16	540.00
550.00	297.49	297.81	298.14	298.47	298.80	299.12	299.45	299.78	300.10	300.43	550.00
560.00	300.75	301.08	301.41	301.73	302.06	302.38	302.71	303.03	303.36	303.69	560.00
570.00	304.01	304.34	304.66	304.98	305.31	305.63	305.96	306.28	306.61	306.93	570.00
580.00	307.25	307.58	307.90	308.23	308.55	308.87	309.20	309.52	309.84	310.16	580.00
590.00	310.49	310.81	311.13	311.45	311.78	312.10	312.42	312.74	313.06	313.39	590.00
600.00	313.71	314.03	314.35	314.67	314.99	315.31	315.64	315.96	316.28	316.60	600.00
610.00	316.92	317.24	317.56	317.88	318.20	318.52	318.84	319.16	319.48	319.80	610.00
620.00	320.12	320.43	320.75	321.07	321.39	321.71	322.03	322.35	322.67	322.98	620.00
630.00	323.30	323.62	323.94	324.26	324.57	324.89	325.21	325.53	325.84	326.16	630.00
640.00	326.48	326.79	327.11	327.43	327.74	328.06	328.38	328.69	329.01	329.32	640.00
650.00	329.64	329.96	330.27	330.59	330.90	331.22	331.53	331.85	332.16	332.48	650.00
660.00	332.79	333.11	333.42	333.74	334.05	334.36	334.68	334.99	335.31	335.62	660.00
670.00	335.93	336.25	336.56	336.87	337.18	337.50	337.81	338.12	338.44	338.75	670.00
680.00	339.06	339.37	339.69	340.00	340.31	340.62	340.93	341.24	341.56	341.87	680.00
690.00	342.18	342.49	342.80	343.11	343.42	343.73	344.04	344.35	344.66	344.97	690.00
700.00	345.28	345.59	345.90	346.21	346.52	346.83	347.14	347.45	347.76	348.07	700.00
710.00	348.38	348.69	348.99	349.30	349.61	349.92	350.23	350.54	350.84	351.15	710.00
720.00	351.46	351.77	352.08	352.38	352.69	353.00	353.30	353.61	353.92	354.22	720.00
730.00	354.53	354.84	355.14	355.45	355.76	356.06	356.37	356.67	356.98	357.28	730.00
740.00	357.59	357.90	358.20	358.51	358.81	359.12	359.42	359.72	360.03	360.33	740.00
750.00	360.64	360.94	361.25	361.55	361.85	362.16	362.46	362.76	363.07	363.37	750.00
760.00	363.67	363.98	364.28	364.58	364.89	365.19	365.49	365.79	366.10	366.40	760.00
770.00	366.70	367.00	367.30	367.60	367.91	368.21	368.51	368.81	369.11	369.41	770.00
780.00	369.71	370.01	370.31	370.61	370.91	371.21	371.51	371.81	372.11	372.41	780.00
790.00	372.71	373.01	373.31	373.61	373.91	374.21	374.51	374.81	375.11	375.41	790.00
800.00	375.70	376.00	376.30	376.60	376.90	377.19	377.49	377.79	378.09	378.39	800.00
810.00	378.68	378.98	379.28	379.57	379.87	380.17	380.46	380.76	381.06	381.35	810.00
820.00	381.65	381.95	382.24	382.54	382.83	383.13	383.42	383.72	384.01	384.31	820.00
830.00	384.60	384.90	385.19	385.49	385.78	386.08	386.37	386.67	386.96	387.25	830.00
840.00	387.55	387.84	388.14	388.43	388.72	389.02	389.31	389.60	389.90	390.19	840.00
850.00	390.48										850.00

Thermocouple Instruments Limited
Pentwyn, Cardiff, CF23 7XJ, UK
Tel: (+44) 029 20 734121 Fax: (+44) 029 20 734 040
Internet: http://www.thermocouple.co.uk
E-mail: thermocouple@thermocouple.co.uk

Appendix D

Gefrane 600 PID control Setup

• Alarm Types

The alarm types are set by the **A1.t-A3.t** parameters in the **Out menu.** Alarms can be set to be absolute, relative or symmetrical.

- "**Direct**" alarm means the alarm contact closes when the input variable (eg. Temperature) exceeds the alarm setpoint
- "**Inverse**"alarm means the alarm contact closes when the input variable drops below the alarm setpoint.
- "**Absolute**" means the setpoint is independent of the active (control) setpoint.
- "**Relative**" means the alarm setpoint is relative to the active (control) setpoint
- "**Symmetrical**" means the alarm is active inside / outside a window around the control setpoint. It is used to detect abnormal deviation (positive and negative) of the input variable from setpoint.
- Alarms can be delayed by adding 32 (delay in seconds)or 64 (delay in minutes) to the selected alarm parameter. The **Hy**-parameter (**Hy.1** -**Hy.4** in **CFG** menu) becomes the delay time.

Examples:
Al.t=0 means that the alarm relay will close when the temperature exceeds the alarm setpoint ("high temperature alarm")
Al.t=2 and an alarm setpoint AL.1=10 means that the alarm relay will energise when the temperature rises by 10°C above the control setpoint.
Al.t=33(1+32) and Hy.1=45 means that a low temperature alarm will come on if the low temperature condition has prevailed for 45 seconds

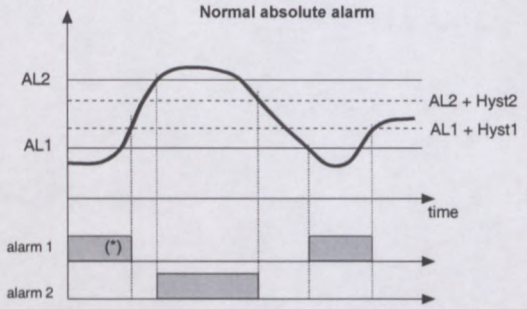

For AL1 = reverse absolute alarm (low) with positive Hyst1, AL1 t = 1
(*) = OFF if disabled on power-up
For AL2 = direct absolute alarm (high) with negative Hyst2, AL2 t = 0

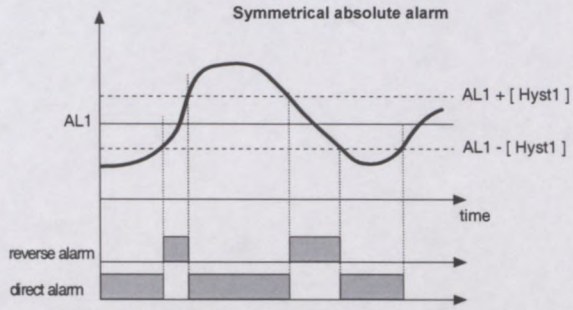

For AL1 = symmetrical Lo absolute alarm with Hyst1, AL1 t = 5
For AL1 = symmetrical Hi absolute alarm with Hyst1, AL1 t = 4

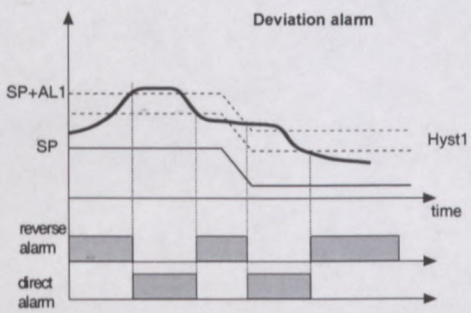

For AL1 = Lo deviation alarm with negative Hyst 1, AL1 t = 3
For AL1 = Hi deviation alarm with negative Hyst 1, AL1 t = 2

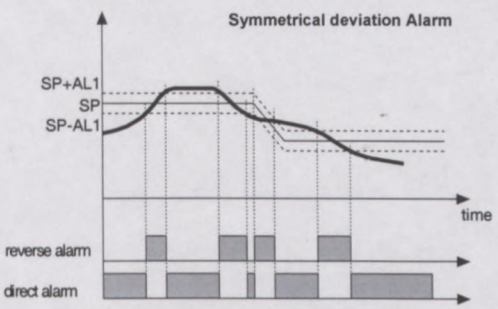

For AL1 = Symmetrical Lo deviation alarm with Hyst 1, AL1 t = 7
For AL1 = Symmetrical Hi deviation alarm with Hyst 1, AL1 t = 6

9.6 SENSOR FAULT AND LOOP BREAK ALARM (LBA)

LBA LOOP BREAK ALARM:

The LBA alarm is enabled by setting **Al.n**= (between 16 and 31) in **Hrd** menu, but can be disabled by setting **Lb.t**=0 in the **CFG** menu.
Lb.t sets the waiting time for a LBA alarm. The % output power under fault condition is set by **Lb.P** in the **CFG** menu. An alarm output can be enabled by setting **rL.1** (2, 3 or4)=6 in the **Out** menu. LBA is triggered when the output power is fully on (100%) but the process variable does not respond. This will typically happen when the heating circuit is defective, a fuse is blown, the thermocouple cable is short circuited or the sensor is not mounted in position.

Apart from triggering an alarm output, the LBA alarm can be configured to force the control output into a preset % output power when a loop fault occurs. The idea is to enter an output power at which the process will continue at normal temperature without causing overheating.

NB: Do not set the **Lb.t** too short to avoid nuisance tripping. Do not set **Lb.t** too long causing overheating before output power is reduced.

SENSOR FAULT

The system will indicate a sensor fault whenever the input signal falls outside the range set by **Lo.S** and **Hi.s** (**InP** menu).
In this condition the main control output power will default to the % set in **FA.P** (**CFG** menu).
This is a useful feature, allowing you to finish a production run before attending to a sensor fault. We recommend monitoring the % output power during normal operation (temporarily set **dSP**=2 in **HrD** menu) and then entering this value as the **FA.P** parameter.
Alternatively set **FA.P**=0 to disable the control output (failsafe mode).

9.7 Heater Break Alarm (aux. Input 3)

Controllers with input/output 3 option ="**H**" monitor the load current via a 50mA secondary current transformer (refer to Gefran CT type 330200 and 330201). The scaling of the input is achieved by setting **LS.2** (normally **LS2**=0) and **HS.2** in the **InP** menu.

The heater Break (HB) Alarm is enabled by setting either **rL.1** or **rL.2** or **rL.3** or **rL.4**=5, 13, 14, 15 or 16, by setting **Hb.F** to the appropriate level (see **Out** menu) and by setting **AL.n** to the correct parameter (see **Hrd** menu).

A.Hb in level 1 menu sets the HB alarm setpoint.
Hb.t in the **CFG** menu sets the waiting period before a HB alarm is triggered.

The direct **HB** alarm trips when the ammeter input value is below the limit set for **Hb.t** seconds of the "ON" time for the selected output.
The **HB** alarm can be activated only with ON times greater than 0.4 seconds (excludes continuous output).
The **HB** alarm also checks load current during the OFF interval of the cycle time for the selected output. The **HB** alarm trips if the measured current exceeds approximately 12.5% of the full scale set for **HB.t** seconds of OFF status of the output (parameter **HS.2** in **InP**).

The alarm is reset automatically if its cause is eliminated.

Setting limit **A.Hb** = 0 disables both types of **HB** alarms, with de-energizing of the assigned relay.
You can display the load current by selecting the item In.2. (level 1) or by setting **dSP**=1 in the **Hrd** menu.

NOTE: ON/OFF times refer to the cycle time set for the selected output.
Continuous alarm **Hb_F** = 3 (7) is active for a load current value below the set limit. It is disabled if the heating (cooling) output value is below 3%.

9.8 Manual mode

The controller can be set into manual mode. This is achieved by setting **but.**=1 in the **Hrd** menu. It is also recommended to set either Ld.1, LD.2 or Ld.3=17 (flashing) in the the **Hrd** menu, thus getting LED indication if the controller is in manual mode.

By operating the AUTO/MANUAL button on the faceplate the controller will switch from normal control to manual control. The PV display (bottom display) will now show the % output power. The power can be adjusted via the UP/DOWN arrow keys.

The controller will return to AUTO mode if the AUTO/MANUAL button is operated again.

9.9 Display functions

SV DISPLAY (BOTTOM DISPLAY)

The function of this display can be configured by setting the **dSP** parameter in the Hrd menu.
Normally **dSP**=0, showing the control setpoint. However the display can also be configured to display the value of the auxiliary input, the output power or the deviation of the process variable from the setpoint.

Display of the % output power (**dSP**=2) is useful to determine the output power during normal running conditions, thus obtaining the value to feed into the **FA.P** parameter in the **CFG** menu. This will then be the % output power the controller defaults to when a LBA (sensor fault) alarm occurs.

L1, L2, L3 LED DISPLAYS

The three LEDs on the left hand side of the faceplate can be configured to indicate various conditions. The function of each LED is determined by the **Ld.1-Ld.3** parameters in the **Hrd** menu. The LEDs can also be configured to flash by adding 16 to the selected parameter.
Each LED can be assigned a different function. It is also possible to assign the same function to all three LEDs . e.g. setting
Ld.1=Ld.2=Ld.3=24 will cause all three LEDs to flash when an error (sensor fault) occurs. This is a very visible indication.

It is recommended to assign these LEDs when any of the following features are being enabled:
Softstart, selftuning, autotuning, Manual/Auto mode.
It makes diagnostics easy if one can see in which mode the controller presently is.

9.10 PID parameters, Autotune and selftune

PID parameters must be tuned to provide accurate control . There is often a tradeoff between rapid response to deviations from the setpoint , elimination of overshoot and stability of the process. PID parameters can either be tuned manually or automatically through selftuning or autotuning.

• PID parameters

The PID parameters determine the control performance and are settable in the **CFG** menu.

P: Proportional band:
The function of the Proportional band (see **h.Pb** and **c.Pb**) is to eliminate the cyclic overshoot/undershoot caused by thermal lag. This is achieved by reducing output power before the setpoint is reached, thus anticipating the overshoot. The closer one gets to the setpoint, the less power is provided. The proportional band is expressed as a percentage of the input scale (**Hi.S-Lo.S**). See example below.

A very narrow proportional band can lead to cyclic overshoot/undershoot. An excessively wide proportional band will slow down the heat up time becvause power is reduced too early.
Proportional control results in an error (offset).

E.g. for a type "J" input with **Lo.S**=0 and **Hi.S**=1000 and **h.Pb**=4.5 the proportional band is 4.5% of (1000-0)=45°C. As a result the output power of the control output will be reduced when the rising temperature enters a 45°C window below the setpoint.

I: Integral parameter
The Integral parameter (see **h.it** and **c.it**) automatically removes the error (offset) caused by the proportional control. It reduces or increases power to counteract any deviation of the process variable from setpoint. The integral parameter represents time ("Integral time") and is expressed in minutes. A long integral time results in slow correction of errors. A very fast integral time can cause ringing (oscillation) as a result of aggressive error correction.

D: Derivative parameter
The Derivative parameter (see **h.dt** and **c.dt**) counteracts rapid changes in the process variable. It is useful to reduce overshoot caused by aggressive Integral action. It also provides fast corrective action to a sudden change in the process variable. The Derivative parameter represents time ("Derivative time") and is expressed in minutes. A long Derivative time results in a strong response to a change in the process variable. Derivative time should be used with caution as it can lead to instability by overreacting to noise (electromagnetic interference) on the sensor input line. As a rule of thumb the Derivative time should be less than 25% of the Integral time. Any higher value will lead to a conflict between Integral and Derivative action, resulting in the process spiraling out of control.

Appendix E

AMBA Code

```
%=========================================================================%
%     Adaptively Mutation Breeder Algorithms (AMBA)                       %
%     File Name: sourcecode_ver11_Water_AMBA_sim.m                        %
%     Version: 11                                                         %
%     Date: 2006-08-29                                                    %
%     Descriptions: +calculated Standard Deviation                        %
%     Test liquid: Water; 1509.1 (m/s)                                    %
%     Transducer: PZ27-Small, ID = 5.2e-3; OD = 6.35e-3; Length = 6.35e-3 %
%=========================================================================%


%========================== Importing Spectrum ==========================%
clear
clc
close all
format long
load('data_Bjorn_small_tube.mat')
%=========================================================================%

velocity_literature = 1509.1;                    %Literature measurement of
Velocity in Water at 30C

%========================== Structure Spectrum ==========================%
G = Admittance .* cos(Phase);                    % Calculate Conductance(G)
B = Admittance .* sin(Phase);                    % Calculate Suceptance(S)
Y_complex = complex(G,B);                        % Complex matrix of G +jB
values for different frequencies
Omega = 2*pi.*frequency;


%============================== Initialization ==========================%
% Load Defined Geometric and Physical Properties of Tube
ID = 5.2e-3;                                     % Inner Diameter
OD = 6.35e-3;                                    % Outer Diameter
Length = 6.35e-3;                                % Length
Thickness = (OD - ID)/2;                         % Thickness

% Properties of Tube
h33 = 0.0267;                                    % Piezoelectric constant
Transformer_A = (((pi*ID*Length) + (pi*OD*Length)) / 2)/(h33 * Thickness); % Electro-
Mechanical Transformer A
Transformer_B = 1/(pi*ID*Length);                % Acoustic-Mechanical
Transformer B
fundamental_freq = 3.33e+6;                      % Resonance Frequency of
Fundamental Thickness mode

% Number of Modes
Mechanical_modes = 1;
Acousticl_modes = 19;
```

```
% Define Breeder Algorith Parameters
Supreme_pool = 10;                                  % Number of genetic sets
created by simply mutation the previous superior solution
Breeder_comb_pool = 100;                            % Number of genetic sets
created by linear combination of top solutions
Genetic_pool = Supreme_pool + Breeder_comb_pool;    % Size of genetic pool
Mutation = 0.09;                                    % Mutation scalar used by
mutation to previous superior solution
Extline_mutation = 0.8;                             % Mutation scalar used by
linear combinations
Generations = 100;                                  % Number of identical
solutions before iterations stop

% Assign Electrical Parameters
co_scale = 4e-8;                                    % Electrical Capacitance
Co = co_scale * rand(Genetic_pool,1);               % Generate genetic pool for
"Co"

% Assign Mechanical Parameters
wm_scale = 2*pi*fundamental_freq;
qm_scale = 80;
rm_scale = rand*100;
Wm = wm_scale * rand(Genetic_pool,Mechanical_modes);    %Initial matrix of trial
solutions
Qm = qm_scale * rand(Genetic_pool,Mechanical_modes);
Rm = rm_scale * rand(Genetic_pool,Mechanical_modes);

% Initialise the starting value of mechaincal parameters
Co(1,:) = 1.7145e-9;
Wm(1,:) = fundamental_freq*2*pi;
Qm(1,:) = 46;
Rm(1,:) = 100;
Lm = (Qm.*Rm)./Wm;
Cm = 1./(Qm.*Wm.*Rm);

% Randomly Assign Accoustic Parameters
Sound_speed_scale = 1500;
nat_freq_acou_fund_scale = 2 * (2 * pi * (Sound_speed_scale / ID));
qa_scale = 8e+3;
ra_scale = 7e+7;

for k=1:Acousticl_modes
   Acoustic_mode_counter(1,k)=k ;
end

WnFa = nat_freq_acou_fund_scale * rand(Genetic_pool,1);
Qa = qa_scale * rand(Genetic_pool,Acousticl_modes);
Ra = ra_scale * rand(Genetic_pool,Acousticl_modes);

% Initial Guessing for Acoustic Parameters
WnFa(1,:) = 1.766e+6;
```

```
Ra(1,:) = 5.3126e+008;
Qa(1,:) = 670;
WnFa = repmat(WnFa,1,Acousticl_modes).*repmat(Acoustic_mode_counter,Genetic_pool,1);
La = (Qa.*Ra)./WnFa;
Ca = 1./(Qa.*WnFa.*Ra);

% Mask Applied to Ra
Mask = ((Ra - fundamental_freq)./abs(Ra - fundamental_freq)+1)/2;
Ra = Mask .* Ra + 2*(1-Mask).*fundamental_freq;

%---------- Initialization Complete ----------%

%=========================================================================%
%================================ Main Codes ==============================%
%============================ Breeder Algorithm ===========================%
Interations = 0
Rating_history = 1:1:Generations;
while ((Rating_history(Generations) ~= Rating_history(1)) && (Interations < Generations))

   Interations = Interations + 1;

% Evaluate genetic sets using modes
   for n = 1:Genetic_pool

      % Acoustic Port Impedance
      Zacoustic = complex(ones(length(frequency),1)*Ra(n,:),(((Omega*La(n,:))-
(1./(Omega*Ca(n,:))))));
      Yacoustic_eff = (Transformer_B^2)./Zacoustic;
      Yacoustic_eff_total = zeros(length(frequency),1);
      Yacoustic_eff_total = sum(Yacoustic_eff')';
      Zacoustic_eff_total = 1./Yacoustic_eff_total;

      % Mechanical Port Impedance
      Zmechanical = complex(ones(length(frequency),1)*Rm(n,:),((Omega*Lm(n,:))-
(1./(Omega*Cm(n,:)))));
      Zmechanical_total = Zmechanical + Zacoustic_eff_total;
      Zmech_tot_eff = (1/(Transformer_A^2)).*Zmechanical_total;
      Ymech_tot_eff = 1./Zmech_tot_eff;

      % Electrical Port Impedance
      ZCo = complex(0,-(1./(Omega*Co(n,:))));
      YCo = 1./ZCo;

      % Total Impedance
      Y_simulation = Ymech_tot_eff + YCo;

% Rate the Model
      Y_err(n) = sum((abs(Y_complex - Y_simulation)));
   end

% Sort Solutions Acording to Ratings
```

```
Rating = 100 * Y_err;
[Rating_sort,Rating_index] = sort(Rating);
WnFa_sort = WnFa(Rating_index,:);
Qa_sort = Qa(Rating_index,:);
Ra_sort = Ra(Rating_index,:);
Rm_sort = Rm(Rating_index,:);
Wm_sort = Wm(Rating_index,:);
Qm_sort = Qm(Rating_index,:);
Co_sort = Co(Rating_index,:);
```

% Sort Adaptive Mutation to determine Whether to Increase or Decrease Extend line Mutation Rate

```
Adaptive_rating_mask =
[1.*ones(1,Breeder_comb_pool/2),(ones(1,Breeder_comb_pool/2)),zeros(1,Supreme_pool)];
Adaptive_rating_mask = Adaptive_rating_mask(Rating_index);

Adaptive_direction = sum(Adaptive_rating_mask(1:Breeder_comb_pool/10));
Adaptive_direction = 2.*Adaptive_direction + 1;
Adaptive_direction = Adaptive_direction./abs(Adaptive_direction);

Extline_mutation = (1.0 + 0.2 * Adaptive_direction).* Extline_mutation;
if (Extline_mutation < 1.2)
   Extline_mutation = 1.2;
end
```

%========== Create New Genetic Pool ==========%

% Linear combinations

```
t(:,1) = round(((Supreme_pool+1) * rand((Breeder_comb_pool/2),1))-2);
t(:,1) = ((t(:,1) + abs(t(:,1))) / 2) + 1;
t(:,2) = round((Supreme_pool * rand((Breeder_comb_pool/2),1))-1);
t(:,2) = ((t(:,2) + abs(t(:,2))) / 2) + 2;

Mask = (ceil((abs(t(:,1) - t(:,2)))/10));
t(:,2) = (Mask.*t(:,2)) + ((1-Mask).*(t(:,1)+1));          %Ensures no inbreading

WnFa = Line_comb_mutation(WnFa_sort(:,1),Extline_mutation,t,Breeder_comb_pool,1);
WnFa =
repmat(WnFa,1,Acousticl_modes).*repmat(Acoustic_mode_counter,Breeder_comb_pool,1);
Qa = Line_comb_mutation(Qa_sort(:,1),Extline_mutation,t,Breeder_comb_pool,1);
Qa =
repmat(Qa,1,Acousticl_modes).*repmat(ones(1,Acousticl_modes),Breeder_comb_pool,1);
Ra = Line_comb_mutation(Ra_sort(:,1),Extline_mutation,t,Breeder_comb_pool,1);
Ra = repmat(Ra,1,Acousticl_modes).*repmat(ones(1,Acousticl_modes),Breeder_comb_pool,1);
Rm =
Line_comb_mutation(Rm_sort,Extline_mutation,t,Breeder_comb_pool,Mechanical_modes);
Wm =
Line_comb_mutation(Wm_sort,Extline_mutation,t,Breeder_comb_pool,Mechanical_modes);
Qm =
Line_comb_mutation(Qm_sort,Extline_mutation,t,Breeder_comb_pool,Mechanical_modes);
Co = Line_comb_mutation(Co_sort,Extline_mutation,t,Breeder_comb_pool,1);
```

```
% Random Mutation on Previous Superior Solutions
   WnFa(Breeder_comb_pool+1:Genetic_pool,1) = repmat(WnFa_sort(1,1),Supreme_pool,1) +
repmat((WnFa_sort(1,1).*Mutation),Supreme_pool,1).*(2.*rand(Supreme_pool,1)-1);
   WnFa(Breeder_comb_pool+1:Genetic_pool,:) =
repmat(WnFa(Breeder_comb_pool+1:Genetic_pool,1),1,Acousticl_modes).*repmat(Acoustic_m
ode_counter,Supreme_pool,1);
   Qa(Breeder_comb_pool+1:Genetic_pool,:) = repmat(Qa_sort(1,:),Supreme_pool,1) +
repmat((Qa_sort(1,:).*Mutation),Supreme_pool,1).*(2.*rand(Supreme_pool,Acousticl_modes)-1);
   Ra(Breeder_comb_pool+1:Genetic_pool,:) = repmat(Ra_sort(1,:),Supreme_pool,1) +
repmat((Ra_sort(1,:).*Mutation),Supreme_pool,1).*(2.*rand(Supreme_pool,Acousticl_modes)-1);
   Rm(Breeder_comb_pool+1:Genetic_pool,:) = repmat(Rm_sort(1,:),Supreme_pool,1) +
repmat((Rm_sort(1,:).*Mutation),Supreme_pool,1).*(2.*rand(Supreme_pool,Mechanical_modes)
-1);
   Wm(Breeder_comb_pool+1:Genetic_pool,:) = repmat(Wm_sort(1,:),Supreme_pool,1) +
repmat((Wm_sort(1,:).*Mutation),Supreme_pool,1).*(2.*rand(Supreme_pool,Mechanical_modes
)-1);
   Qm(Breeder_comb_pool+1:Genetic_pool,:) = repmat(Qm_sort(1,:),Supreme_pool,1) +
repmat((Qm_sort(1,:).*Mutation),Supreme_pool,1).*(2.*rand(Supreme_pool,Mechanical_modes)
-1);
   Co(Breeder_comb_pool+1:Genetic_pool,:) = repmat(Co_sort(1,:),Supreme_pool,1) +
repmat((Co_sort(1,:).*Mutation),Supreme_pool,1).*(2.*rand(Supreme_pool,1)-1);

%====================== Generating Lm, Cm, La and Ca ======================%
   La = (Qa.*Ra)./WnFa;
   Ca = 1./(Qa.*WnFa.*Ra);
   Lm = (Qm.*Rm)./Wm;
   Cm = 1./(Qm.*Wm.*Rm);
   Rating_history = circshift(Rating_history,[0,1]);
   Rating_history(1) = Rating_sort(1);
   Rating_sort(1)
   Interations
end

%================== Evaluating best solution using previous solutions ==========%
n=1
      % Toatal acoustical conductance
      Zacoustic = complex(ones(length(frequency),1)*Ra(n,:),((Omega*La(n,:))-
(1./(Omega*Ca(n,:)))));
      Yacoustic_eff = (Transformer_B^2)./Zacoustic;
      Yacoustic_eff_total = zeros(length(frequency),1);
      Yacoustic_eff_total = sum(Yacoustic_eff')';
      Zacoustic_eff_total = 1./Yacoustic_eff_total;
      % Toatal mechanical conductance
      Zmechanical = complex(ones(length(frequency),1)*Rm(n,:),((Omega*Lm(n,:))-
(1./(Omega*Cm(n,:)))));
      Zmechanical_total = Zmechanical + Zacoustic_eff_total;
      Zmech_tot_eff = (1/(Transformer_A^2)).*Zmechanical_total;
      Ymech_tot_eff = 1./Zmech_tot_eff;
      % Total electrical capactiance
      ZCo = complex(0,-(1./(Omega*Co(n,:))));
      YCo = 1./ZCo;
```

```
% Simulated conductance
Y_simulation = Ymech_tot_eff + YCo ;
Zacoustic_eff_total;

%====================== Velocity of Sound Calculation ======================%
Lv = La(1,:);
Cv = Ca(1,:);
fv = 1./(2*pi*sqrt(Lv.*Cv));                                    %Calculate the Velocity of
Sound in Liquid

for n = 1: (Acousticl_modes-1)
changing_fv(n) = fv(n+1) - fv(n);
end

Speed_of_sound_sim = changing_fv * ID;
torrance = ((velocity_literature - mean(Speed_of_sound_sim))/mean(Speed_of_sound_sim))*100;

%========================== Standard Deviation ============================%
Xmean = mean(abs(Y_complex(n)));
di = 0;
for count  = 1:1:801
   di = (di + (abs(Y_complex(count)) - Xmean)^2 )
end
model_variance = di/(count-1);
standard_deviation = sqrt(model_variance);

clc
fprintf('Speed of sound in Water = 1509.1  (m/s) --- Literature\n')
fprintf('Speed of sound in Water = %g (m/s) --- Simulation \n', mean(Speed_of_sound_sim))
fprintf('Torance = %g\n', torrance)
fprintf('Variance =%g \n' , model_variance)
fprintf('Standard Deviation =%g \n' , standard_deviation)

%---------------------------- Plot Graphs ----------------------------%
figure(1)
set(1,'Name','Admitance and Susceptance vs frequency')
hl1_2 = line(frequency,abs(Y_complex),'Color','b');
hl1 = line(frequency,abs(Y_simulation),'Color','r');
title('Measured and Simulation of absolute admittance')
legend('Measured','Simulated')
xlabel('frequency (Hz)');
ylabel('Absolute Admittance (Siemens)');

figure(2)
hl1_2 = line(frequency,real(Y_complex),'Color','b');
hl1 = line(frequency,real(Y_simulation),'Color','r');
title('Admitance(real) v.s frequency')
legend('Measured','Simulated')
xlabel('frequency (Hz)');
ylabel('Conductance (G)');
```

```
figure(3)
hl1_2 = line(frequency,imag(Y_complex),'Color','b');
hl1 = line(frequency,imag(Y_simulation),'Color','r');
title('Admitance(imaginary) v.s frequency')
legend('Measured','Simulated')
xlabel('frequency (Hz)');
ylabel('Susceptance (B)');

figure(4)
plot(frequency, Phase,'b')
hold on
Phase_sim = atan(imag(Y_simulation)./real(Y_simulation));
plot(frequency, Phase_sim,'r')
title('Phase v.s frequency')
legend('Measured','Simulated')
xlabel('frequency (Hz)');
ylabel('Phase (Radian)');

figure(5)
plot(real(Y_complex),imag(Y_complex),'Color','b');
hold on
plot(real(Y_simulation),(imag(Y_simulation)+offset ),'Color','r')
title('B v.s G plot')
legend('Measured','Simulated')
xlabel('Conductance (G)');
ylabel('Susceptance (B)');
axis equal
axis tight

figure(6)
plot(1:Acousticl_modes-1,changing_fv(n),'*')
hold on
title('Mode numbers v.s chaning frequency')
xlabel('Mode numbers (N)');
ylabel('df/dN (Hz)');
```

Appendix F

Measurement Setup